UNIVERSITÀ
DEGLI STUDI
FIRENZE

DOTTORATO DI RICERCA IN
INGEGNERA INDUSTRIALE

CICLO XXXII

COORDINATORE Prof. Maurizio De Lucia

On the design, realization, and preliminary run of a novel grazing flow test rig for acoustic liners' assessment under high temperature condition

Settore Scientifico Disciplinare ING/IND 09

Dottorando	**Tutore**	**co-tutore**
Dott. Pourreza Atabak	Prof. De Lucia Maurizio	Ing. Taddei Francesco

Coordinatore
Prof. De Lucia Maurizio

Anni 2016/2019

Ph.D. thesis

Engineering Department

University of Florence, Italy

Title:

On the design, realization, and preliminary run of a novel grazing flow test rig for acoustic liners' assessment under high temperature condition

Candidate: **Atabak Pourreza**

Ph.D. cycle XXXII

Student number: DT23363

Tutor: **Prof. Maurizio De Lucia**

Co-tutor: **Ing. Ph.D. Francesco Taddei**

Florence, 2016-2019

To my dear family for their endless love and all those days that I lived far away from them

Abstract

The installation of acoustic liners can represent an effective strategy for noise reduction in aero engines. The performance of an acoustic liner as a sound absorbing device is expressed by the acoustic impedance which mainly depends on its geometry and on the peculiar flow conditions acting on its surface. Several parameters are involved in the estimation of the impedance through a non-trivial dependence; this is even more complex when such devices are installed within a high-speed and high-temperature flow field such the one characteristic of the core nozzle of an aeroengine. Within such a scenario the experimental investigation is fundamental in order to assess the liner performance accurately. The most reliable way to determine the acoustic impedance is through a grazing flow rig which allows to experimentally investigate the acoustic liner performances under different flow conditions by using a controlled acoustic signal as excitation. At the Department of Industrial Engineering in Florence, a novel grazing flow rig for testing liners at flow conditions representative of the Low-Pressure Turbine (LPT) exit, i.e. at high speed and high temperature, has been designed and realized. The present work describes the design of the test rig and the preliminary experimental outcomes achieved for assessing the rig performances. The design of all the main components has been addressed following a comprehensive approach in order to meet the acoustic and aerodynamic requirements and by considering the thermo-structural effects as well. The design process has been supported by the use of Finite Element Analyses, the main results and the design solutions achieved are shown. As the rig is supposed to work under high temperature conditions, the sensors to be used for collecting the acoustic data shall withstand the hot flow as well. Hence, an experimental analysis has been carried out in order to compare the main market solutions available. As a result, the most suitable measurement device was identified. Once the design and the construction of the rig was finished, a preliminary set of tests was performed to prove the eligibility of the rig for the designed purpose. The uniformity of the flow field into the test section has been verified through a preliminary measurement of the flow profile. From the acoustic point of view, the reflection coefficient was measured at the duct ends and the results demonstrated very low reflections proving the effectiveness of the designed anechoic terminations. In addition, a first test on an acoustic liner sample was performed, i.e. the transmission loss was measured at cold flow condition. The overall results demonstrate that the rig is properly designed for the desired purposes.

ACKNOWLEDGEMENTS

I would like to sincerely thank my supervisor, Prof. Maurizio De Lucia, for his supports and guidance during my doctorate career and especially for his trust on me.

A very especial thanks goes to Dr. Francesco Taddei for his limitless and kind guides and scientific supports and helping me to grow in the current research field. Undoubtedly, it would be very challenging for me to finish this work without his helps.

The presented work is the result of a group work and I would like to thank my colleague Ing. Hamid Rashidi for his useful helps during my research activity.

I also want to appreciate the availability and supports of all my groupmates; Giacomo, Federico, Michele, Matteo and Sahand and all my students.

At the end, I would dedicate my thesis to my family and my friends Adel and Hadi that always encouraged me to pursue my academic career.

Contents

List of figures:

List of tables:

Chapter 1

Introduction

Aircraft noise and regulations

1. The reduction of the noise generated by the aircrafts is critical for the growth of air transports and for the quality of human life in residential areas around the airports and it is becoming more problematic as the public air transportation grows. New designs for aircrafts and engines are needed to solve the conflict between the growth of air traffic because of a customer's high demand and the noise pollution. Increasingly stringent rules for noise emission control for the novel engines are being applied by the international authorities and governments which have considered noise one of the most important factors affecting the environmental pollution and, as a consequence, people health. According to the Advisory Council of Aeronautics Research in Europe (ACARE), a significant reduction in the total aircraft noise must be achieved in the near future. To meet these targets, it is demanded to have a deeper understanding on noise sources and propagation mechanism in the jet engine and, more importantly, to develop and introduce more effective noise reduction techniques.

1.1.

1.2. Noise sources in the jet engines

In a civil aircraft engine, basically air is sucked by the intake and then it is separated into 2 parts; one flows into the core duct and the other part passes through the bypass duct. The bypass duct is where the larger part of the mass flow is passed. The most important sources of noise are the fan, where the main noise generation mechanism is due to the rotor and stator interaction, the combustor, the jet and the turbine. Mainly, tonal noise is generated by moving parts such as turbomachinery rotors, and the broadband noise is mainly due to the turbulent flow interaction with solid parts and flow mixing.

Compared to the typical 1960s design (low by-pass ratio design, Figure 1), the modern high by-pass ratio aircraft engines have a lower jet noise. However, such a design causes the fan noise to become the major noise source in the engine.

Although in high by-pass ratio design the fan provides the major contribution to the overall engine noise emission, other modules such as the Low-Pressure Turbine (LPT), can become important from an acoustic perspective, especially at the approach condition where the fan and jet noise is lower. The use of liners in the core nozzle duct can represent a promising strategy to reduce the LPT emissions

without affecting the aero design optimization or when other design solutions are not applicable, or to recover unexpected signature.

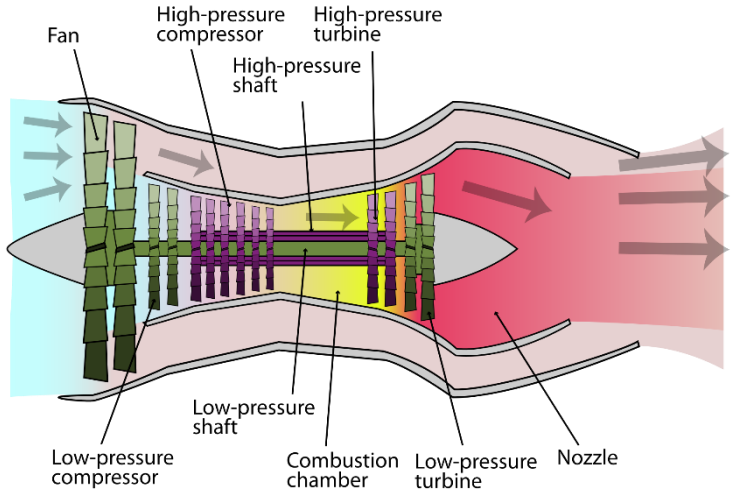

Figure 1, low by-pass ratio turbofan – picture by K. Aainsqatsi, CC BY-SA 3.0 [1]

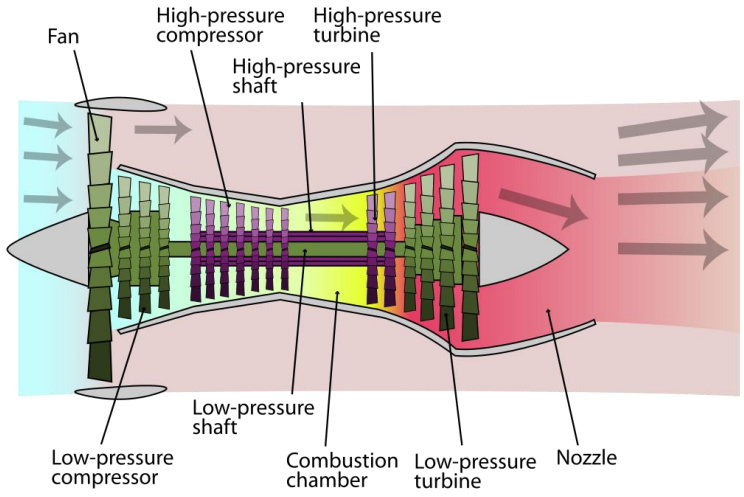

Figure 2, high by-pass ratio turbofan – picture by K. Aainsqatsi, CC BY 2.5 [2]

1.3.

Passive noise control in jet engines; Acoustic liner

The installation of acoustic treatments at the wall of the flow passages (i.e. intake, bypass and exhaust) in modern turbofans is a consolidated design strategy to keep the acoustic signature within specific requirements. Conventionally, liners convert the acoustic energy to turbulent motions of flow, therefore the acoustic energy is dissipated by viscous effects during the flow oscillations through the cavities of the liner. Helmholtz resonator has the maximum sound dissipation at its resonance frequency. Several liner configurations are normally considered to damp both broadband

and tonal noise components, including locally and non-locally reacting panels. The simplest and traditionally most investigated configuration is the single layer or single degree of freedom (SDOF) treatment, consisting in a porous face-sheet joined on top of a honeycomb core that is fixed to a rigid back-plate. Different types of liner can be installed on the different parts of the engine.

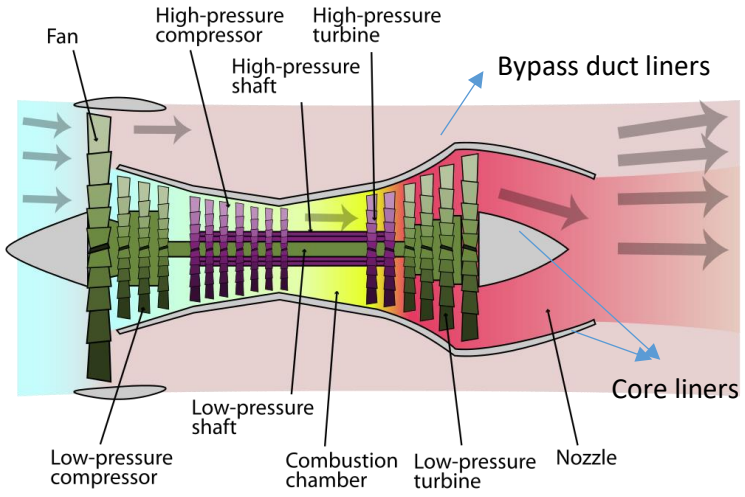

Figure 3, Acoustic liner installation on the inner wall of the jet engine, Low-pressure turbine

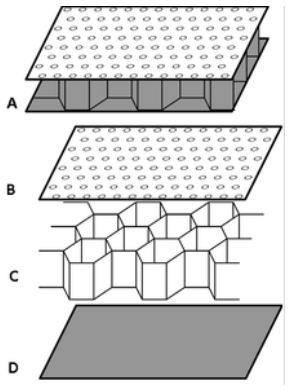

Figure 4, typical structure of an acoustic liner

The acoustic performance of a liner is obviously dependent on its geometry that should be optimized to find out the best acoustic performance. Furthermore, the interaction of the porous surface with the air flow plays a key role in the liner effectiveness and the effect of the flow should be carefully addressed too [3]–[7].

Thanks to the computational aero-acoustic tools (CAA), numerous studies has been carried out for better understanding the acoustic liner mechanism and useful indications have been achieved, however the experimental investigations are fundamental to gain the physical insights and have a supporting material to validate the CAA. There are different experimental methods to evaluate the acoustic liner performance, ranging from simple no-flow tests to more complex and representative setups.

Experimental methods for acoustic liner investigations

Acoustic performance of a liner is characterized by its impedance $Z(\vec{x};\omega)$. Experimentally, there are different ways to determine the acoustic impedance of a liner. In each method specific assumptions are taken into account to model the physics and the most important one, which simplifies the determination of the liner impedance, is that in each method the liner is considered as locally-reacting.

1.4.1. Standing wave tube

The experimental bench consists of a tube, an axially moving probe, a signal generator and the test article that is installed at the end of the tube. Plane wave propagation is applied. The method is basically developed on the relationship between the standing wave characteristics and the impedance of the test article. The probe can move inside the tube so it can be used to measure the acoustic pressure at different positions. The absorption coefficient is calculated by measuring the ratio of maximum and minimum sound pressure level inside the tube [8], [9].

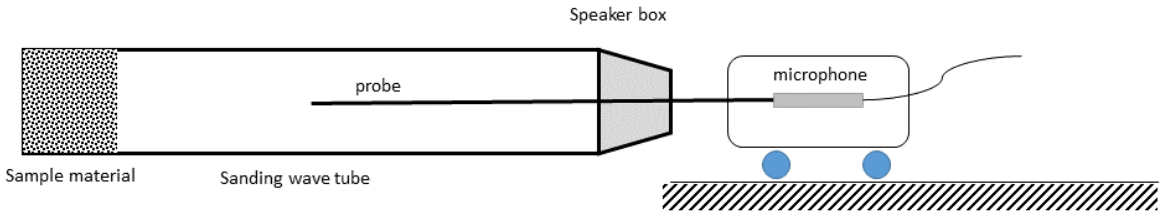

Figure 5, schematic of standing wave tube method for acoustic liner impedance investigations [9]

1.4.2. Kundt's tube (Two microphones method)

The normal incidence impedance of a sample can be measured with a so-called Kundt's tube which is based on the two-microphones method [10] and it is widely used as a standard for impedance measurement. With reference to the scheme shown in Figure 6, the method relies on the determination of the normal acoustic impedance from the reflection coefficient which is estimated through the measurement of a transfer function by means of two microphones which are installed on the tube wall. It is the most commonly used technique for determining the impedance of the acoustic liner but it does not consider the presence of a mean flow.

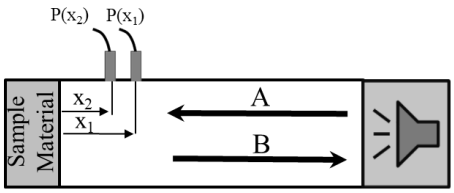

Figure 6, two-microphone method [10]

1.4.3. Impedance direct measurement; PU-probe

Another technique that gives the value of the impedance at the surface of a test sample is to measure directly the acoustic pressure and the particle velocity at the sample surface in any desired location.

This method employs the so-called PU-probe. The probe is installed directly on the test sample and the impedance is obtained by measuring the local pressure and velocity at the same time. The method is successfully used for the no flow condition but it is not completely applicable for the condition with grazing flow [11].

1.4.4. Grazing flew test rigs

All the techniques that are mentioned above are suitable for determining the liner impedance but none of them can be used for measuring the impedance at the presence of the flow on the liner surface. As the flow effect on the liner impedance is considerable, a test facility able to provide a well-known grazing flow on the liner surface is required. One of the first bench to fulfil this was developed by NASA [12]. In the test rig, basically, an acoustic tube is used in which one of the walls is holding a flush mounted liner while the other one is holding an array of microphones. In this way the pressure field is measured by microphones in the opposite wall of the liner (in the first attempt, a moveable microphone was used to measure the pressure at different positions). Loudspeakers are used to generate the excitation signal inside the tube. The test rig was limited to the plane wave regime as at higher order modes the error magnitude rises considerably. An anechoic termination is installed at the downstream end of the tube to avoid sound wave reflections. The impedance of the liner in such a system is achieved through an indirect measurement and by deploying a so-called impedance eduction method to determine the impedance of the liner. Desired aerodynamic conditions inside the tube can be provided to reproduce the actual liner working conditions.
In last decades, a significant number of similar test benches were developed. Hereafter, some of the remarkable working test rigs will be introduced and their features will be pointed out.

1.4.4.1. State of the art of grazing flow rigs for acoustic liners investigations

Several grazing flow rigs have been realized during the last decades and the realization of novel facilities with increasingly representative envelopes and even more sophisticated and reliable measurement techniques is still a topic of interest. Following, up to the best of the author knowledge, some of the most noticeable grazing flow test rigs are reviewed.
The GIT-TB (Grazing flow Impedance Tube Transverse Bar) has a square cross-section of 50.8 * 50.8 cm and a liner with a 50.8 cm width and a 406.4 cm length can be installed. The liner is placed in the middle of the test section. The acoustic field inside the duct is provided by four 120W speakers that can generate discrete signals from 0.5 to 3 kHz with a maximum sound pressure level (SPL) of 130 dB. The acoustic field enters the tube which has an anechoic termination at its end. Two ¼”

condenser microphones are used for acoustic measurement. One is installed in the region upstream the liner, close to it, while the other one is placed on the wall opposite to the liner in a traversing system. The rig is suitable to work at room temperature and Mach number up to 0.5 [13], [14].

The GIT-M95, as it can be seen also from the name, has the same structure of the GIT-TB except that instead of the Traversing Bar (TB), 95 microphones are used for acoustic measurements. This modification was made to ease the testing as it was very time consuming to make test with a traversing microphone for different flow conditions at different frequencies. So that, the large number of microphones can help to faster the tests. Furthermore, using a traversing bar can cause some leakage that can disturb the flow. GIT-TB was limited to work under plane wave excitation, while the GIT-M95 is capable to capture also the higher order wave modes thanks to the large number of microphones. Further, two ring arrays of four microphones each were installed at the upstream and downstream boundaries of the liner section for modal decomposition purposes. Such measurement setup allowed the analysis of higher order modes up to 10 kHz [14].

The Grazing Flow Impedance Tube (GFIT) is another facility that is used by NASA for acoustic liner evaluations. The rig consists of an upstream nearly anechoic settling chamber, acoustic drivers, a test section and a downstream anechoic termination. The test rig has a modular design, so different configurations are easily installed for providing different rig configurations. The test section has a rectangular cross-section area, 2.0 by 2.5 inches and the acoustic liner has a maximum length of 24 inches. The chosen cross-section area allows the propagation of higher order modes in horizontal and vertical directions. 95 flush-mounted condenser microphones are used. The high number of microphones allows the evaluation of the impedance within the frequency range from 0.4 to 3.0 kHz. The maximum mean flow velocity at the test section is Mach 0.6 and the rig works at ambient pressure and temperature. The test section is placed at the farthest position in the downstream side of the wave guide to have a fully developed boundary layer. The acoustic field is generated through 18 acoustic drivers (120W each), which allow a remarkable SPL up to 160 dB [15], [16].

The Curved Duct Test Rig (CDTR) is placed at NASA Langley Research Center and its dimensions are quite representative of the actual engine ones (up to 50% of the bypass duct size). The rig can be fed by high speed mean flow up to Mach 0.3 (later is modified to support the flow up to Mach 0.5) and the sound generation is controlled to guarantee both magnitude and modal distribution. The rig is mainly designed to study the effect of the curvature on the liner performance as it can be found in the actual turbofan engines. The duct has a cross-section of 0.762*0.762 m and the test section 0.152*0.381. The microphones are placed at both upstream and downstream sides of the liner section to measure the acoustic field evolution across the treatment. Each array of microphones consists of 31 piezo-ceramic sensors, flush-mounted with the duct inner wall. The signal quality is improved by

a proper signal conditioning system. 16 loudspeakers generate the desired sound field. Amplifiers are used to increase the sound pressure level and it is expected to generate also higher order modes, up to mode number 2 in the shorter side and number 5 in the longer side of the duct [17]–[19].

A square cross-sectioned duct (DUCT-S, DUct aCoustic Test rig with Square cross section) with grazing flow testing capability was installed at German Aerospace Center (DLR) and equipped with two anechoic terminations at both sides to minimize the end reflections. The duct cross-section is 80 mm * 80 mm and the flow can reach Mach 0.3. A liner sample with a maximum length of 220mm could be inserted at the middle of the test section. A set of 5 microphones is installed at each side of the liner section in an axial exponentially distributed arrangement. The pressure field was recorded using flush mounted ¼ inch condenser microphones. Furthermore, some slots are foreseen opposite to the liner and a ring of six microphones is located at both liner sides. High sensitivity loudspeakers at both ends are installed via a horn to generate the signal. The measurements can be performed under the plane wave regime up to 2110 Hz [20]–[22].

The DUCT-R (DUct aCoustic Test rig with Rectangular cross section) instead has a 60 mm * 80 mm rectangular cross-section and it is an upgraded version of the DUCT-S with some improvements and a liner length up to 800 mm. A radial compressor is employed to provide the flow inside the test section and Mach 0.3 is achieved at the liner section. 106 microphones and two sets of loudspeakers are mounted at the two sides of the test section. The microphones are mounted in 16 ring arrays and each array consists of 6 microphones. The arrays are placed by using an exponential positioning rule. 1/4” condenser microphones were used for acoustic data collection. An arbitrary frequency generator with amplifier was used to produce the testing signal. In addition, temperature probes were used upstream and downstream the liner section for the sound speed determination [21].

A hot-stream test facility [23], [24] has been designed and commissioned at the National Aerospace Laboratory (NLR, the Netherlands). The rig consists of a compressor, combustion chamber, a contraction, a rectangular duct of 1.2 m length with an exit nozzle that has a cross section dimensions of 0.15 x 0.05 m. The hot gases flow into a collector, with the 1.2 m diameter and then to an exhaust system. The duct has a modular design with a 300 mm long source section, a liner test section with two boxes (400 mm), two measurement sections upstream and downstream of the liner section (2 x 140 mm) for acoustic and aerodynamic data collection and an exit nozzle (100 mm). Acoustic drivers are connected to the source section by means of two air-cooled horns. In-situ acoustic impedance measurements are applied in the liner test panels which are located at the side-wall of the test section. Acoustic impedance and insertion loss measurements can be measured within the frequency range from 1.0 to 6.0 kHz with an overall SPL of 142 dB. The maximum feeding temperature for flow Mach

number 0.35 is 500 °C while for Mach 0.4 is 440 °C. Air-cooled sensors were used for acoustic data measurements.

Another hot-flow test facility, the Hot-Acoustic-Testing rig (HAT), was constructed in Berlin to experimentally investigate the acoustic performances of liners at high temperature flow conditions [25], [26]. The rig allows a high accuracy measurement at nearly realistic engine conditions up to Mach 0.7. The rig can provide a high temperature (up to 550 °C) and pressure (up to 11 bar absolute) condition. The acoustic measurement is done by means of microphone probes which are mounted at both sides of the test sample section. The probe microphones are designed to protect the microphone from damages due to the working high temperature condition. The probe microphones are positioned at ten points in the axial direction upstream and downstream the liner section. The circular cross-section of the tube has a diameter of 70 mm and a total length of about 5.4 meter. The total rig is insulated with a custom tailored two-layer insulation material. The test section is placed between two anechoic terminations. The acoustic excitation through the air-cooled loudspeakers is from 160 to 2800 Hz for the plane wave regime. Several temperature and static pressure taps are used in different positions at upstream and downstream sides of the liner section for monitoring the aerodynamic quantities.

The B2A test bench at ONERA has a 50 mm * 50 mm cross section, and it is made of stainless steel. The total length is about 4 m and the test section is equipped with two windows made of silica for optical access. The anechoic termination at the end of the tube lets the reflection coefficient not to be more than 0.2 for frequencies higher than 500 Hz. The highest temperature and Mach numbers are 300 °C and 0.3, respectively. Acoustic drivers at the upstream side of the wave guide can provide tones at up to 140 dB within the frequency range 0.3 – 3.5 kHz. Sixteen microphones are installed on the wall in front of the test article to monitor the pressure field. Flush mounted microphone probes with 1.2 mm diameter are used. For the impedance eduction, a moving probe is considered which can scan along all the microphone locations [27]–[29].

An experimental facility was built by Le Mans University with the aim of testing the acoustic liners at high flow speed (up to 0.6 Mach) and under the multi-modal acoustic field of large amplitudes [30]. Attention has been paid to have the higher order modes under control during the generation process. The main duct where the test sample is installed has a rectangular cross-section of 280 mm * 150 mm. Another design requirement was to have a sufficiently high SPL for each mode at the frequency range 0.3 - 5 kHz. To achieve this, the rig is equipped with two sets of acoustic sources at both liner sides: loudspeakers for low frequency excitation and compression chambers for mid and high frequency ranges. 24 loudspeakers and 60 compression chambers in total were installed on the rig to generate the desired acoustic field with enough SPL.

Recently, a new experimental test apparatus referred as the Heated, Optimized Tube for Multimodal Evaluation of Sound Scattering (HOTMESS) recently was introduced at the Georgia Tech Research Institute to measure the acoustic reflections and transmission properties of a test sample with mean flow at high temperature, high amplitude, and higher-order mode propagation situation. The rig can reproduce low subsonic flow rate, temperature at the test article up to 260 °C, high sound pressure level up to 160 dB and higher-order modes propagation for both circumferential and radial modes. Test rig is a two-side circular wave guide which is mainly composed of a heater, sound sources at upstream and downstream, measurement sections at upstream and downstream test article. The test rig has a modular construction for enabling future modifications. The inner diameter of the tube is 101.6 mm and thickness of 6.35 mm. The heater temperature can be set up to 650 °C and it is controlled by its own PID controller. To enable the higher order modes excitation, 32 compression drivers are used, 16 at the upstream and 16 at the downstream section of the test bench. The acoustic drivers are mounted in four sets around the circumference via a finned tube for keeping the temperature low nearby the drivers. 16 sensors are mounted at each side of the test article. For the cold condition, piezoelectric sensors are used to measure the acoustic pressure, however for hot working condition dynamic pressure transducer with a water-cooled adapter were used. The reason to use the microphone in the cold condition is the lower floor noise as it has a higher sensitivity with respect to the dynamic pressure transducer. The position of the sound sources and sound recording points were optimized for having the best configuration [31], [32].

1.5. Motivation of the work and thesis outline

1.5.1. Motivation of the activity

The use of acoustic liner for noise reduction purposes is a well-known strategy and a large number of studies are being done to investigate deeply its performance. Experimental studies must be considered as well as analytical and numerical models for acoustic liner research. Although different test facilities are available at the moment, each one with a given envelope and measurement capabilities, the development of a test rig able to reproduce operating conditions representative of the engine exhaust could be still of a great importance and interest. Surfing on the literature and up to the author knowledge, there is a lack of sufficient studies on the acoustic liners' assessment under hot working condition and high sub-sonic Mach numbers, representing the LPT exhaust features. The main challenge would be from the aerodynamic point of view and even more effort would be required to develop an acoustic measurement system at such high temperature conditions. UniFi test rig target is to provide a hot temperature flow up to 450 °C with a Mach number up to 0.5 and investigate acoustic

sources up to 7 kHz. A significant effort is required to design and construct the rig in order to meet at the same time the acoustic, aerodynamic and structural requirements, and to establish a reliable and accurate method to analyze the measured data. Furthermore, a set of aerodynamic and acoustic instrumentations are foreseen to properly measure all relevant quantities in a wide range of working conditions.

1.5.2. Thesis outline

The aim of this thesis is to illustrate the design approach and logic followed in the construction of UniFi grazing flow test rig. In the first part, an introduction is given about the noise emission issues in the jet engines and the benefits of using acoustic liners as passive noise control devices at the engine wall. A review was carried out on the existing solutions for acoustic liner investigations at different conditions.

In the second section, a description of the theory underlying the UniFi test bench is reported. Duct acoustics, with a major focus on rectangular duct, is the main theoretical background for the rig modeling. The characteristics of the acoustic liner (impedance as the objective parameter) are also explained to some extent. A brief explanation of the measurement technique that is employed for acoustic pressure is put in this section as well.

In the third section, where the most focus of the thesis is on, the UniFi rig logic is described and the design of the overall rig and the features of its main components are illustrated in detail from a thermo-structural and acoustic point of view. This section includes the design parameters and the adopted design solutions. Finite Element Analysis (FEA) software is used to analyze the components under the most challenging test condition and the model results are brought in detail. The employed instrumentations for aerodynamic and acoustic characterization are introduced and the adopted solution for acoustic measurements at high temperature is presented.

A preliminary commissioning of the rig was carried out and the main evidences are shown in the fourth section. These results contain the aerodynamic description of the rig inlet and some acoustic results proving the eligibility of the rig for the acoustic liner investigation purposes. The activity is still ongoing, however the main stage of the project focused on the design and manufacturing, is finished.

Chapter 2

Methodology

Theory of wave propagation in a stationary and moving medium

2.1.1. Plane wave propagation inside a duct with an inviscid stationary medium

2.

2.1.

A straight duct with circular or rectangular cross-sections is usually used as a wave guide to study the acoustic liners. Since UniFi test rig has a rectangular cross-section, the theoretical part of this thesis is focused on the acoustics within rectangular ducts.

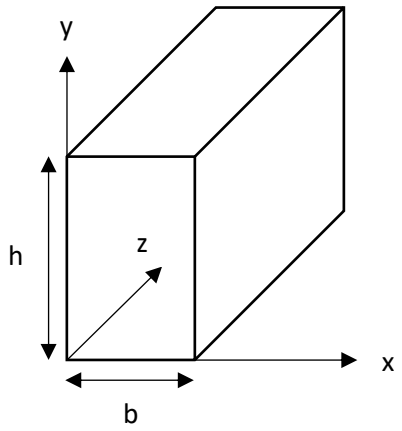

Figure 7, rectangular duct cross-section as the wave guide [33]

In the ideal condition with a small enough duct cross section area and stationary non-viscous fluid, small-amplitude waves travel as plane waves. Acoustic pressure perturbation p as well as particle velocity u at all points of any surface normal to the waves' propagation direction are the same. The phase surface (the surface in which p and u have the same amplitude and phase) is a plane normal to the propagation direction which is the duct longitudinal axis.

Considering the small perturbances hypothesis, the linearized equations for mass continuity, dynamical equilibrium (momentum equation) and energy equation (isentropicity) are given below:

$$\rho_0 \frac{\partial u}{\partial z} + \frac{\partial \rho}{\partial t} = 0 \qquad \text{eq. 2–1}$$

$$\rho_0 \frac{\partial u}{\partial t} + \frac{\partial p}{\partial z} = 0 \qquad \text{eq. 2–2}$$

$$\left(\frac{\partial p}{\partial \rho}\right)_s = \frac{\gamma(p_0 + p)}{\rho_0 + \rho} \cong \frac{\gamma p_0}{\rho_0} \qquad \textit{eq. 2–3}$$

A linear, one-dimensional, space and time dependent equation satisfying all the mentioned relations is the classical wave equation:

$$\left[\frac{\partial^2}{\partial t^2} - a_0^2 \frac{\partial}{\partial z^2}\right] p = 0 \qquad \textit{eq. 2–4}$$

Which admits the following general solution:

$$p(z,t) = C_1 f(z - a_0 t) + C_2 g(z + a_0 t) \qquad \textit{eq. 2–5}$$

Where $\rho = \frac{p}{a_0^2}$; $\frac{\partial \rho}{\partial t} = \frac{1}{a_0^2}\frac{\partial p}{\partial t}$; $\frac{\partial p}{\partial z} = \frac{1}{a_0^2}\frac{\partial p}{\partial z}$ *eq. 2–6*

And *z* is the axial coordinate and p_0 and ρ_0 are, respectively, the mean pressure and density which are assumed to be uniform, and *s* is the entropy.

a_0 is the speed of sound which, for the approximations considered here, is independent of *z* and *t*.

By application of Fourier transform, the solution becomes

$$p(z,t) = C_1 e^{j\omega\left(t - z/a_0\right)} + C_2 e^{j\omega\left(t + z/a_0\right)} \qquad \textit{eq. 2–7}$$

Where the time dependent part is assumed to be in the $e^{j\omega t}$ form. Looking carefully at the general solution one can consider that, the first part represents the forward going wave with constant amplitude C_1 traveling at constant speed a_0, and the second part is the backward moving wave with the constant amplitude C_2 and speed a_0.

The free field wave number is defined as:

$$k = \frac{\omega}{a_0} = \frac{2\pi}{\lambda} \qquad \textit{eq. 2–8}$$

Where *k* is the wave number and λ is the wavelength, so the acoustic pressure can be written as:

$$p(z,t) = \left[C_1 e^{-jkz} + C_2 e^{+jkz}\right] e^{j\omega t} \qquad \textit{eq. 2–9}$$

The acoustic pressure is linked to particle velocity through the linearized momentum equation and it is derived as:

$$u(z,t) = 1/Z_0\left[C_1 e^{-jkz} - C_2 e^{+jkz}\right]e^{j\omega t} \qquad \textit{eq. 2–10}$$

$Z_0 = \rho_0 a_0$ is the so-called characteristic impedance of the medium and it is given by the ratio of acoustic pressure to the particle velocity for a progressive wave without reflections.

2.1.2. 3-D wave propagation inside a duct with an inviscid stationary medium

Moving from 1D to 3D wave propagation and considering a rectangular duct with *(x,y,z)* coordinate system with an inviscid stationary medium, the general solution for the equation becomes:

$$p(x,y,z,t) = \left(C_1 e^{-jk_z z} + C_2 e^{+jk_z z}\right)\cdot\left(e^{-jk_x x} + C_3 e^{+jk_x x}\right)\cdot\left(e^{-jk_y y} + C_4 e^{+jk_y y}\right)e^{j\omega t} \qquad \textit{eq. 2–11}$$

With the compatibility condition

$$k_x^2 + k_y^2 + k_z^2 = k_0^2 \qquad \textit{eq. 2–12}$$

Assuming rigid wall as the boundary condition we have:

$$\frac{\partial p}{\partial x} = 0 \; for \; x = 0 \; and \; x = b \qquad \textit{eq. 2–13}$$

$$\frac{\partial p}{\partial y} = 0 \; for \; y = 0 \; and \; y = h \qquad \textit{eq. 2–14}$$

So that C_3 and C_4 are determined:

$$C_3 = 1,\; k_x = \frac{m\pi}{b}, \qquad m = 0,1,2,\cdots \qquad \textit{eq. 2–15}$$

$$C_4 = 1,\; k_y = \frac{n\pi}{h}, \qquad n = 0,1,2,\cdots \qquad \textit{eq. 2–16}$$

For a duct with rigid walls with width b and height h the sound wave propagation would be

$$p(x,y,z,t) = \sum_{m=0}^{\infty}\sum_{n=0}^{\infty}\cos\frac{m\pi x}{b}\cos\frac{n\pi x}{h}\times\left(C_{1,m,n}e^{-jk_{z,m,n}z} + C_{2,m,n}e^{+jk_{z,m,n}z}\right)e^{j\omega t} \qquad \textit{eq. 2–17}$$

$m = 0,1,2,\cdots$

$n = 0,1,2,\cdots$

And the wave number $k_{z,m,n}$ for th mode (m,n) is calculated by the relation

$$k_{z,m,n}{}^2 = \left[k_0^2 - \left(\frac{m\pi}{b}\right)^2 - \left(\frac{n\pi}{h}\right)^2\right] \quad \textit{eq. 2–18}$$

Any mode (m,n) could propagate un-attenuated if

$$k_0^2 - \left(\frac{m\pi}{b}\right)^2 - \left(\frac{n\pi}{h}\right)^2 > 0 \quad \textit{eq. 2–19}$$

$$\frac{4}{\lambda^2} - \left(\frac{m}{b}\right)^2 - \left(\frac{n}{h}\right)^2 > 0 \quad \textit{eq. 2–20}$$

$$\lambda < \frac{2}{\left\{\left(\frac{m}{b}\right)^2 + \left(\frac{n}{h}\right)^2\right\}^{1/2}} \quad \textit{eq. 2–21}$$

Consider $h > b$, mode (0,1), as the first higher order mode, would propagate if

$$\lambda < 2h \quad \textit{eq. 2–22}$$

$$f < \frac{a_0}{2h} \quad \textit{eq. 2–23}$$

h is the bigger side of the duct cross-section.

In rectangular duct, the transverse nodes in the transverse pressure distribution are represented by m and n. Figure 8 shows the nodal lines in a rectangular ducts up to m=2 and n=2.

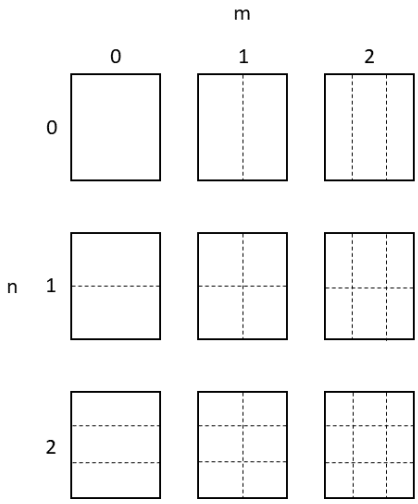

Figure 8, Transverse pressure distribution nodal lines for in a rectangular duct [33]

2.1.3. Plane wave propagation inside a duct with an inviscid moving medium with a uniform velocity U

When the fluid is not stationary and is moving with a constant uniform velocity *U*, the propagation speed for the forward going and backward going waves are respectively $a_0 + U$ and $a_0 - U$ from a static observer point of view. It has to be noted that the gradient of *U* in the *r* and *z* direction is negligible, and the one-dimensional equation becomes:

$$p(z,t) = \left(C_1 e^{j\omega/(a_0+U)z} + C_2 e^{j\omega/(a_0-U)z}\right) \cdot e^{j\omega t} = \left(C_1 e^{-jk_0 z/(1+M)} + C_2 e^{+jk_0 z/(1-M)}\right) \cdot e^{j\omega t} \quad \text{eq. 2–24}$$

2.1.4. 3D wave propagation inside a duct with an inviscid moving medium with a uniform velocity U

In the presence of mean flow, which is constant in space and time, for a rectangular duct the equation becomes:

$$p(x,y,z,t) = \sum_{m=0}^{\infty}\sum_{n=0}^{\infty} \cos\frac{m\pi x}{b}\cos\frac{n\pi y}{h} \times \left(C_{1,m,n} e^{-jk^{+}_{z,m,n}z} + C_{2,m,n} e^{+jk^{-}_{z,m,n}z}\right) e^{j\omega t} \quad \text{eq. 2–25}$$

Where *M* is the flow Mach number inside the duct.

And

$$k_{z,m,n}^2 + \left(\frac{m\pi}{b}\right)^2 + \left(\frac{n\pi}{h}\right)^2 = \left(k_0 + Mk_{z,m,n}\right)^2 \qquad \text{eq. 2–26}$$

$$k_{z,m,n}^{\pm} = \frac{\mp Mk_0 + \left[k_0^2 - (1-M^2)\left\{\left(\frac{m\pi}{b}\right)^2 + \left(\frac{n\pi}{h}\right)^2\right\}\right]^{1/2}}{1-M^2} \qquad \text{eq. 2–27}$$

Thus, for higher order modes *m,n > 0* the propagation would take place un-attenuated if

$$k_0^2 - (1-M^2)\left\{\left(\frac{m\pi}{b}\right)^2 + \left(\frac{n\pi}{h}\right)^2\right\} \geq 0 \qquad \text{eq. 2–28}$$

In other words, if the frequency is small enough only plane wave would propagate. eq. 2–28 can be written in terms of wavelength or frequency limits as follows:

$$\lambda > \frac{2h}{(1-M^2)^{1/2}} \qquad \text{eq. 2–29}$$

$$f < \frac{a_0}{2h}(1-M^2)^{1/2} \qquad \text{eq. 2–30}$$

Where h is the larger of two side dimensions of the rectangular duct. Apparently, the cut-off frequency for each mode is lower than that in the no-flow (stationary-medium) condition. Another point to be mentioned is that the cut-off frequency for the downstream wave is the same as for upstream going wave.

2.1.5. Wave propagation in a non-uniform moving medium

So far, uniform flow was considered in this essay. However, the effect of shear flow should be considered as it plays an important role in the acoustic liner performance. The non-uniform flow effects was analyzed first by Pridmore-Brown, The model covers a fairly wide range of velocity profiles [34].

$$\frac{1}{c^2}\frac{\partial^2 p}{\partial t^2} = (1-M^2)\frac{\partial^2 p}{\partial x^2} + \frac{\partial^2 p}{\partial y^2} - \frac{2M}{c}\frac{\partial^2 p}{\partial x \partial t} + 2\rho_0 c\frac{\partial M}{\partial y}\frac{\partial v}{\partial x} \qquad \text{eq. 2–31}$$

$$a_0 = c$$

Later the Pridmore-Brown equation was extended in order to consider also the viscous effects [35].

2.2. Impedance boundary condition

In the previous section, it was assumed a hard wall boundary condition at the duct wall. As the duct with lined wall is of interest here, the impedance wall condition is discussed. The normal impedance of a wall expresses the dynamical behavior of the surface under the action of an incident acoustic wave. The surface can be considered as locally or non-locally reacting. In the first case its behavior depends only on the specific point where the wave-surface interaction takes place and not on the motion of the other parts of the surface, while in the second case the motion at one point depends on the motion of all the points of the surface. In case of traditional acoustic liners, they could be considered as locally reacting since, as it will be described more in detail in the next paragraph, they are usually built up by a honeycomb structure with separated cells for which the acoustic motion on each cell is independent from the acoustic motion on the surrounding ones. The wall with a normal impedance Z_ω could be considered as a boundary condition and the wave equation shall be solved accounting for the corresponding impedance value at any wall. In case of locally reacting lined wall, stationary medium and no viscous effects, the impedance is constant, Z_ω. The mean flow can considerably affect the wall impedance as well as the wave propagation. In case of mean flow, the wall impedance should be assumed as a function of the flow Mach number [33].

The $b \times h$ duct with the lined walls should satisfy the boundary conditions below:

$$\frac{p(0,y,z,t)}{-u_x(0,y,z,t)} = \frac{p(b,y,z,t)}{u_x(b,y,z,t)} = Z_{\omega x} \qquad \text{eq. 2–32}$$

$$\frac{p(x,0,z,t)}{-u_y(x,0,z,t)} = \frac{p(x,h,z,t)}{u_y(x,h,z,t)} = Z_{\omega y} \qquad \text{eq. 2–33}$$

Where Z_ω could be a function of M, $Z_\omega = Z(M)$.

It is worth mentioning that at the presence of flow, the boundary condition for the lined wall could be affected by the boundary layer refraction effects. Although for the hard-wall these effects are neglected, for lined wall it should be considered for a better prediction of the liner impedance. The boundary layer effect was modeled first by Ingard [36] and then the model was improved by Myers [37]. The so-called Ingard-Myers boundary condition was formulated and investigated more deeply by other authors [38]–[40].

Acoustic liner working principle

2.3.1. Structure

The traditional acoustic liner is normally composed of a honeycomb core which is placed in between a perforated sheet and a rigid back plate. Roughly speaking, it is nothing but a series of Helmholtz resonators, that are assembled together on a single plate [26] [4]. The acoustic treatments are passive noise control devices and could be locally or non-locally reacting. In locally reacting case each cell performs independently from the other cells and it is independent from the imposed acoustic field [3]–[5], [41], [42]. Mainly the acoustic impedance of a single layer liner depends on the geometry of the cell i.e. the hole diameter, cell depth, perforated sheet thickness and porosity of the perforated plate.

2.3.

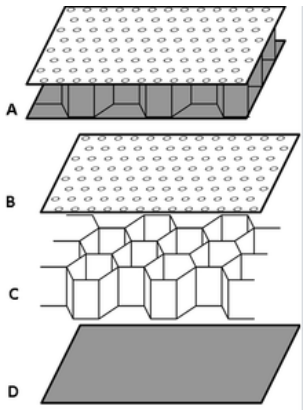

Figure 9, Single degree of freedom acoustic liner

If the liner is composed of a single layer honeycomb, it is called single-degree-of-freedom (SDOF). Other kinds of absorbers have been developed, such as the DDOF (Double-Degree-of-Freedom) or MDOF (Multiple-Degree-of-Freedom).

2.3.2. Acoustic liner impedance

The effectiveness of the acoustic liner is assessed through the acoustic impedance, defined as the ratio between the acoustic pressure and the particle velocity.

Using the Fourier transform it can be expressed as:

$$Z(\vec{x};\omega) = \frac{p(\vec{x};\omega)}{\vec{u}(\vec{x};\omega)\cdot\overline{n_s(\vec{x})}} \qquad \text{eq. 2–34}$$

At a position *x* of the surface *s* with *n* as the normal vector.

The impedance is a complex number and is a function of frequency ω and position x. The real part is the resistance, the imaginary part is the reactance, and its inverse 1/Z is called admittance. The impedance in general cannot be a function of the surface alone because it also depends on the incoming acoustic field; however, the impedance can be actually considered to be dependent only on the surface properties if it is locally reacting.

The specific acoustic impedance can be defined as the ratio between the acoustic impedance and the characteristic impedance of the medium: $Z/\rho_0 c_0$.

The acoustic impedance of a locally-reacting liner in the low frequency band can be explained by a mechanical analogy. For a single Helmholtz resonator, the equivalent mechanical mass-spring-damper system is shown as reported in Figure 10:

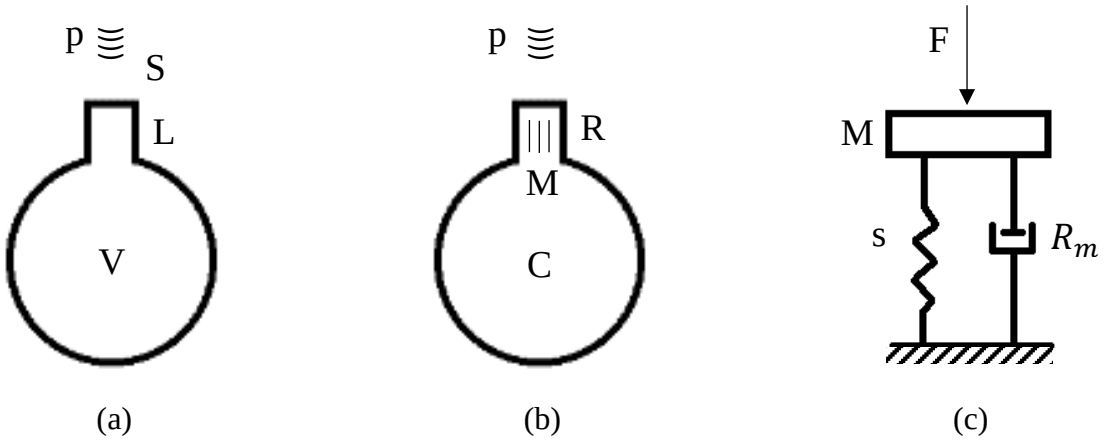

Figure 10 (a) single Helmholtz resonator, (b) equivalent acoustic parameters, (c) equivalent mechanical system

Mathematically, for a mechanical system with a given mass M, a spring with stiffness s and a damping effect R_m, which is accelerated by a sinusoidal force F, the impedance is defined as a complex number:

$$Z = R_m + i\,X_m \qquad \textit{eq. 2–35}$$

In which *Rm* is the resistance and *Xm* is the reactance. X_m is obtained as

$$X_m = \omega_m - (^{s}/_{\omega}) \qquad \textit{eq. 2–36}$$

The same analogy could be considered for the Helmholtz resonator to obtain the acoustic impedance. Consider a single Helmholtz resonator with a rigid-walled cavity with volume V and neck length L and area S. The mass element in this case is the fluid within the neck, which oscillates due to the forcing term. The imposed acoustic pressure in the cavity causes the stiffness element effect because of the compressibility. The dissipation happens because of the radiation effects at the opening as well as the viscous effects due to the very small neck area, however the later one is neglected in this analysis as it is less than the radiation effects. By equalizing the main 3 elements of the mass-spring-damper mechanical system to the ones of the Helmholtz resonator, the mechanical impedance parameters of a Helmholtz resonator can be achieved as follows:

$m = \rho_0 s l'$	l' effective length of the neck	*eq. 2–37*
$s = \rho_0 C^2 \frac{S^2}{V}$	s effective stiffness of the Helmholtz resonator	*eq. 2–38*
$R_r = \rho_0 C k^2 \frac{S^2}{2\pi}$	Radiation resistance (for flanged neck)	*eq. 2–39*

Finally, for the acoustic impedance Z definition, the elements could be considered as in Figure 10, in which the system is described by inertance M (m, in mechanical system), Compliance C (1/s in mechanical system) and resistance *R* (R_m in mechanical system).

$$Z_m = R_r + i(\omega_m - {}^{s}/_{\omega}) \quad \textit{eq. 2–40}$$

$$Z = R + i(\omega_m - {}^{1}/_{\omega C}) \quad \textit{eq. 2–41}$$

Where *R* is the energy dissipation component ad the second part ($\omega_m - {}^{1}/_{\omega C}$) represents the energy saving component [20], [43]–[45].

2.3.3. The extended Helmholtz resonator

In the previously mentioned theory of the Helmholtz resonator, the model is limited to the low frequency range and it is assumed that the medium in the neck moves as a solid body and additional simplifications are considered for the volume inside the cavity. A more general model is proposed by Rienstra [46] (extended Helmholtz resonator, EHR) for high-frequency applications.

$$Z(i\omega) = R_f + i\omega m - i\beta \cot(0{,}5\omega T_l - i0{,}5\varepsilon) \qquad \text{eq. 2–42}$$

Where R_f and m stand for the resistance and reactance of the face sheet respectively, the cavity reactance β , the cavity resistance parameter ε and T_l for the response time (time step) [20], [22], [46].

Acoustic measurement techniques

2.4.1. Two-microphones method

2.4.

Figure 11, shows the well-known configuration for two-microphones method. The simplest configuration is composed of an acoustic driver, two fixed microphones at defined positions and a material sample. The method could be used to assess the absorption of a material by measuring the reflection coefficient and it was proposed first by Seybert and Ross [47]. The two microphones method is a standardized method according to ISO 10534-2:1998 [10].

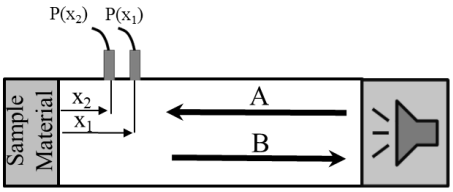

Figure 11, two-microphone method configuration

The method could be extended to more than two microphones installed in the axial direction alongside the duct i.e. multi-microphones method. Multi-microphones method yields an overdetermined system of equations and in general, the results from multi-microphones method are more accurate than that coming from the two-microphones method [48].

If there is no attenuation and considering the plane wave propagation, one can write

$$p(x,t) = p_i(x,t) + p_r(x,t) = Ae^{-ikx} + Be^{ikx} \qquad \text{eq. 2–43}$$

Where $p_i(x,t)$ and $p_r(x,t)$ are the incident and reflected wave, respectively, and A and B are the corresponding amplitudes.

For the situation reported in Figure 11, the reflection coefficient (R) is defined as

$$R = \frac{Reflected\ waves\ pressure}{Incident\ waves\ pressure} = \frac{p_B}{p_A} \quad \text{eq. 2–44}$$

And the transfer function between two microphones (H_{12}) at the positions x_1 and x_2 can be calculated as a complex ratio P2/P1:

$$H_{12} = \frac{P(x_2)}{P(x_1)} = \frac{S_{12}}{S_{11}} = \frac{S_{22}}{S_{21}} \quad \text{eq. 2–45}$$

Where S_{11} is the auto spectrum of sound pressure at position 1 and S_{12} is the cross spectrum of sound pressure at two microphone positions 1 and 2.

The transfer function could be written as below, and it is used to calculate the reflection coefficient inside the duct in both wave propagation directions

$$H_{12} = \frac{P(x_2)}{P(x_1)} = \frac{Ae^{-ikx_2} + Be^{ikx_2}}{Ae^{-ikx_1} + Be^{ikx_1}} = \frac{e^{-ikx_2} + Re^{ikx_2}}{e^{-ikx_1} + Re^{ikx_1}} \quad \text{eq. 2–46}$$

$$R = \frac{H_{12} - e^{-jk\Delta x}}{e^{jk\Delta x} - H_{12}} * e^{2jkx_1} \quad \text{eq. 2–47}$$

Where the wave number is defined as $k = {}^{\omega}/_{c}$. If there is flow inside the duct, it should be considered in the wave number calculation and the *R* becomes:

$$R = \frac{H_{12} - e^{-jk_0^+\Delta x}}{e^{jk_0^-\Delta x} - H_{12}} * e^{2j(k_0^+ - k_0^-)x_1} \quad \text{eq. 2–48}$$

$$k_0^+ = \frac{\omega}{c(1+M_0)} \ \ and \ \ k_0^- = \frac{\omega}{c(1-M_0)} \quad \text{eq. 2–49}$$

One important consideration to be done on the application of the two-microphones method is the definition of the spacing between microphones [49]. The microphones could be installed either with a fixed distance or with an exponential distribution law. Equidistant microphone spacing with a large enough number of microphones are expected to give the best results [41], [48]. However, it still needs to be pay attention to the microphone spacing. In order to reduce the analyses error the microphone positions shall respect the following general rulebe [33]:

$$x_1 - x_2 \leq \frac{a_0}{2f_{max}}(1 - M^2) \quad \text{eq. 2–50}$$

In which the flow effect is accounted for.

Another standard method used for the assessment of the acoustic absorption of a material sample e.g. the transmission loss of an acoustic liner, is described below.

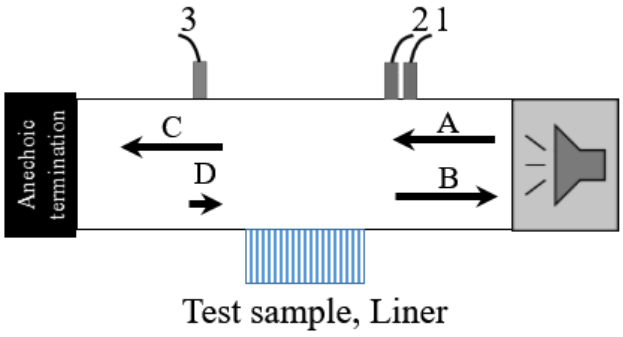

Figure 12, schematic of the method for transmission loss measurements

Figure 12 shows the simplified schematic of the test rig. There are axially mounted microphones at both sides of the acoustic liner and, at the end of the duct, an anechoic termination is foreseen to avoid undesired back reflections. To find the transmission loss at least 3 microphones are required; two in the upstream side and another one right downstream the liner section. Decomposing the wave field into its forward and backward going components leads to find the magnitude of the transmission loss due to the sample.

The transmission loss determines how much the liner can absorb the incoming sound perturbation and is defined as:

$$TL = L_{WA} - L_{WB} \qquad \text{eq. 2–51}$$

Where L_{WA} and L_{WB} are the acoustic power levels of, respectively, the incident and transmitted sound wave. If an anechoic termination is installed downstream of the test sample, the TL can be computed as:

$$TL = 20 \times log_{10} \frac{p_A}{p_C} \qquad \text{eq. 2–52}$$

If *R* is very small, then $p_d \ll p_c$ so

$$p_c = p_3 \qquad \text{eq. 2–53}$$

Hence TL can be expressed as follows:

$$TL = 20 \times log_{10} \frac{p_A}{p_3} \quad \text{eq. 2–54}$$

A random signal is excited by the speaker then the Auto-spectrum (S_{x1x1}) and the cross-spectrum (S_{x1x2}) at any x position are estimated by applying the Fourier transform to the microphone signals. Then a system of equations is set up where the unknown amplitudes will be the forward running and reflected waves [47], [50]:

$$\bar{P}_x(f,T) = \frac{1}{T}\int p(x,t)\, e^{-i\omega t} dt \quad \text{eq. 2–55}$$

$$S_{11}(f) = \left(\frac{1}{T}\right)[\bar{P}_1(f,T)\bar{P}_1^*(f,T)] = f(S_{AA}(f), S_{BB}(f), S_{AB}(f), Q_{AB}(f)) \quad \text{eq. 2–56}$$

$$S_{22}(f) = \left(\frac{1}{T}\right)[\bar{P}_2(f,T)\bar{P}_2^*(f,T)] = f(S_{AA}(f), S_{BB}(f), S_{AB}(f), Q_{AB}(f)) \quad \text{eq. 2–57}$$

$$\begin{aligned} S_{21}(f) = C_{21}(f) + iQ_{21}(f) &= \left(\frac{1}{T}\right)[\bar{P}_2(f,T)\bar{P}_1^*(f,T)] \\ &= f(S_{AA}(f), S_{BB}(f), C_{AB}(f), Q_{AB}(f)) \end{aligned} \quad \text{eq. 2–58}$$

$$\hat{S}_{33}(f) = \left(\frac{1}{T}\right)[\bar{P}_3(f,T)\bar{P}_3^*(f,T)] \quad \text{eq. 2–59}$$

Where * denotes the complex cunjugate of the complex number.

Solving the above system of equations, the magnitudes of $S_{AA}(f)$, $S_{BB}(f)$, $C_{AB}(f)$ *and* $Q_{AB}(f)$ will be obtained. It is worth mentioning that at position 4 there is very little reflecting wave component as the AT is installed at the end of the tube. The transmission loss in the frequency domain could be calculated by the formulation below:

$$TL = 10 \times log_{10} \frac{S_{AA}(f)}{S_{33}(f)} \quad \text{eq. 2–60}$$

2.5

Review of Impedance eduction methods for acoustic liner

Waveguide methods are operationally convenient for educing the liner impedance in a grazing flow environment. Waveguide methods combine experimental measurements and data reduction techniques to infer the impedance of the liner. These methodologies are referred to as impedance eduction techniques.

Different impedance eduction techniques can be categorized according to the test rig configuration they rely on. This means that the methods are classified based on some relevant rig constraints, such as the mutual position between microphones and liner. Two widely used rig configurations have been first defined by NASA and DLR. The proposed data reduction methods are described hereafter.

Mainly two different strategies can be implemented, relying on different bench configurations: iterative closed loop methods, such as LEE[1] [51]–[53], CHE[2] [51]–[53], CDTR[3] [15], and D-S[4] [22] and the straightforward methods, such as SMM[5] [51] and SFM[6] [54]–[56].

The iterative method uses a sound propagation model based upon a finite-element methodology and evaluates the liner impedance by iterating on an assumed value of test liner impedance (via a gradient based optimizer) until the predicted (from FEA) and measured wall pressures are matched along the microphone array. Here the impedance eduction method is formulated as an optimisation problem in which impedance functions are iterated upon until the finite element solution of the acoustic pressure matches the measurement within a defined error band.

[1] Linearized Euler Equations
[2] Convected Helmholtz Equation
[3] Curved Duct Test Rig
[4] DUCT with square cross section
[5] Single Mode Method
[6] Straight Forward Method

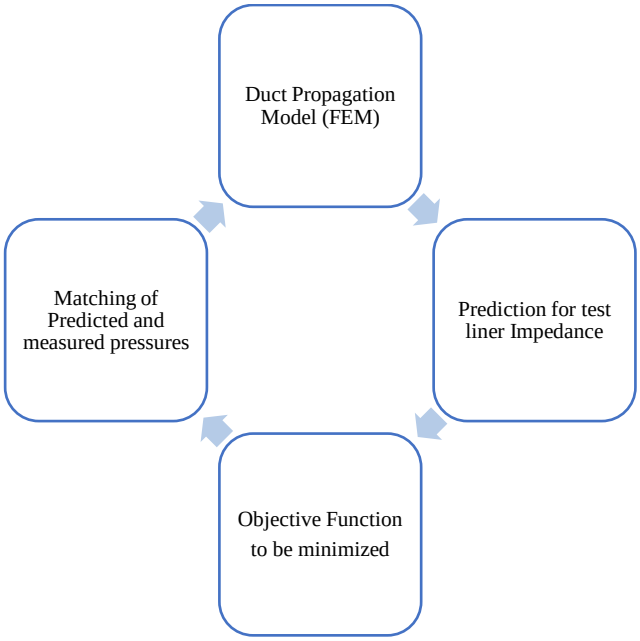

Figure 13, optimization process for acoustic impedance estimation

The straightforward methods, which are typically easy to be implemented and computationally efficient, firstly determine the axial wave numbers from measured pressure results in front of the liner, and the impedance values are obtained from the wave number and eigenvalue equation.

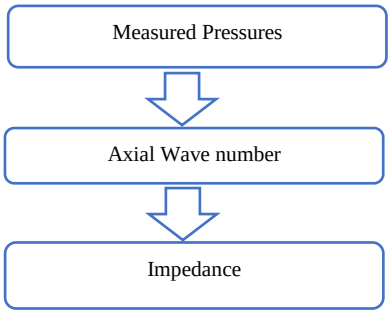

Figure 14, the steps in the straight forward method for determining the impedance

In both mentioned methods, there are some key requirements which have to be fulfilled and can be listed as below:

- Configuration of the test rig
- Positions of the microphones
- Acoustic wave excitation
- Flow characteristics inside the duct

Following these considerations, the most suitable method should be selected. The UniFi grazing flow rig has been designed to allow the application of both methodologies for impedance eduction purposes.

Chapter 3

UniFi grazing flow test rig

Conceptual design

3. As mentioned in the first section, the objective of this work is to design a grazing flow test rig aimed at evaluating the performance of the acoustic liners under test conditions representative of an aircraft engine, and specifically the turbine exhaust. To achieve this goal, a test rig operating at high flow speed and high flow temperature shall be developed. The design of such a rig, which would be the combination of a high-speed wind tunnel and an acoustic test facility, must be carefully addressed.

3.1 The typical architecture of a grazing flow rig dedicated to the measurement of the liner acoustic impedance is based on the following main components [57], [58]:

1. A flow duct
2. A test section where the liner is installed
3. A measurement system for both aerodynamic and acoustic data
4. A controlled acoustic source
5. Anechoic terminations at one or both ends of the flow duct

A schematic of a typical grazing flow rig is shown in Figure 15.

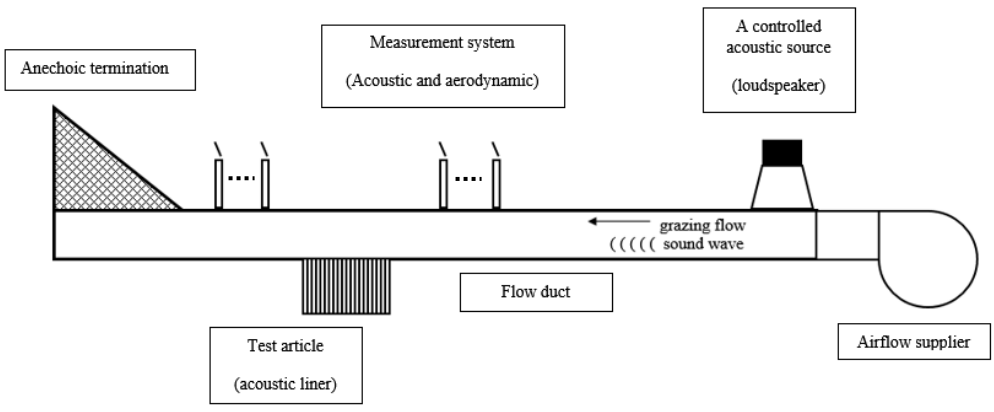

Figure 15, schematic of a typical flow duct configuration with its main components

The grazing flow tube is a hard-wall duct with a determined cross-section area. A known sound field is excited inside the duct at the presence of an air flow. The lined-wall can be installed on this tube at

a specified position and the impedance of the test-article can be estimated based on measured data (both aerodynamic and acoustic). The acoustic impedance of the liner mainly depends on the liner geometry, the flow condition inside the tube and the incoming waves. For the proposed grazing flow rig, a flow is considered to be representative of the LPT exhaust i.e. high speed and high temperature flow. The requested air flow is provided by a centrifugal fan and a plenum, followed by a nozzle, guarantees the uniformity of the flow within the test-section. A closed cycle is considered to recover the hot air within a recirculating system.

3.2. Acoustic design

The propagating acoustic field inside the tube is defined by the wave guide geometry. The duct dimensions should be selected in such a way that the plane wave regime has a sufficiently wide frequency range. This is useful to calibrate both the measurement system and the impedance eduction technique based on a well-known acoustic field (the plane wave is the only cut-on mode). Furthermore, the rig shall enable the propagation of a high number of acoustic modes with well separated cut-on frequencies, to enable the testing of absorbers with different incoming perturbations.

According to the mentioned requirements, a rectangular test section has been selected for the duct. The rectangular geometry has the advantage of imposing different cut-on frequencies for transverse modes that relate to different directions. The transverse area is small enough to guarantee a minimum extension of the plane wave regime, but not too small to allow the propagation of higher order acoustic modes within the frequency band of interest.

Figure 16 shows the nomenclature used throughout this thesis for indicating the transverse modes within a rectangular cross section.

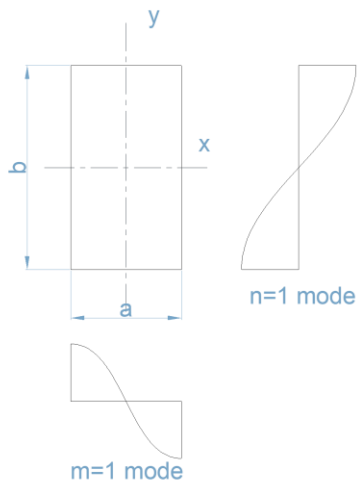

Figure 16, transverse modes in a rectangular duct

Moreover, a pronounced reduction of the test section area dramatically rises the head losses inside the test duct, and the required fan power as well. This aspect is critical especially when air flows at high Mach number and high temperature. The test section area and the aspect ratio have been chosen as the best trade-off among the plane wave range extension, the separation among cut-off frequencies of transverse modes, and head losses.

The desired operating envelope for the test rig is summarized in Table 1.

Table 1, UniFi test rig design targets

Description	**Symbol**	**Value**
Maximum flow Mach number in the test section under hot flow conditions	Ma	0.50
Maximum temperature of the flow	T [°C]	450
Maximum frequency	f [Hz]	7000
Maximum order of the cut-on (m,0) mode	m	2
Maximum order of the cut-on (0,n) mode	n	4

3.3. UniFi grazing flow test rig preliminary configuration

Considering all the aforementioned requirements a basic configuration for the test rig is identified, as in Figure 17 . The required flow is provided by a fan and fed into the test section through an inlet plenum. The flow is expanded by a final diffuser after passing the test section and, at the end, it could

be either dispatched to the environment or returned back to the fan using a dedicated circuit. Table 2 summarizes the main required components to be assembled together.

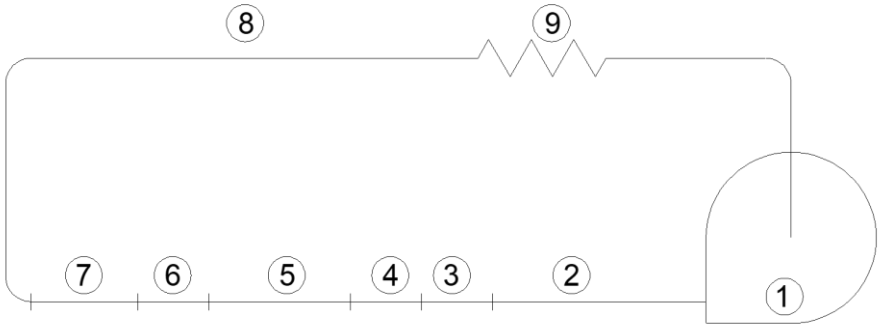

Figure 17, UniFi test rig preliminary configuration as a closed cycle

Table 2, UniFi test rig main required components

ID number	**Description**
1	Fan/Compressor
2	Inlet plenum: settling chamber
3	Inlet nozzle
4	Anechoic termination
5	Test Section
6	Anechoic termination
7	Outlet diffuser
8	Return duct
9	Heat exchanger

The main part of the rig is the duct, which is a flow tube and works as a wave guide as well. The cross-section of the duct was chosen with an aspect ratio of about 1.8, and basically it is a long duct with a fixed cross-section and includes anechoic terminations, liner section and measurement sections upstream and downstream the liner. The overall duct length is given by the summation of all these components. To have a uniform flow inside the duct, a plenum followed by a high contraction nozzle is foreseen at the beginning of the test-section. The head losses (ΔP) for the flow (with max Mach=0.5) that passes through these components can be numerically estimated. The air supply machine should be capable to recover these losses by providing a sufficient pressure ratio (PR). Based on the required pressure ratio and mass flow rate, the air supply system can be selected.

The operating conditions that are considered for the design can be mainly summarized as “cold” and “hot” working conditions as shown in Table 3.

Table 3, UniFi test rig two main operating condition

	Flow temperature (°C)	Mach	Max internal pressure (kPa)	Air density (kg/m^3)	Reynolds number (-)
Cold operation	20.0	0.50	50.0	1.20	>500000
Hot operation	450.0	0.50	25.0	0.49	>200000

All the components mentioned above should be designed respecting the general design rules to guarantee the lowest possible head losses as well as the best acoustic performance. The design of each component should also consider the thermo-structural effects which could affect the component integrity under the most challenging working conditions.

Afterwards, the overall layout of the UniFi test rig is described and details on the main rig components are provided.

3.4. UniFi grazing flow test rig overall layout

The layout of the test rig located at the University of Florence is shown in Figure 18 and Figure 19. The rig is substantially a long straight duct, acting as a wave guide, in the middle of which a liner is installed. An air flow at desired temperature and speed is generated by a fan, and a specific acoustic perturbation is produced too, by means of a dedicated loudspeakers system. When the acoustic waves reach the liner and interact with it, the acoustic field is expected to experience a reduction in its amplitude.

Figure 18, complete schematic of UniFi grazing flow test rig

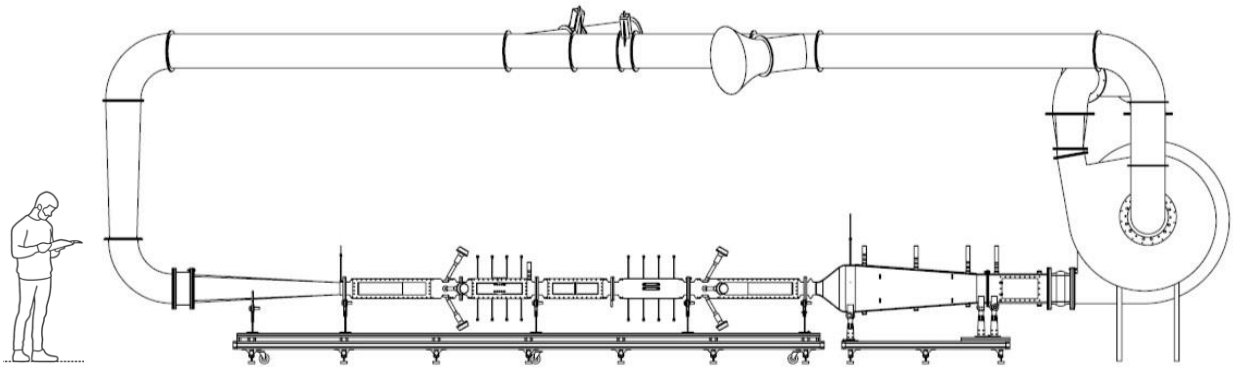

Figure 19, UniFi grazing flow test rig, side view

The incoming and outgoing pressure fields are acquired by two measurement modules composed by several flush-mounted sensors, located upstream and downstream the liner according to optimized patterns. The possibility to install the sensors in front of the liner is foreseen too. Thanks to dedicated numerical techniques, the raw acoustic signals are post-processed, and the impedance and the insertion loss can be assessed in the frequency band of interest. Furthermore, the implementation of anechoic terminations at the boundaries of the test section is foreseen, to avoid detrimental spurious back-reflections. The rig should satisfy testing conditions representative of an aircraft engine and specially the turbine exhaust. In order to achieve this goal, the rig must operate at high temperature

(up to 450°C) and Mach number (up to 0.5) and the excitation signal must cover the low as well as the high frequency band (up to 7 kHz). Following, the design of each component is described from thermo-structural and aero-acoustic points of view.

Fan

3.5.1. Fan selection

3.5. The early design stage was aimed at identifying the air-supply plant characteristic curves, and therefore the power requirements for the driving compressor. The most critical working conditions are those corresponding to the maximum temperature, hence they have been considered as the design parameters. Beside the need to withstand the high temperature of the gas, the most demanding requirement for fan design was to provide high pressure while dealing with hot air, i.e. low-density air, and relatively high flow rate.

A two-stages centrifugal fan has been selected from manufacturer's data. Figure 20 shows the non-dimensional performance curves of the fan. The parameters on the axes are, respectively:

non-dimensional mass flow: $m = \frac{\dot{m}\sqrt{T_{01}}}{p_{01}}$

Pressure ratio: $PR = \frac{p_{02}}{p_{01}}$

The parameters are scaled with the respective values at rig design point. The dash-dot curves are the constant efficiency contours.

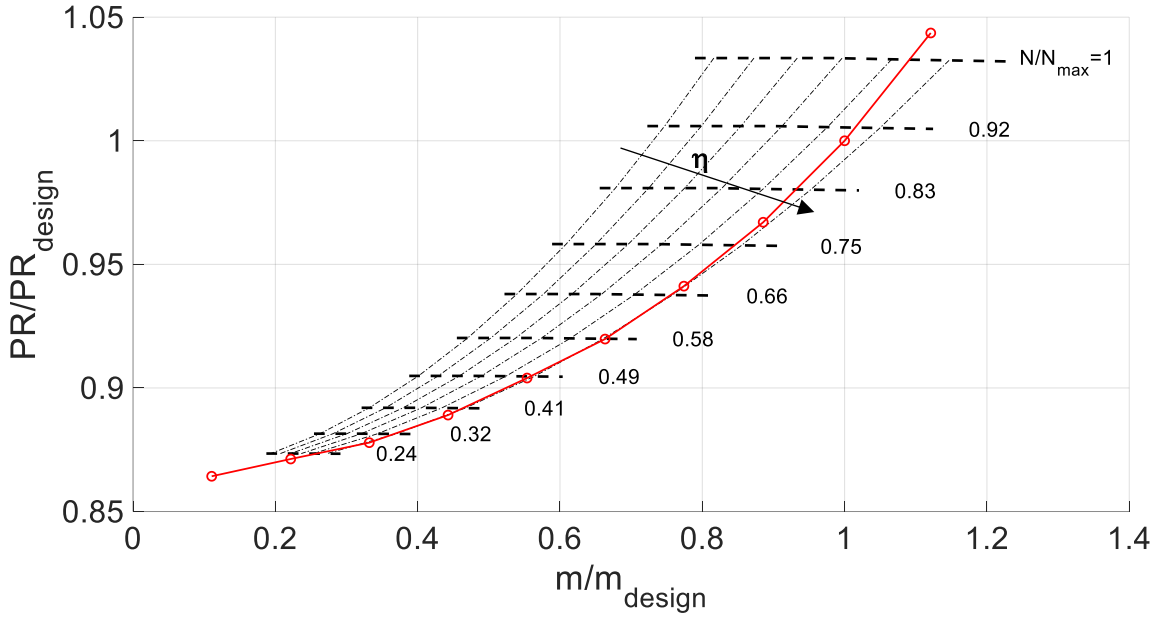

Figure 20, Fan performance curves (dashed lines) and plant characteristic curve (red line) at the maximum working temperature. Dash-dot curves are constant efficiency (η) curves, the arrow indicates the sense of increasing efficiency.

As reported in the picture, the selected fan is able to provide the required flow rate by working at nearly the highest efficiency (indicated as η) over all the expected range of testing, spanning from almost no flow up to slightly above the design conditions. The flow range is expected to be wider when working at lower temperature.

Figure 21 Fan, installed at UniFi grazing flow test rig laboratory

3.5.2. Fan commissioning

A fan commissioning activity has been performed. Both open and closed-circuit tests have been carried out to assess the performance of the fan at various inlet conditions, focusing on the capabilities of the fan at working with a low inlet flow density, representative of high temperature conditions. A performance recovery plan was needed to meet the desired specifications. Such a plan included the design and the installation of special sealing features and the modification of the second rotor geometry. After the recovery plan, the measured performance curves matched in a very satisfactory way the required ones as shown by the following picture.

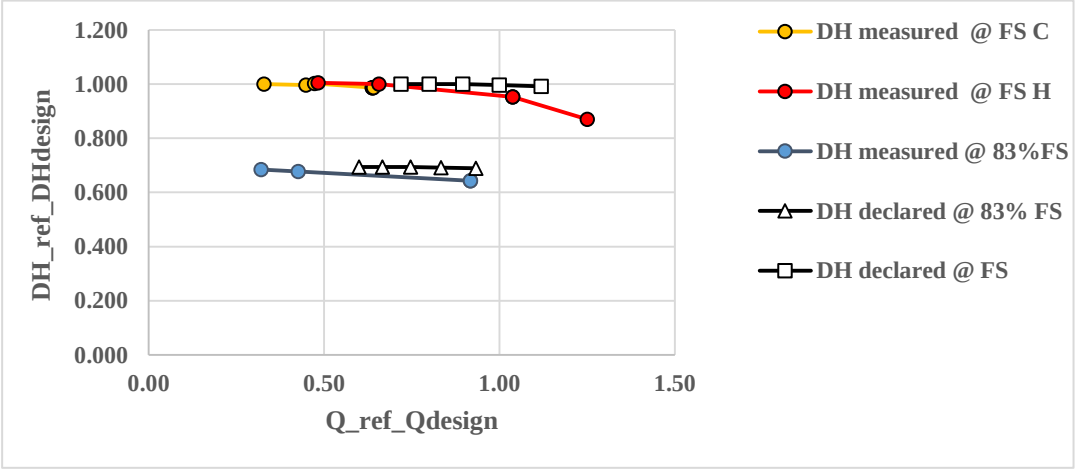

Figure 22, Measured fan performance curves - FS=Full Speed; C: conditions representative of low temperature flow, H: conditions representative of high temperature flow; "declared": factory performance curves, i.e. required performances. Curves are scaled with the design values

3.6. Inlet plenum

An inlet plenum is installed at the fan exit in order to guarantee a uniform flow inside the duct. With reference to Figure 23, the plenum is a duct with rectangular cross section and varying area composed by a slowly increasing diffuser followed by a converging nozzle. The high contraction ratio which is provided by the nozzle is expected to improve the flow quality significantly while the upstream diverging duct allows to settle the flow non-uniformities which could be produced by the fan outlet. Furthermore, the sudden area contraction could help to reduce the fan noise by acting as a reactive filter for low frequency noise components. The fan exit has a rectangular shape and it is bigger than the test section (nozzle exit).

The plenum shape and dimensions were selected in order to provide a smooth area transition between the fan outlet and the test duct cross section. The overall geometry was initially defined by considering maximum axial length constraint due to the available space in the laboratory while avoiding the detachment of the flow into the initial diffuser. The detailed geometry achieved through aerodynamic and thermo-structural analyses will be explained in the next sections.

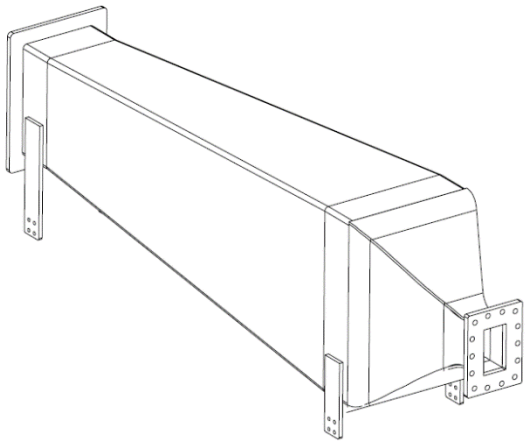

Figure 23, inlet plenum geometry

3.6.1. Aerodynamic design

CFD simulations have been performed to analyze the aerodynamic behavior of the plenum and the overall test-section geometry. The verifications are required to estimate the overall pressure losses at the highest flow temperature and pressure, to check the uniformity of the flow in the test section and the evolution of the flow along the test section. The simulations were carried out from the fan exit to the final diffuser exit by means of a computational fluid dynamics software tool with $k - \varepsilon$ turbulence model and scalable wall functions. 3M grid elements were used in simulating one quarter of the geometry.

The investigations confirmed that the main design requirements are satisfied, such as the overall pressure losses, the flow uniformity, all relevant quantities of the mean flow and the boundary layer at testing conditions representative of the LPT exhaust. As an example, the figures below show, respectively, on the left, the streamlines within the plenum and at the nozzle exit and, on the right, the 2D distribution of the modulus of the velocity in the test section at the design operating point of the rig at hot conditions.

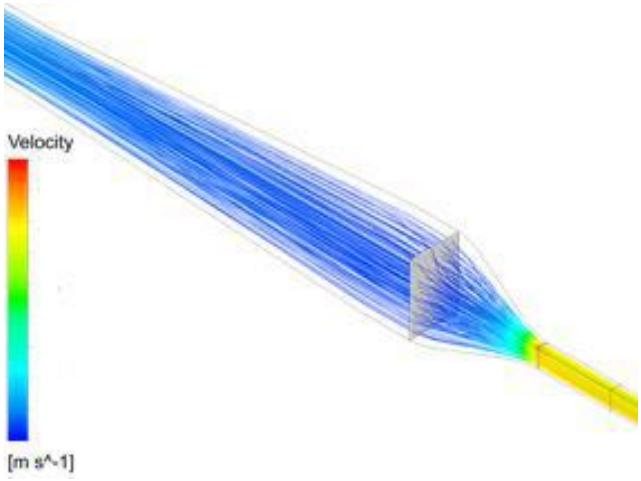

Figure 24, Flow condition in the plenum, ¼ of geometry

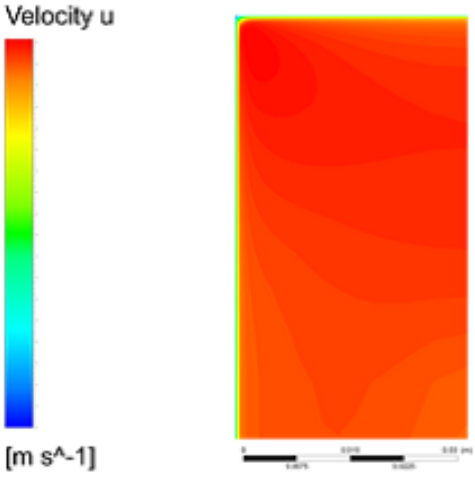

Figure 25, Flow map in the test section, ¼ of geometry

The adopted aerodynamic configuration for the test rig guarantees a uniform flow in the test section without any distortions and the nozzle can also recover possible non-uniformities coming from the fan exit. Figure 26 shows the flow profile for two different scenarios: one with uniform flow produced by the fan, and a strongly distorted (sheared) one. In both cases, the uniform flow is recovered in the liner section (Figure 27).

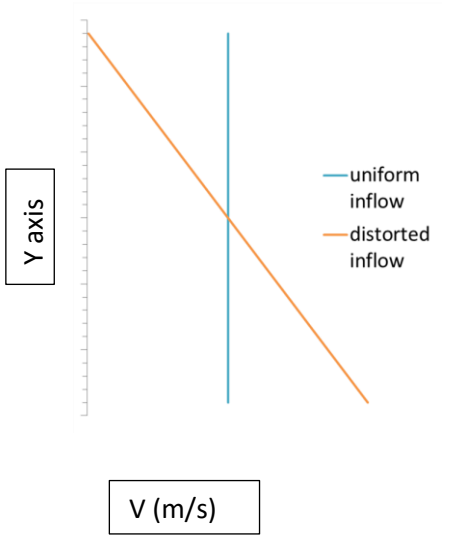

Figure 26, different imposed flow profiles at the inlet of the plenum in the CFD model

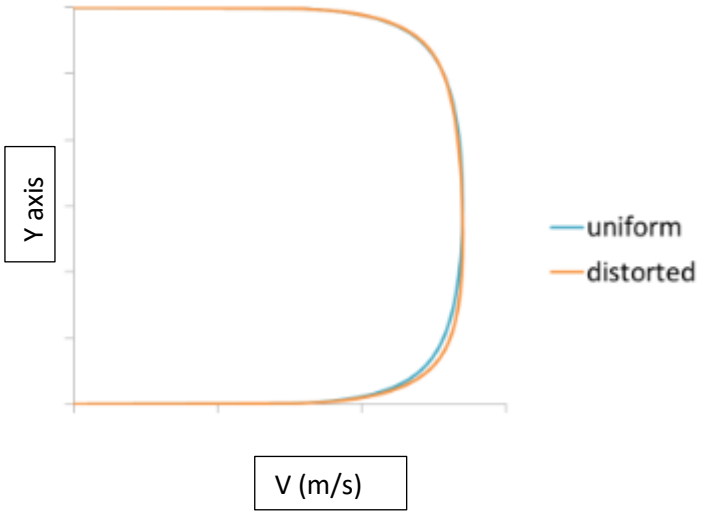

Figure 27, achieved flow profiles at the liner section for different inflow profiles in the CFD model

3.6.2. Thermo-structural design

The test rig is supposed to work at both cold and hot flow conditions (Mach up to 0.5). Obviously, the most critical conditions from a structural point of view are those at high temperature and high speed. However, as the air density at cold condition is higher, the internal pressure in the rig components is bigger, making this operative condition critical for the mechanical resistance as well.

Two extreme cases were considered for design purposes:

1) Cold condition: 25 °C and 50 kPa internal pressure

2) Hot condition: 450 °C and 25 kPa internal pressure

The cold working condition must be considered, as already mentioned, because it foresees the highest working pressure for the rig components. The second one, the hot condition, is of concern as there is a superposition of the internal pressure and the thermal stresses.

Thermo-structural analyses were performed through a multi-physics commercial FEA software to assess the component integrity. Structural mechanics module was employed for the analysis. The inputs for the analyses are the internal pressure (p) and the temperature (T) in the inner surface of the plenum (it is supposed that the flow temperature is equal to the metal surface). Solid mechanics and heat transfer computational modules were coupled together. The software takes advantages of the one-way coupling and solves the problem sequentially using the segregated solver. The model is firstly solved for the heat transfer and then, based on the calculated temperature map, the equation below is solved to compute the thermal strain:

$$\varepsilon_{th} = \alpha \times (T - T_{ref}) \qquad \textit{eq. 3–1}$$

Here α is the coefficient of thermal expansion, T is temperature (Kelvin), and T_{ref} is the strain-free reference temperature (also Kelvin).

The total stress is the summation of structural stress σ_0 plus the stress due to the thermal strain:

$$\sigma = C \times \varepsilon_{th} + \sigma_0 \qquad \textit{eq. 3–2}$$

In this equation, σ is the stress, *C* is the elasticity matrix, and ε represents the strain.

For the first case, the load is due to the pressure inside the plenum. To reduce the modeling effort, symmetry condition is used and ¼ of the geometry was studied. The plenum is made of AISI 316L

stainless steel and to insulate it, as well as all the other components of the rig, a layer of glass wool is considered to be installed all around it. The schematic of the model and the imposed boundary conditions to assess the mechanical stress due to the pressure and thermal dilatation is shown in Figure 28 and Figure 29.

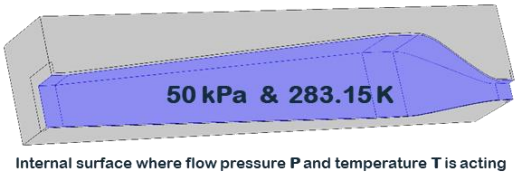

Figure 28, FEM inputs for the cold operating condition

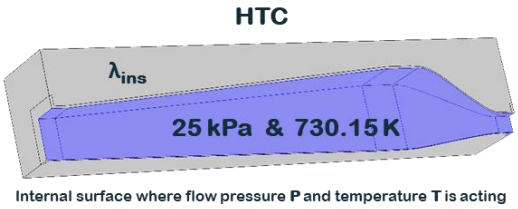

Figure 29, FEM inputs for the hot operating condition

The mesh size is sufficiently fine to have the desired accuracy for the stresses and thermal expansions. The mesh is refined in the corners where the stress concentration takes place to accurately locate the position and to estimate the amplitude of the maximum stress. For the thermal insulator modelling (glass wool) the mesh size is coarser. For the ¼ geometry of plenum with a 20 cm thick glass wool, 8.60*10^5 mesh elements were used, the computational mesh is depicted in Figure 30.

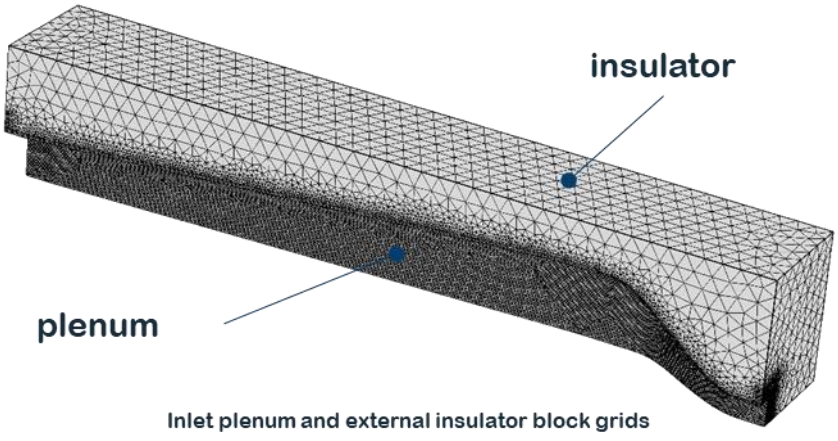

Figure 30, adopted mesh in the FEM model for plenum thermo-structural analysis

The stainless-steel properties were found in the software material library. Figure 31 shows the von-Mises stress distribution for the cold working condition. The maximum stress is located in the plenum corner (inner side) and it is sufficiently lower than the yield stress.

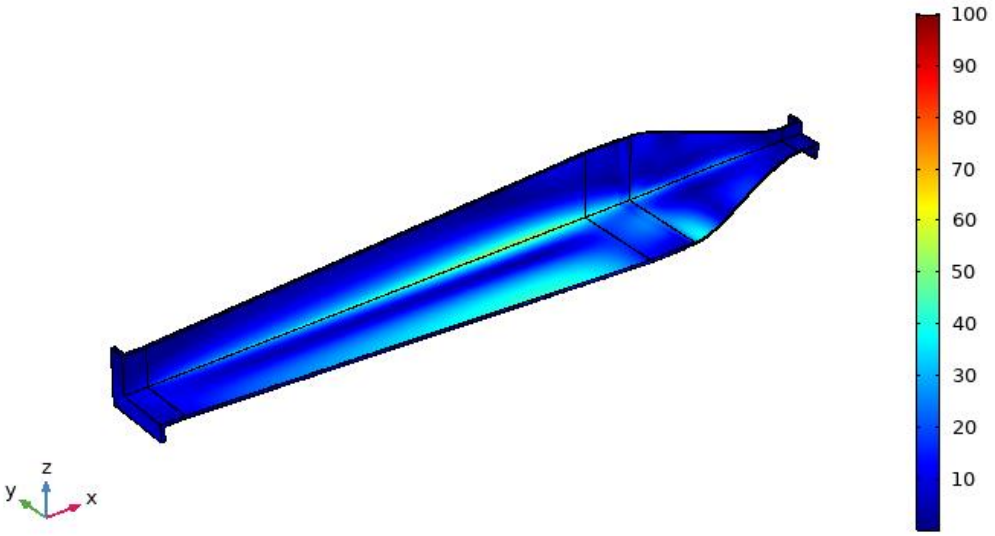

Figure 31, von-Mises stress ([MPa]) distribution in the plenum for the cold working condition

For the hot operating condition instead, the results consider not only the mechanical stresses due to the internal pressure but also due to the thermal gradients. The yield stress for the material in the hot condition is lower than that at cold conditions. However, the maximum stress, which takes place at the plenum corner, is 2.3 times lower than the yield stress, see Figure 32.

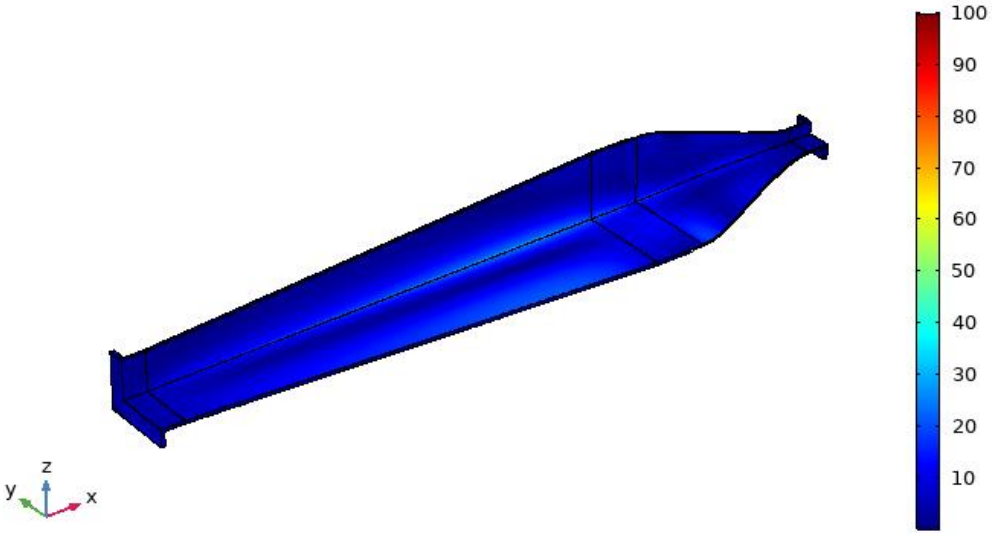

Figure 32, von-Mises stress ([MPa]) distribution in the plenum for the hot working condition

A heat transfer study was carried out too for safety purposes, and the objective was to calculate the heat losses for a given thickness of the glass wool. Constant temperature of 450 °C is supposed for the plenum inner surface and the natural heat transfer boundary condition is imposed on the outer surface of the insulator (Figure 33). The laboratory ambient temperature is assumed to be 25 °C. Figure 34 shows the thermal map of the plenum and glass wool together. The results demonstrate that the use of a 20 cm thick glass wool is sufficient for the thermal insulation as well as the safety of people in the lab, since the temperature on the outer surface is close to the ambient temperature (Figure 34).

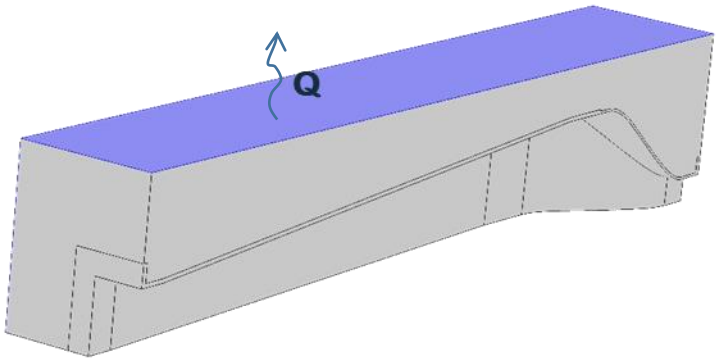

Figure 33, natural convection heat transfer on the glass wool surface as the boundary condition for the FEM model

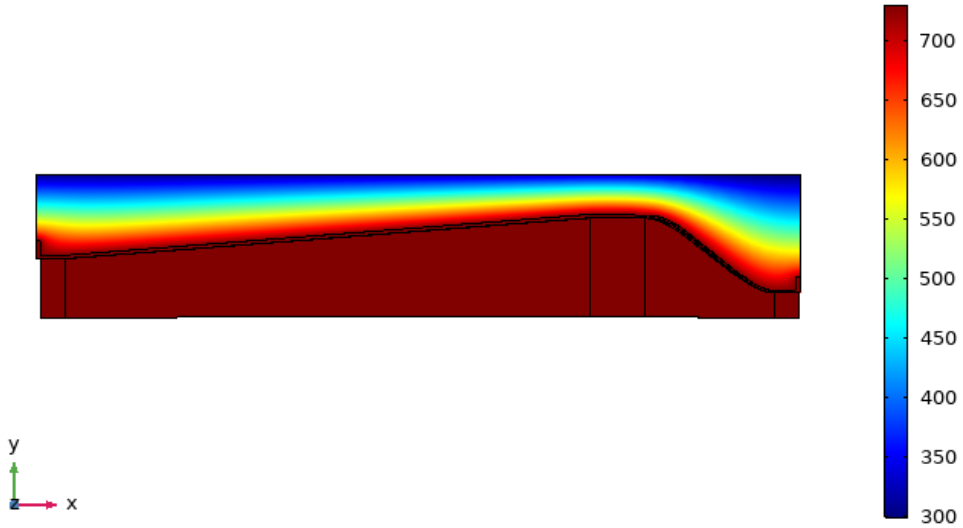

Figure 34, surface temperature ([K]) of the plenum at the hot working condition

The plenum will experience also a thermal expansion while operating at high temperature. The maximum displacement happens clearly in the axial direction as shown in Figure 35. It is worth

mentioning that this expansion (as well as all the other components) in the axial direction is supposed to be compensated by two expansion joints that are placed at the inlet and outlet portions of the duct. The expansion joints are made of special semi-flexible material that can withstand high temperatures.

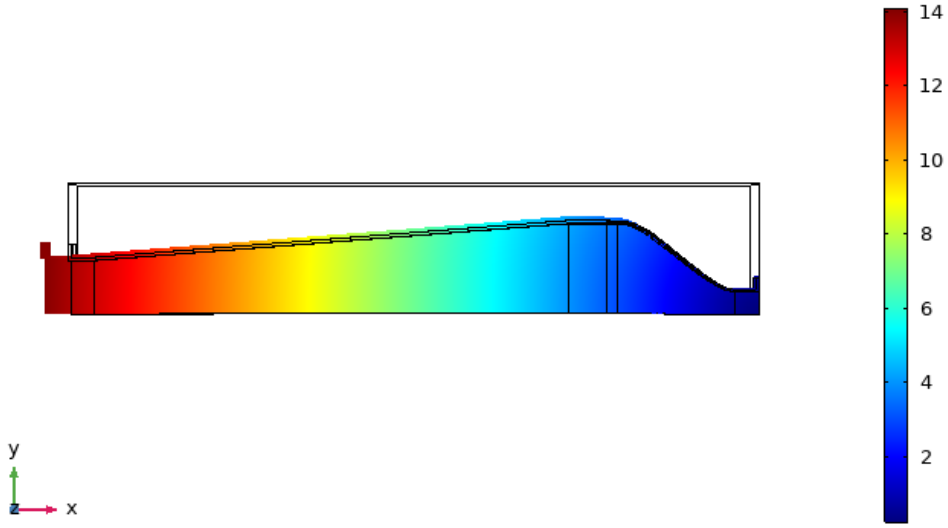

Figure 35, axial displacement ([mm]) of the plenum due to the thermal expansions

Table 4 summarizes the main design parameters of the plenum and most relevant evidences from the numerical investigations. Figure 36 shows the final design solution, produced and installed on the rig.

Table 4, design parameters and numerical results for the plenum

parameter	Plenum material	Thickness (mm)		Max structural stress (MPa)	Yield stress (MPa)	Safety factor	Thermal dilatation (mm)
		diffuser	nozzle				
Cold condition	AISI 316L	8	6	75	170	2.3	0
Hot condition	AISI 316L	8	6	37	90	2.5	14

Figure 36, plenum installed on the test rig

3.7. Anechoic terminations

Anechoic terminations (AT) are fundamental to avoid spurious wave reflections at the boundaries of the test section. In the UniFi rig, two anechoic terminations are placed at both sides of the test section.

Basically, the AT consists of a lined duct portion, with a variable thickness layer of sound absorbing material separated by a perforated sheet from the flow within the duct. Various geometries are reported in technical literature for anechoic terminations such as the one-slope, the two-slope, the exponential slope design, etc. Anechoic terminations could be installed either in one or two sides of the duct [59]. Apart from the cavity geometry, the flow resistance, which is in turn linked to the density of the sound absorbing material, can impact on the acoustic performance. The geometry with two slopes has been selected due to its better performance with respect to the one-slope or exponential profile.

The anechoic termination is able to provide the sound absorption in a wide range of frequency thanks to the varying thickness (due to the slope profile) of the absorbing material within the cavity. The performance of the anechoic termination is normally evaluated by means of the two-microphones method [59].

For the current work, the proposed geometry with two-slope has been presented hereafter. The first slope has a very small angle in order to avoid abrupt changes for the wall impedance moving from the hard-walled duct to the anechoic termination. The second slope has a bigger angle to reach the maximum thickness while limiting the overall axial length (Figure 37).

Figure 37, typical shape of a 2-slope anechoic termination

Once the geometry of the anechoic termination was decided, more detailed and comprehensive studies were carried out for optimizing the shape of the termination from acoustic and thermo-structural points of view to ensure the lowest possible wave reflection inside the test section.

3.7.1. Acoustic design

Figure 38 shows the 3D model of the anechoic termination. The rectangular cross-section is the same as the duct. AT has a modular design consisting of the two sound absorbing wedges at two sides of the duct. They are made of different parts: the cavity, which is filled by metal wool, the perforated sheet (acoustically transparent component), the two slopes external case and the flanges (

Figure 39). In the installation of the anechoic termination, attention was paid to avoid any step or discontinuity in the flowpath and a ceramic gasket is used for the sealing.

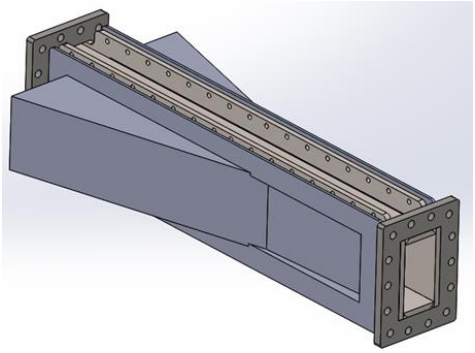

Figure 38, anechoic termination in the UniFi test rig

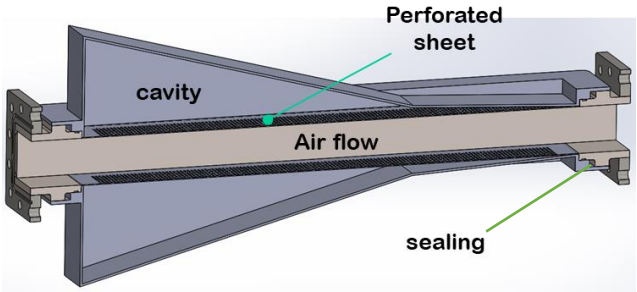

Figure 39, inner structure of the anechoic termination

The anechoic terminations are installed at both sides of the test section since it is supposed to have the wave excitation in both upstream and downstream direction inside the duct. The target is to reach a reflection coefficient lower than 0.2 in whole frequency band of interest. Once the geometry of the anechoic termination is defined, a FEM model was developed to verify the AT acoustic performance.

For this purpose, different lengths of the AT at both cold and hot conditions and a wide range of incoming frequencies were considered. Metal wool is considered as a porous domain with a defined flow resistivity in the model for the analyses.

In the acoustic module of the employed FEA software, the acoustic pressure p is the dependent variable that is solved for in the frequency domain. The frequency domain uses the Helmholtz equation in which pressure is a function of position and frequency. The equation could be presented as below if there is no acoustic source and the attenuation is neglected.

$$\nabla.\left(-\frac{1}{\rho}\nabla p_t\right)-\frac{1}{\rho}\left(\frac{\omega}{c}\right)^2 p_t = 0 \qquad \textit{eq. 3–3}$$

The governing equation and boundary conditions in the employed FEA software are formulated in terms of a so-called scattered field formulation in which the total acoustic pressure (p_t) is defined as eq. 3–4:

$$p_t = p_s + p_b \qquad \textit{eq. 3–4}$$

p_b is the background pressure field that is imposed as a boundary condition within a defined domain of the model to generate a given incident wave field, e.g. an incoming plane wave.

p_s is the scattered pressure field which is the dependent variable. Its value is determined once the equation 3-3 is solved for p_t and by applying it in the eq. 3–4.

The scattered field formulation is selected since the solution contains both information for the imposed and solved pressure field and it makes possible to distinguish the scattered pressure field from the imposed pressure field; so that it could be effectively used to assess the reflection coefficient of a duct termination or the transmission loss of an acoustic filter. By the application of non-reflective boundary conditions at the ends of the domain, the reflected wave is then given only by the effect of the AT itself, and it coincides with the scattered acoustic field. Hence, the reflection coefficient is calculated as the ratio between the values of the scattered pressure to the background pressure averaged on a surface parallel to the duct cross-section.

$$R = abs(P_s)/abs(P_b) \qquad \textit{eq. 3–5}$$

The sound pressure level is calculated based on the root mean square (rms) pressure as below:

$$L_p = 20log(\frac{p_{rms}}{p_{ref}}) \qquad \text{with} \qquad p_{rms} = \sqrt{\frac{1}{2}pp^*} \qquad \textit{eq. 3–6}$$

$$p_{ref} = 2 \times 10^{-5}$$

In the simulations, by taking advantage of geometric symmetry, ¼ of the geometry was considered. The volume filled with air was considered as a fluid domain where classical wave equation has to be solved, while the volume filled by sound absorbing material was modeled as a porous material. The used model represents the porous medium through complex propagation constants, i.e. the characteristic impedance and propagation velocity, which were determined through empirical correlations. The domain at the end of the AT was modelled in a conservative manner, by exalting the eventual back-reflections due to the final diffuser installed at the very end of the test-section. The computational domain consists of a sphere with two layers; the first layer promotes the generation of reflections due to the free-field radiation while the second one acts as a Perfectly Matched Layer (PML). PML is a layer of virtual domain that is put all around the physical region of interest and includes a complex coordinate scaling to absorb all outgoing wave energy, avoiding spurious reflections. PML does not cause any impedance mismatch at the boundary layer. Another PML boundary condition was put at the beginning of the duct to model the infinite tube in such a way that there is only the wave propagation in one direction. The background pressure field is used to generate the plane wave excitation with the amplitude of 1 *pa* for providing the acoustic field in the model.

The stand-alone duct without AT was compared to the solution with anechoic termination installed. Figure 40 to Figure 43 show the adopted boundary conditions in the FEM model.

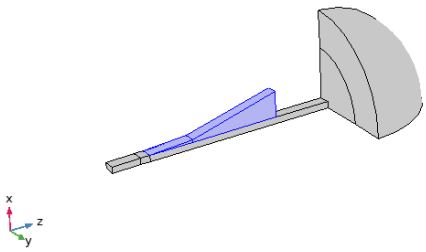

Figure 40, Poro-acoustic domain

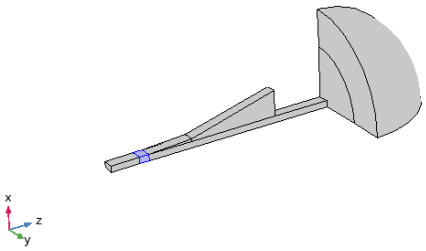

Figure 41, Background pressure field

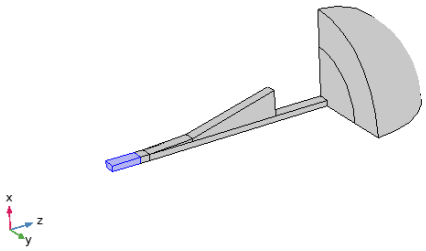

Figure 42, inlet PML boundary condition

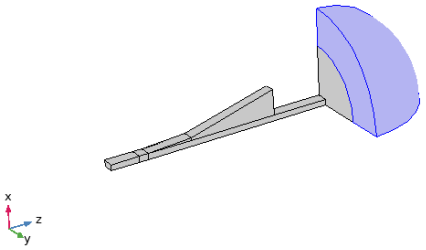

Figure 43, outlet PML boundary condition

In the acoustic model, to guarantee a proper description of the wave propagation in the desired frequency band, the mesh size has been selected to have a sufficient number of elements for the smallest wavelength. Figure 44 shows the mesh sample in the ¼ of the domain.

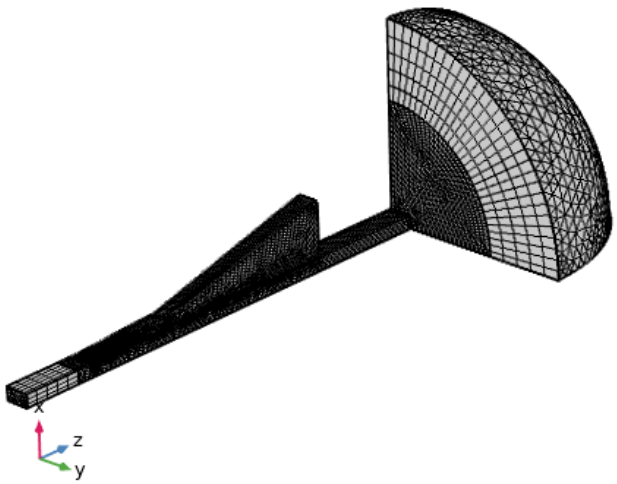

Figure 44, A sample of the mesh shape implemented in the acoustic model for AT

Figure 45 represents the acoustic field inside the duct: it can be noted that the acoustic pressure amplitude decays after interacting with the AT. At the same time, the acoustic pressure pattern shows only a forward running wave, proving the goodness of the anechoic termination. For what concerns the sound pressure level at the exit of the domain, as it is shown in Figure 46, the amplitude comes to zero inside the PML proving the effectiveness of the damping strategy.

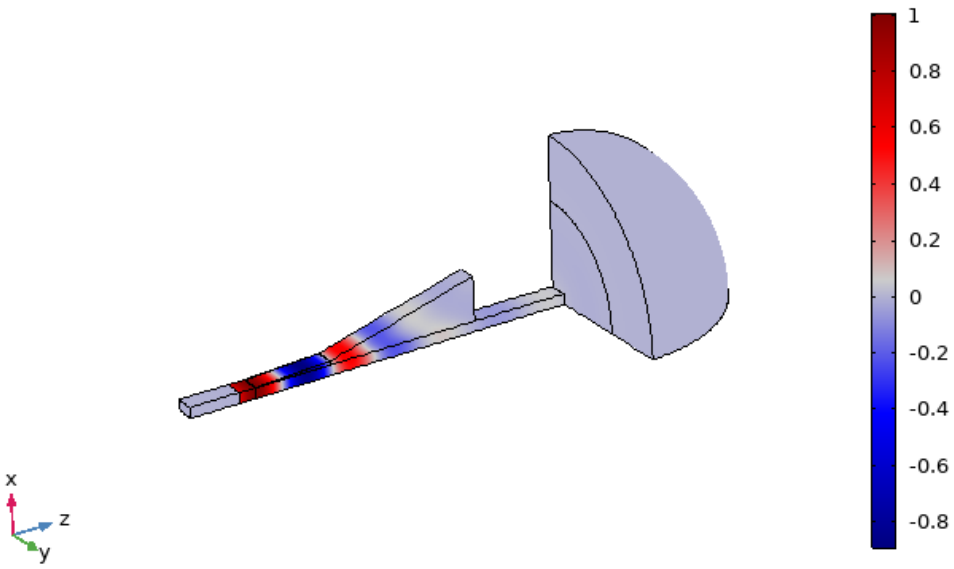

Figure 45, acoustic pressure field ([Pa]) @1000 Hz

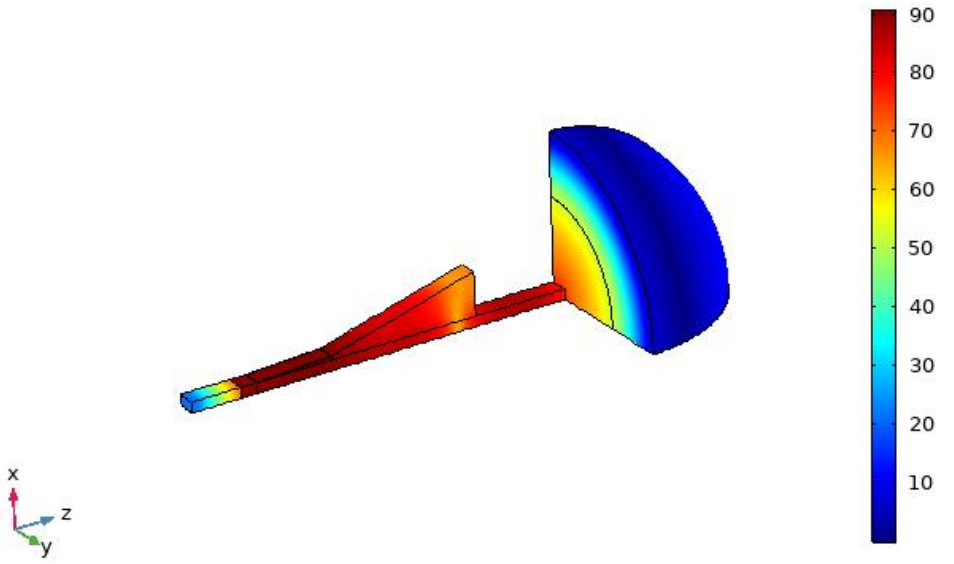

Figure 46, Sound Pressure Level ([dB]) @ 1000 Hz

Figure 47 reports the results in terms of reflection coefficient versus non-dimensional frequency (*kr*) numerically obtained for different lengths and temperatures.

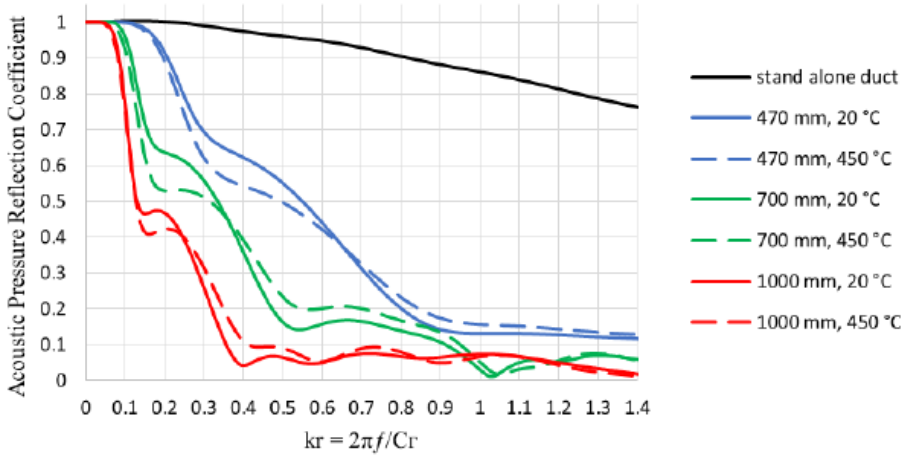

Figure 47, reflection coefficient ([-]) vs reduced frequency ([-]) for different lengths and temperatures in the AT

First of all, it is demonstrated that the AT is crucial for the reliability and goodness of the acoustic facility since the stand-alone duct shows very high (and detrimental) reflection coefficients. The use of an AT can satisfy R<0.2 in whole frequency range of interest. More about the results, although the AT with 1000 mm length has the best performance, it was decided to install the 700 mm long termination because of the limited room within the Laboratory. It is worth noticing that the homologous curves obtained at different temperatures compare quite well together when the non-dimensional frequency is used as abscissa, due to the scaling of temperature effects on the speed of sound. The residual differences may arise from the dependence on the temperature of the sound absorption parameters in the material model used for the computations, i.e. the characteristic impedance and propagation constant.

It should be mentioned that in these models the frequency band is limited to 1 kHz to reduce the computational costs. It is expected that for higher frequencies the reflection coefficient is sufficiently low.

3.7.2. Thermo-structural design

The AT is made of AISI 316L stainless steel and the dismountable parts are installed together carefully to avoid any steps or discontinuities as they could be the sources of reflections and acoustic

distortions inside the wave guide. The cavity must be filled by a sound absorbing material. The glass wool represents a good candidate and was already used for cold operating conditions [60]. However, considering the hot working conditions, metal wool was finally chosen as sound absorbing material, because its high thermal conductivity [61] will reduce the thermal stresses due to the temperature gradient between the internal (hot) and external (cold) part of the AT. The eligibility of metal wool is validated as will be discussed later.

In the interfaces between different parts, a high temperature resistant ceramic gasket was used to avoid flow leakages. A numerical model is used to assess the stresses on the AT structure. Two operating conditions (cold and hot) were considered, similar to what performed for the inlet plenum. Figure 48 shows the boundary conditions used for the simulation.

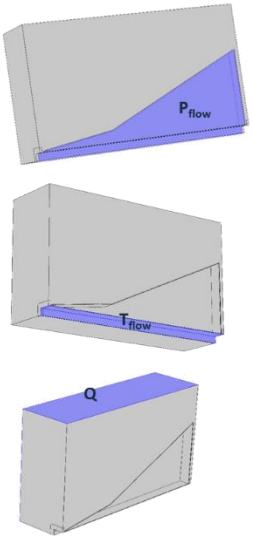

Figure 48, boundary conditions for thermo-structural modeling of the AT

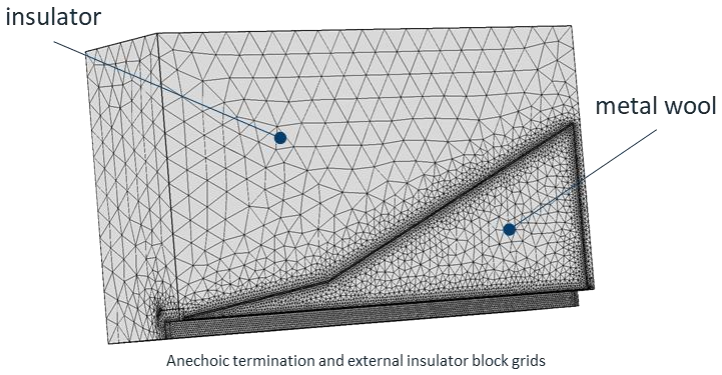

Figure 49, Mesh adopted for thermo-structural modeling of the AT

¼ of geometry with imposed symmetry condition was analyzed. A block of mineral/glass wool is considered as the external thermal insulator while metal wool is filling the cavity as the sound absorber. As mentioned before, the selection of the metal wool allows the heat transfer through the component to relax the thermal stresses due to the temperature gradients between the inner and outer sides of the AT. The pressure inside the anechoic termination was set on the inner surface as well as the temperature due to the air flow inside the duct. Natural convection was imposed on the external shell of the insulating material. Around 6.5*10^5 elements were used to properly mesh the component and a grid refinement was applied at the corners to increase the accuracy of the analysis where peaks and strong gradients of stresses are expected (Figure 49). A coupled multi-physics approach was used:

thermal analysis based on B.Cs. was firstly performed, followed by a structural analysis including deformations due to the calculated thermal map. As the thermal gradient inside the AT is key in its structural integrity, a sensitivity analysis was carried out to find the best choice for the metal wool (as sound absorbing material) and mineral wool (as external insulating material). The design logic is that the metal wool must be as conductive as possible, while the mineral wool should have a very low thermal conductivity for better insulation. This trend was observed also through the FEM models results. The simulations were carried out for the worst condition to guarantee the rig safety.

Figure 50 shows the thermo-structural stress distribution in the AT. The maximum stress happens in the inner corners and is strongly localized, while in the rest of the component there are no significant stresses. A summary of the FEM analysis settings and outcomes is brought in Table 5.

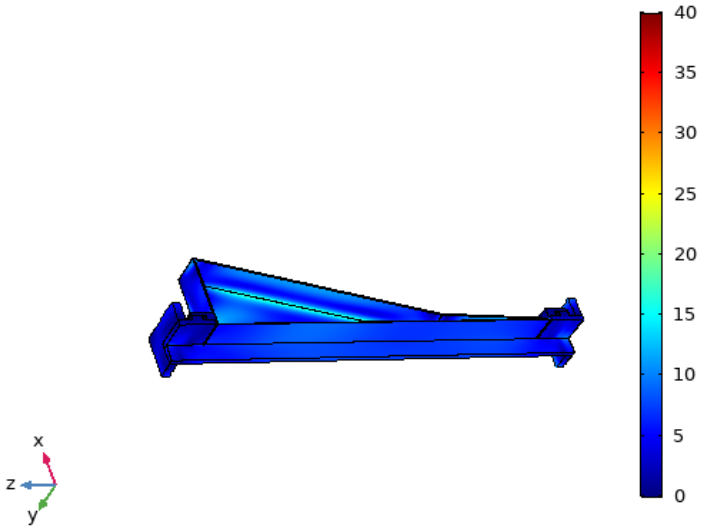

Figure 50, von-Mises stress ([MPa]) distribution

The surface temperature gradient that is obtained through the simulation is shown in Figure 51. The whole AT is at high temperature however the external temperature is controlled due to the insulator shell. The high temperature causes considerable dilatation in the axial direction of the AT and this represents a concern. To calculate the elongation due to the high temperature, a fixed point constraint was imposed on the model at one side, so the part is free to expand in the other direction (Figure 52).

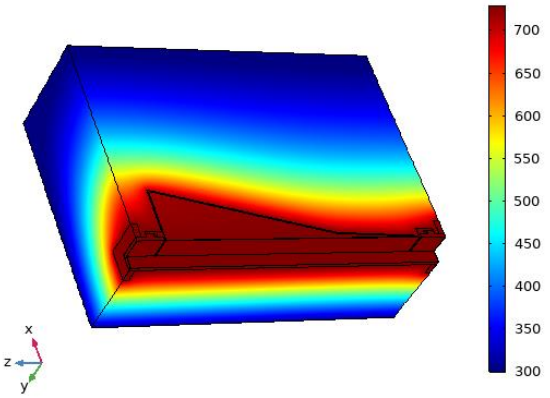

Figure 51, Surface temperature ([K]) for the AT at hot working condition

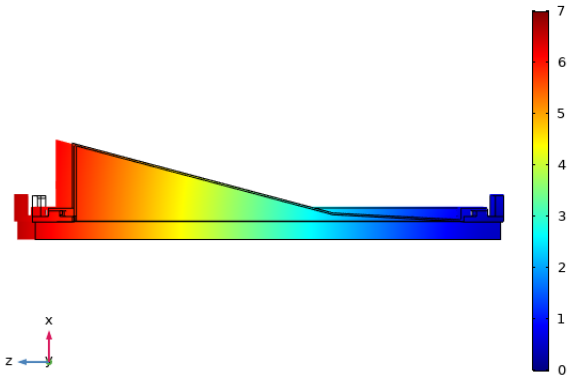

Figure 52, AT axial displacement ([mm]) due to the thermal expansions

Table 5, FEM numerical results for the anechoic termination

parameter	Plenum material	Cavity Shell Thickness (mm)	Mineral wool conductivity (W/mK)	Metal wool conductivity (W/mK)	Max structural stress (MPa)	Yield stress (MPa)	Safety factor	Thermal dilatation (mm)
Cold condition	AISI 316L	3	-	-	115	170	1.5	-
Hot condition	AISI 316L	3	0.09	24.8	67	90	1.3	8
Hot condition	AISI 316L	3	0.09	12.4	79	90	1.1	8
Hot condition	AISI 316L	3	0.18	24.8	80	90	1.1	8
Hot condition	AISI 316L	3	0.18	12.4	71	90	1.25	6.5

Figure 53 shows the manufactured and installed AT. The cavity shell is filled with the metal wool and then the perforated sheet is installed on (Figure 54). All the assembly is then flanged on the rig, inside the slots that are specifically foreseen for this component.

Figure 53, AT installed on the UniFi test rig

Figure 54, AT components

Test section

3.8.1. Structure

The test section is a long straight duct with rectangular cross-section that works as the wave guide. The test section has a modular structure and it is composed of 3 portions, having the same shape and flanged together, as can be seen in Figure 55. Each duct side has windows that allow the easy mounting and dismounting of side plates that can be used for the installation of the aerodynamic as well as acoustic instrumentations. The liner too can be installed in these lateral windows.

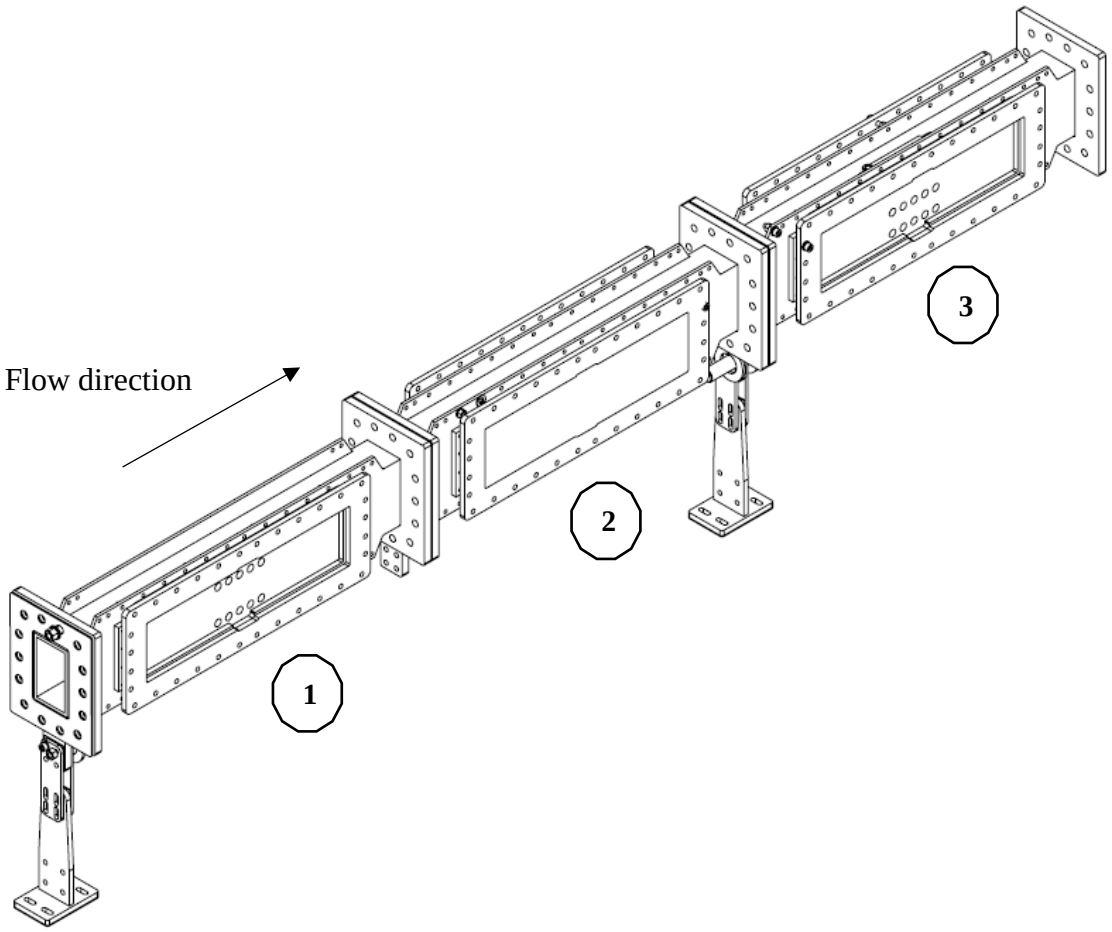

Figure 55, Test section: upstream section, 1. Liner section, 2. Downstream section, 3.

The duct is made of AISI 316 L and the inner surface is polished to have a very small roughness. The duct wall is 6 mm thick in order to provide the system with a proper stiffness and to allow the installation of the sensors.

The flanges connecting the different portions of the test-section have a 15 mm thickness and are welded on the tube. A machine-worked face is considered for a proper sealing. To allow a perfect sealing and avoid any step or discontinuity on the inner surface of the duct, a throat is considered on

the flange as a sit for the ceramic gaskets. Further, to set a uniform pressure on the gasket, it is recommended to put the bolts by following a best practice rule, where $D_{b\text{-}b}$ is the inter-bolt distance and d_b is the bolt nominal diameter.

$$3 < D_{b\text{-}b}/d_b < 6 \qquad \text{eq. 3–7}$$

Figure 56, the flange with bolts positions and the seat for gasket

3.8.2. Acoustic design

The rectangular cross-section with an aspect ratio of ≅1.8 is chosen considering the trade-off between an efficient aerodynamic behavior (acceptable head losses) and the possibility to propagate higher order modes. The cross-section dimensions allow to sufficiently extend the plane wave propagation frequency limit and, at the same time, they enable the separation of the cut-off frequencies of transverse modes. The aspect ratio is selected in such a way that the difference Δf between adjacent cut-on frequencies is not less than 120 Hz (Δf_{min} > 120 Hz). With reference to Figure 16, Table 6 shows some acoustic parameters while varying the aspect ratio of the cross-section. For the UniFi test rig, an aspect ratio of 1.845 was finally chosen.

Table 6, acoustic parameters as function of the duct aspect ratio

b/a	Δf_{min} [Hz]	N. cut on modes	(m,n) max	(m,0) max	(0,n) max	First cut on [Hz]	T (°C)	Mach
1.883	126.3	13	(2,3)	(2,0)	(0,4)	1226.2	20	0.5
1.880	134.9	13	(2,3)	(2,0)	(0,4)	1227.3	20	0.5
1.876	143.4	13	(2,3)	(2,0)	(0,4)	1228.5	20	0.5
1.873	151.2	13	(2,3)	(2,0)	(0,4)	1229.6	20	0.5
1.869	147.5	13	(2,3)	(2,0)	(0,4)	1230.8	20	0.5
1.866	143.9	13	(2,3)	(2,0)	(0,4)	1231.9	20	0.5
1.862	140.2	13	(2,3)	(2,0)	(0,4)	1233.1	20	0.5
1.859	136.6	13	(2,3)	(2,0)	(0,4)	1234.2	20	0.5
1.855	133.0	13	(2,3)	(2,0)	(0,4)	1235.4	20	0.5
1.852	129.3	13	(2,3)	(2,0)	(0,4)	1236.5	20	0.5
1.848	125.7	13	(2,3)	(2,0)	(0,4)	1237.7	20	0.5
1.845	**122.1**	**13**	**(2,3)**	**(2,0)**	**(0,4)**	**1238.8**	**20**	**0.5**
1.215	123.5	13	(2,3)	(3,0)	(0,3)	1526.5	20	0.5
1.214	127.2	13	(2,3)	(3,0)	(0,3)	1527.4	20	0.5
1.212	130.8	13	(2,3)	(3,0)	(0,3)	1528.4	20	0.5
1.211	127.6	13	(2,3)	(3,0)	(0,3)	1529.3	20	0.5
1.209	124.3	13	(2,3)	(3,0)	(0,3)	1530.2	20	0.5
1.208	121.1	13	(2,3)	(3,0)	(0,3)	1531.2	20	0.5

Figure 57 shows some of the possible higher order mode shapes that can propagate in the duct. The cut-on frequency of the first transverse mode is f=1238 Hz at Ma=0.5.

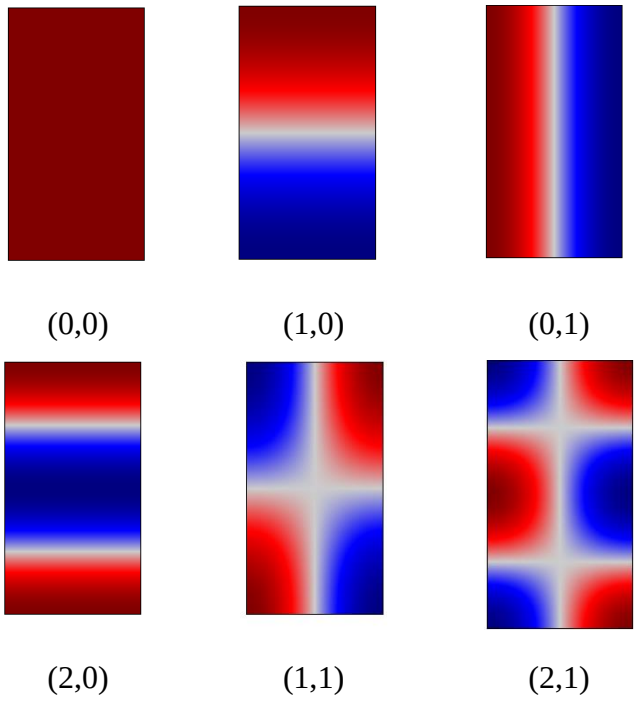

Figure 57, higher order mode shapes (m,n)

3.8.3. Liner installation

The test article (acoustic liner, Figure 58) is mounted in a dedicated window in the middle of the test section and it is carefully sealed by a ceramic gasket (Figure 59 and Figure 60). The liner could be installed in whether one or both sides of the duct and there is the flexibility to investigate liners with different geometries as the mounting system can, as an example, easily manage different axial length and cavity depth.

Figure 58, acoustic liner sample with the sealing

Figure 59, acoustic liner installation on the dedicated window in the test section

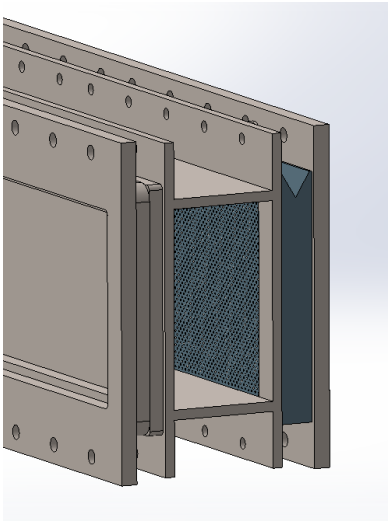

Figure 60, acoustic liner installation flush mounted with the duct wall

3.9. Excitation signal generation, source section

Two sets of four high-sensitivity compression drivers with a maximum power of 50W and a frequency range from 160 to 7000 Hz can provide a maximum SPL of about 140 dB that ensures a sufficient SNR (> 10 dB) at the desired testing conditions. The speakers are installed both upstream and downstream the liner section, so that there is the possibility to excite the sound waves in the flow direction or in the opposite one. The speakers are connected to the duct walls by means of long enough stainless-steel tubes, to keep them far from the hot region. Inclined connections are chosen for linking the tube to the duct to minimize the interaction between flow and the connecting tubes. In addition, thermal resistive Teflon joints are used to install the speaker on the tube in order to improve the thermal barrier between speaker and rig. Figure 61 and Figure 62 show the speakers configuration and their installation on the rig.

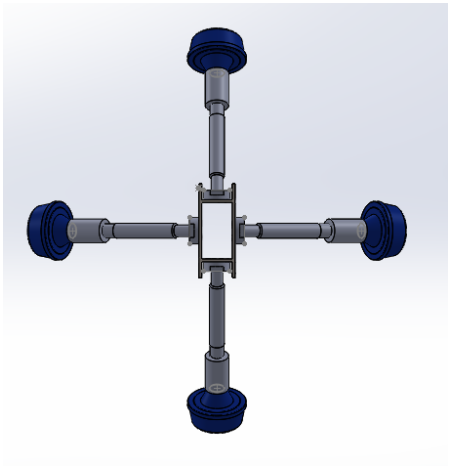

Figure 61, speakers' configuration

Figure 62, speakers installed on the rig

The speakers can be either set to work at the same phase (plane wave excitation) or controlled to generate higher order mode waves. There is the capability of exciting broadband noise as well as tonal noise.

3.10. Rig thermal control

The rig is designed to work in both closed and open circuit condition. Each configuration could be reached by properly setting the valves that are placed on the returning circuit which control the mixing between cold external air and hot recirculating air inside the system. There is a discharge valve at the outlet port, which vents part of hot air to the external environment, and a recirculation valve providing a pressure difference between inlet and discharge ports. In the fully open condition, the discharge valve is fully open and recirculation valve is fully closed: in this condition the fan is fed completely by the ambient air. In the hot conditions, the flow is expected to reach the target temperature through the air recirculation in the closed loop. An electrical heater at the fan exit is foreseen to support the heating process. The whole rig is thermally insulated from the environment by a thick layer of glass wool. Figure 63 shows some of the thermal control strategies deployed in the rig.

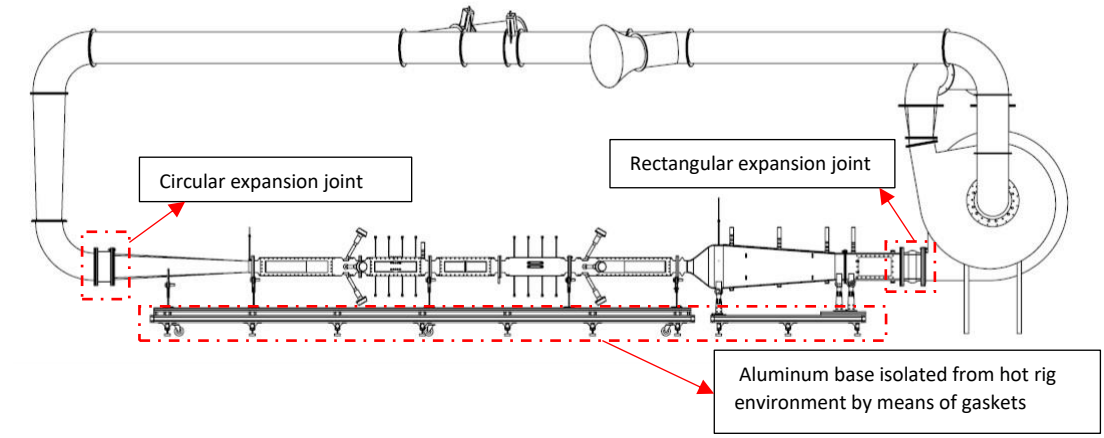

(a)

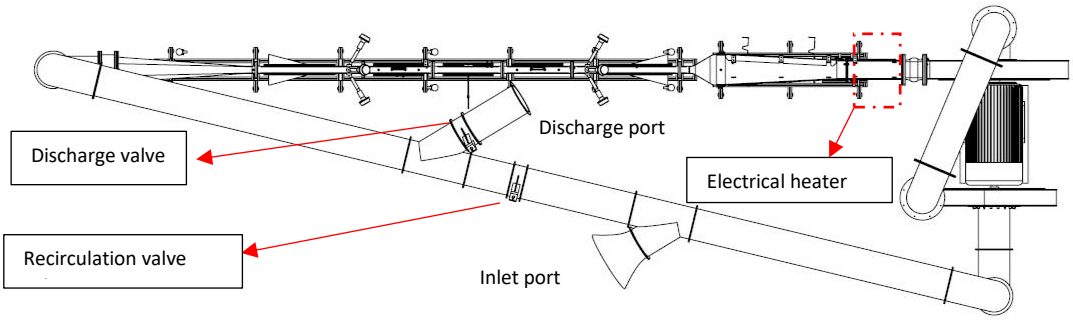

(b)

Figure 63, rig thermal control considerations; side view of the rig (a), top view of the rig (b)

Figure 64, picture of the returning duct of the UniFi test rig

To investigate the effectiveness of the proposed temperature control system, a simulation has been performed through a dynamic simulation software. The test bench is simply modelled by means of different pipe sections, having appropriate lengths and areas in order to reproduce the aero losses expected within the circuit. The mass flow rate is inserted through the model by means of the fan and it is gradually increased until reaching the desired target value. The outlet is modelled by the aforementioned discharge valve, whose working condition is described by a percentage of the fully open position. A PID controller is dedicated to change the position of discharge valve and keep the temperature in the desired range. The outlet port is followed by a recirculation valve, which is located between the discharge and inlet ports to control the pressure difference between these two axial stations.

An example of simulation's results is reported hereafter. In the current simulation, the mass flow rate of the fan is linearly increased from 0 to the target value in the first 50 seconds and then, for the entire simulation, it is kept constant. The target temperature is set to 450 °C while the recirculation valve is set to the 50% of its fully open position throughout the entire simulation. It is worth considering that, at the beginning of the simulation, the discharge valve is completely closed. It can be seen from Figure 65 and Figure 66 that meanwhile the temperature is below 450 °C, the PID controller keeps the discharge valve closed until the temperature exceeds the target temperature. At this point the PID controller partially opens the discharge valve to keep the temperature close to the desired value. When the discharge valve is close to the 6% of its opening position, the operating condition is guaranteed. From Figure 66, it can be noticed that, according to the control system logic, the transient phase is of short duration and the stabilization is achieved without temperature oscillations or severe unsteady spikes which could represent a concern for the structural integrity of the test bench. Therefore, according to this preliminary investigation, the system seems able to control the working temperature in a rather quick and stable manner.

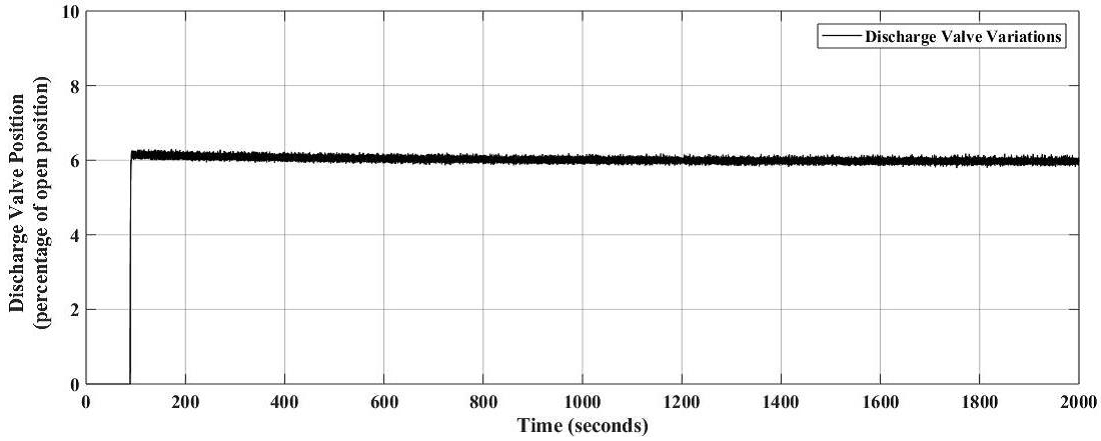

Figure 65, discharge valve position through simulation

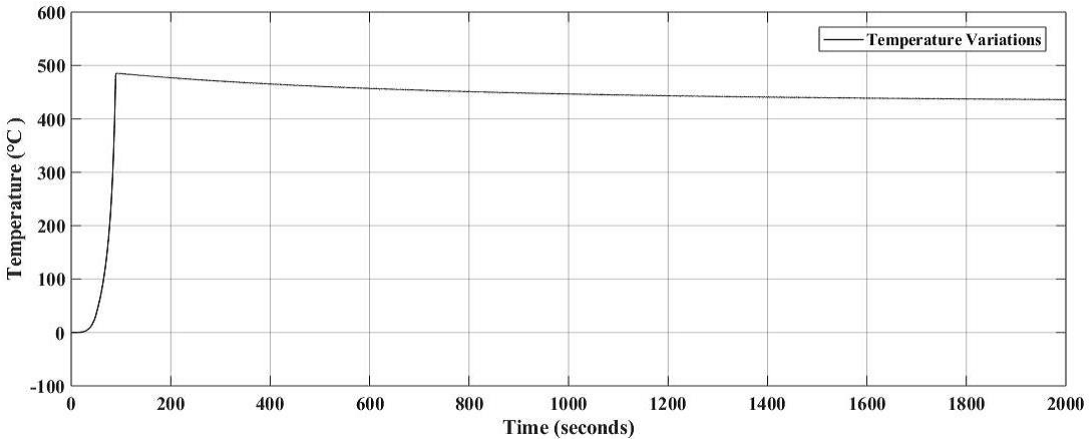

Figure 66, temperature variation through the simulation

Two thermal expansion joints are placed at fan and diffuser exit (Figure 63) to compensate the thermal expansion and displacement of the long test section. The thermal joints (Figure 67 and Figure 68) are made of a special fabric that could stand for high temperature and high pressures.

Figure 67, a picture of the rectangular expansion installed at the fan exit

Figure 68, a picture of the circular expansion joint installed at the final diffuser exit

The whole rig is mounted on a sliding aluminum structure (Figure 63) that can recover the stresses due to the thermal elongation. A concrete basement provides a good leveling and stability to the overall system.

Aerodynamic measurement and instrumentation

Part of this study is dedicated to the design of an aero measurement system for the monitoring of the rig and the characterization of the flowfield within the duct. It is well known that the grazing flow impact on the liner performance is crucial and therefore the flow conditions have to be accurately measured and considered for the assessment of the acoustic impedance. The aerodynamic mapping of the rig is obtained through different probes mounted in the test section and along the rig circuit. A list of instrumentations and their installation on the rig is discussed hereafter.

3.11.1. Kiel Probe

A Kiel probe equipped with a K-type thermocouple is mounted inside the plenum in a traversing system to measure the total quantities before entering the nozzle.

Figure 69, a picture of the Kiel probe equipped with a thermocouple used in the rig, suitable for high temperature applications

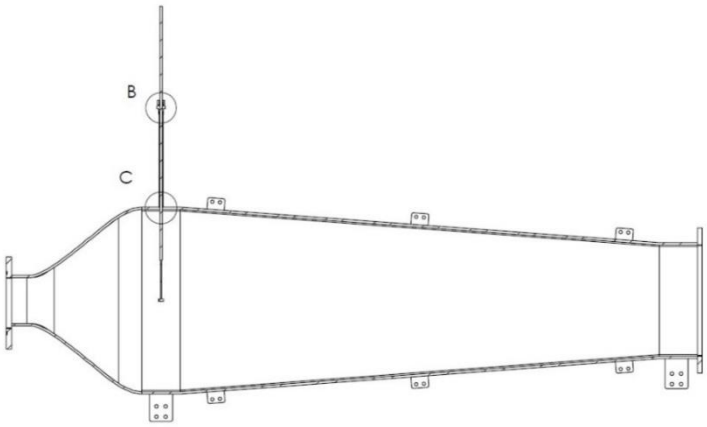

Figure 70, the Kiel probe mounted on the plenum in a traversing mode

The probe is manufactured to withstand the maximum testing temperature and it is long enough to keep the end part far from the hot region.

3.11.2. Static pressure taps and thermocouples

A set of static pressure taps and thermocouples are foreseen in different parts of the rig. In the test section, upstream and downstream the liner, there are four pressure taps for static pressure (bottom surface of the duct) and four J-type thermocouples (upper surface of the duct) for temperature recordings as reported in Figure 71. These sets of measurement points allow the monitoring of the flow right before and after the liner and along the duct.

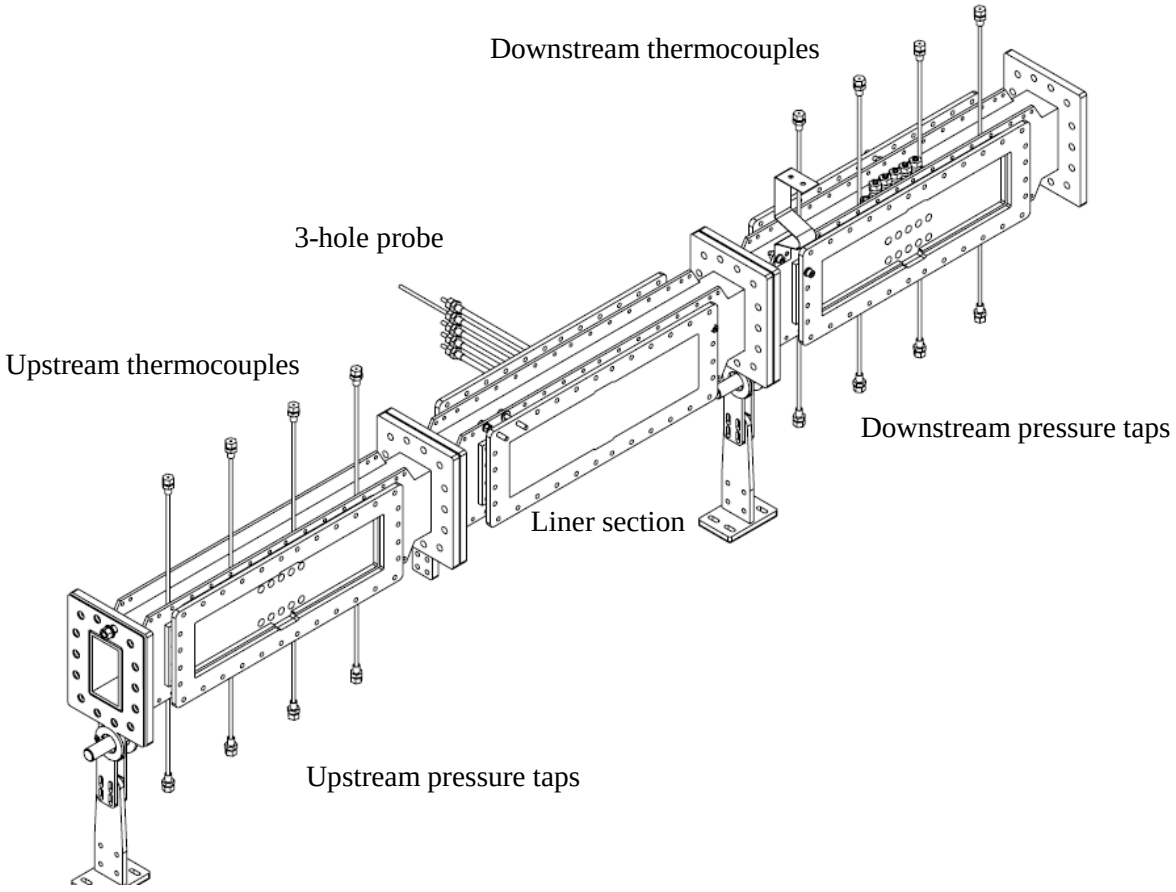

Figure 71, measurements stations upstream and downstream the liner section

3.11.3. 2-dimensional 3-hole probe

A calibrated 3-hole probe is used to measure total and static pressure, yaw angle and total temperature at the liner section. A full 2D Mach number map can be obtained by the collected measurements from the 3-hole probe. A traversing system that covers the cross-section area is designed and installed on the rig at the liner section (Figure 71) to determine the complete mapping of the flow. The measurement position is farther than eight equivalent diameters from any discontinuity or bend, i.e. from the nozzle exit, to ensure that measurement will be made in a well-developed flow without distortions.

Figure 72, a picture of 2-dimensional 3-hole probe

In order to assess the 2D flowfield in the cross-section with a good resolution and, at the same time, to reduce the duration of the test, it is necessary to consider an optimized distribution for the measurement points. The figure below shows an example of the sampling grid that was used for the aero measurements during the preliminary commissioning of the rig, but more refined distributions can be considered in the future.

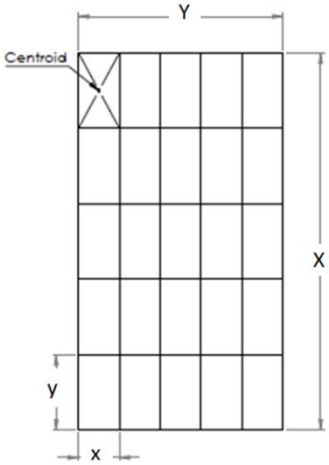

Figure 73, measurement grid sample for 2D flow mapping

An acceptable grid for flow measurements in rectangular ducts should be composed of equal area elements in which each element has the same aspect ratio of the duct cross-section. As in practice it is difficult to reach the optimum design for grid, the parameter (S) is defined as follow to achieve a sufficiently high accuracy in the duct measurements [62], [63]:

$$2/3 \leq S \leq 4/3$$

In which S is calculated as:

$$S = \frac{Aspect\ ratio\ of\ elemental\ area}{Aspect\ ratio\ of\ duct\ cross\ section}$$

The number of measurement points should not be less than 24 and it must be at least 1 measurement point per 2 square feet.

The traversing system (Figure 74 and Figure 75) has been designed as to permit to change the position of the probe during the tests at high temperature while the rig is running.

Five tubes are mounted as measurement rows on the longer side of the duct and the probe can slide through these tubes so that 5 rows of measurement are available on the long side of the duct while for the shorter side (liner face), an theoretically infinite number of measurement points (Figure 75) is possible, thus implying a higher resolution. This is important because the large number of measurement points allows a more refined assessment of the flow Mach profile in the plane normal to the liner.

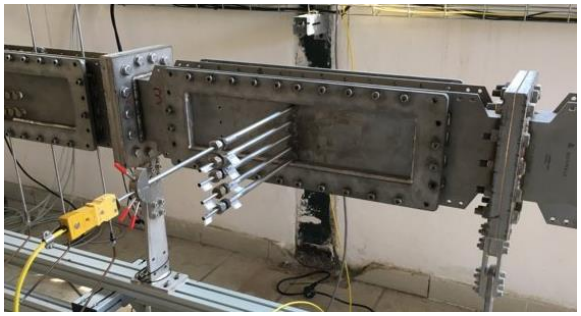

Figure 74, installation of the 2 dimensional 3-hole probe on the rig

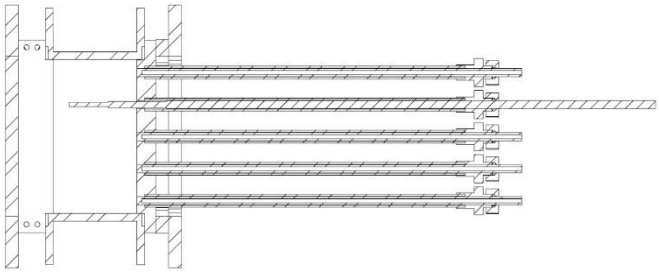

Figure 75, the 3-hole probe traversing system

The probe is equipped with a thermocouple that is beneficial to get the temperature of the flow at each measurement point and in order to have a more accurate calculation of the flow characteristics.

3.11.4. Hot-wire probe

The mean flow measurements are carried out through the 3-holes probe as it was described in the section 3.11.3. However, the boundary layer measurement is critical for the acoustic liner characterization and has to be addressed as well. In the UniFi test rig a hot-wire probe can be installed on a plate in front of the liner window by means of a traversing system allowing the measurement of the boundary layer profile on the liner surface. The probe has been selected and is going to be purchased.

3.11.5. Other aerodynamic measurement sections

In addition to the aforementioned instrumentations, a pitot tube is installed at the end of the test section (in the final diffuser) to monitor the flow conditions at the end of the wave guide. The pitot was installed downstream the anechoic termination to mitigate any possible acoustic disturbance caused by the pitot itself.

Several pressure taps and thermocouples are placed on the returning duct as well as on the fan, to record the pressures and temperatures at different positions of the rig.

3.12. Acoustic instrumentation and microphones arrangement

3.12.1. Microphone arrangements

The duct is equipped with several acoustic sensors and devices, i.e. acoustic drivers and microphones. Speakers are mounted both upstream and downstream the liner section. The input acoustic signal could be generated by an arbitrary wave generator and then amplified to a desired level. The input waves can be excited as to propagate along the same or opposite direction of the flow, to evaluate both upstream and downstream running waves.

The wave guide has been designed to allow the propagation of higher order modes. The first higher order mode to become cut-on at ambient temperature and Mach number 0.5, is m=0 and n=1 at 1238 Hz, where m and n correspond to the nodal lines in the larger and smaller sides of the cross-section, respectively. The cut-on frequencies for the other possible orders are reported in Table 7.

Table 7, number of cut on modes and required microphones

f max Hz	T	Ma	Ncuton max	Max n cut-on	Max m cut-on	Nmics min/section	Nmics source + termination
6000	20	0,5	14	(0,4)	(2,0)	28	56
5000	20	0,5	11	(0,4)	(2,0)	22	44
4000	20	0,5	7	(0,3)	(1,0)	14	28
3000	20	0,5	5	(0,2)	(1,0)	10	20
2000	20	0,5	2	(0,1)	(0,0)	4	8
1000	20	0,5	1	(0,0)	(0,0)	2	4

To allow modal decomposition of the acoustic field consisting in all the propagating modes at a given frequency and operating condition, a sufficient number of microphones should be considered.

According to Table 7, the decomposition analysis at 6000 Hz (14 cut-on modes) requires at least 56 microphones which should be located at both sides of the liner. Different arrangements for microphone's positions are available in the literature. Linear arrays can be used at both sides of the liner and/or in front of the liner. Ring arrays as well can be considered at the two sides of the liner. Among the different setups, UniFi test rig benefits both linear and ring array configurations that can help to leverage various impedance eduction methods. 5 ring arrays of microphones (each ring contains 6 microphones) are available at upstream and downstream side of the liner (ring 1 to ring 5 upstream; ring 1 to 5 downstream the liner) and a linear array is foreseen in front of the liner. The axial distance between adjacent rings is constant. Figure 76 shows the cross-section of the test bench where the microphones positions are shown at the upstream and downstream sections on the front sidewall. The other microphones are installed on the other walls (side, top and bottom) to complete each ring array pattern.

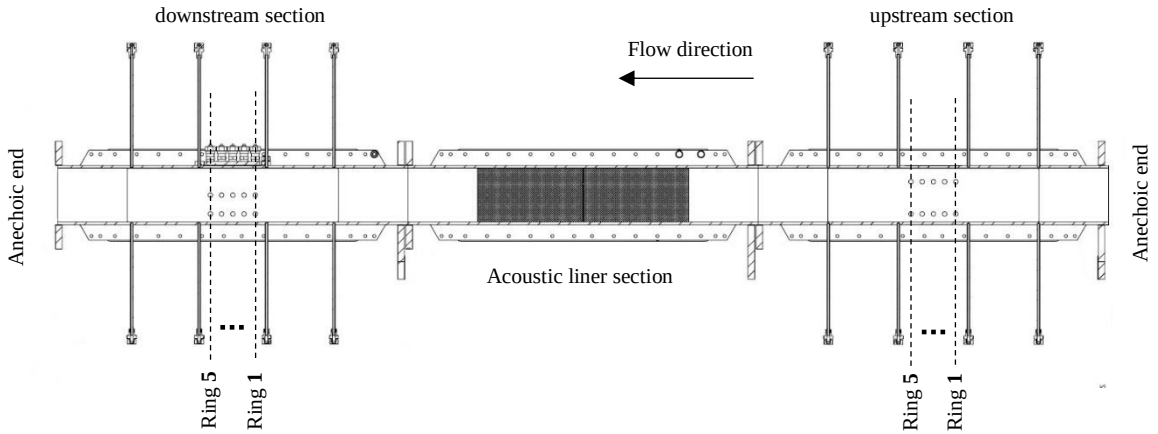

Figure 76, test section with microphones positions at liner sides

The microphones positions within the same ring array are optimized to minimize the error propagation during the modal decomposition process. Condition number analysis is carried out to evaluate the sensitivity of the microphone arrangement to any external error or perturbation on the estimated modal distribution, which is the solution of a large linear system where the unknowns are the amplitudes of each propagating waves and the inputs are the measured acoustic pressures. The optimum distance among sensors is a trade-off between condition number (that should be as low as possible) and the possibility of fabrication and installation of the microphone holders. Below, Figure 77 shows the results coming from the condition number analysis for a given ring array (Figure 78) as

a function of the non-dimensional frequency $k_0'b = k_0 b/\sqrt{1-M^2}$ and the non-dimensional axial distance between the rings $Dx'/b = Dx/\left(b\sqrt{1-M^2}\right)$ [64].

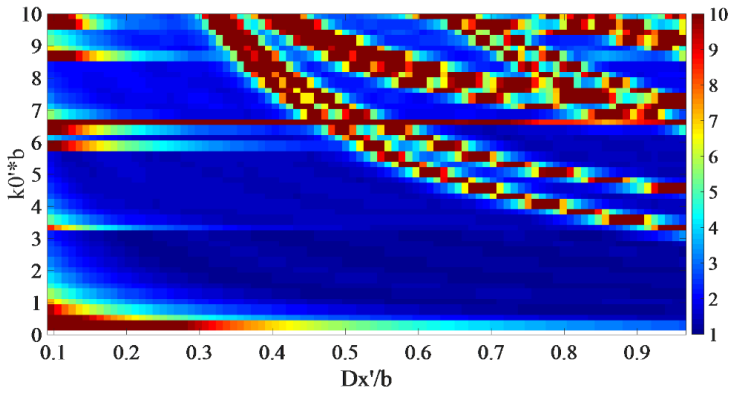

Figure 77, Condition number analysis for microphones' arrangement

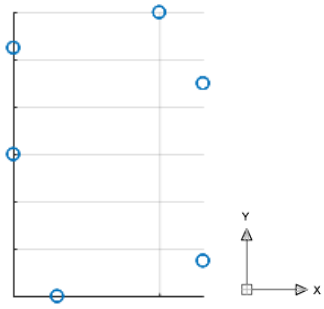

Figure 78, microphones position in the ring array

A set of microphones has been used for the rig preliminary commissioning at cold conditions. Figure 79 shows the outer view of the microphones' installation Highly sensitive ¼" pressure-field microphones were used for measuring sound pressure level inside the flow duct.

Figure 79, a picture of microphones and taps installed on the rig

The microphones are flush mounted on the duct wall (Figure 80 and Figure 81). Dedicated holders were designed and built. The holders allow to easily regulate the position of the microphone to reach the flush-mounted configuration. Besides this, to ensure the microphones' performance, they are

electromagnetically isolated from the rig body by a plastic adapter that is provided in the mounting system for cold operating condition. It is worth to notice here that, for the tests at hot conditions, high temperature resistant piezoresistive sensors will be used for the acoustic measurements as will be described in the next paragraph.

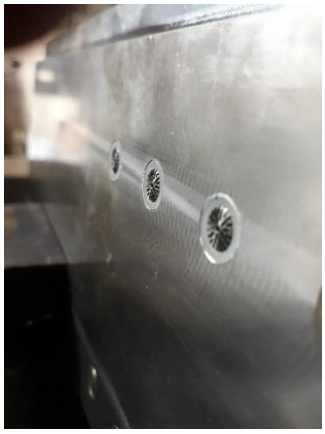

Figure 80, flush mounted microphones on the duct wall

Figure 81, microphones installed on the rig, duct inner view

To complete the acoustic measurement chain, a 24 bit resolution dynamic data acquisition system is employed for high-speed synchronous sampling of the acoustic signals. The maximum sampling rate per channel is 204.5 kHz. The system allows also to use high speed sampling board for bridge-type channels with a passband up to 40 kHz to acquire data from piezo-resistive dynamic sensors.

3.12.2. Measurement approach at high temperature and sensor selection

Standard microphones are not capable to work under hot condition. As the UniFi test rig is supposed to work under high temperature condition, it was required to find a solution for acoustic measurements. There are different but limited typologies of sensors available on the market for acoustic pressure measurements at high temperature. The selection of the measurement technique was driven by a list of technical requirements:

- Working fluid: clean air
- Maximum flow speed: Mach number 0.5
- Maximum operating temperature: 450 °C
- Maximum static pressure: 20 to 30 kPa ref. atmospheric pressure
- Operating bandwidth: 500 -7000Hz

- Maximum SPL: 160 dB (overall 0-20kHz)
- Low diameter of sensing element required, best is equal or less than ¼”
- Flush installation at duct wall
- Floor noise: the lowest possible. Considering a liner test and assuming a tonal signal at 120 dB with a maximum liner attenuation of 40 dB, a narrowband floor noise around 70 dB would be requested to make accurate measurements (acceptable SNR).

Considering the aforementioned specifications, the parameters which are considered to select the sensor are:

1) Maximum operating temperature
2) Floor noise of the sensor
3) Frequency response function with reference to the standard microphone
4) Cost
5) Additional Hardware required
6) Sensitivity
7) Sensing element dimensions
8) Maximum flow speed allowed
9) Temperature impact on FRF and or floor noise
10) Availability of the dynamic calibration certificate.

All possible candidates were carefully studied to identify the most appropriate device for UniFi test rig. After a preliminary comparison among the available solutions in the market, a piezo-resistive pressure sensor, a probe microphone and a piezo-electric sensor were down-selected for deeper investigations as they meet most of the specifications and they have a good performance to cost ratio.

The selected sensors have been preliminarily evaluated on a calibration rig. A set of comprehensive tests was carried out on the sensors to have a clearer scenario before selecting the most suitable sensor to be employed on the UniFi rig. In the next section, the calibration tests that were performed are briefly described. Hereafter a description of the sensors considered within the comparative analysis performed is given.

3.12.2.1. Piezo-resistive sensor

The proposed solution is a piezo-resistive dynamic pressure sensor which is ideal for hot testing. The device is suitable to be used in most liquids and gases media. It is an absolute 4-mm diameter sensor

for a wide range of pressure, and it can operate at temperature up to 500 °C with a compensated temperature range up to +454 °C. Thermal zero shift for this sensor is ±1.5% FS/100°F and the thermal sensitivity shift is around ±1.5 /100°F. The device is designed for high temperature applications, however it requires additional investigations because of the lack of enough information in the frequency domain response. The sensor was installed on a dedicated rig for dynamic calibration and cold and hot tests were performed on it.

3.12.2.2. Piezo-electric sensor

The piezoelectric sensor is a ½" ceramic high sensitivity sensor for high temperature applications up to 345 °C. The device is designed to measure low-level pressure in severe environments such as engines, hydraulic and pneumatic devices, compressors and turbines. The sensor measures transient or repetitive phenomena relative to the initial or average pressure level, over a wide amplitude range and the usable frequency range is from 20 Hz to 30 kHz.

3.12.2.3. Probe Microphone

The solution is based on the assembly of a ¼ inch pressure-field microphone model with a probe tip which allows the microphone to be far enough from the hot environment in a recessed mounting system. The probe tip length is important: it has to be selected in such a way that it keeps the microphone far from the high temperature zone and, at the same time, it shall provide a satisfying frequency response function with respect to the flush mounting microphone. The stand-alone microphone is the best suited device for acoustic measurements, but it can withstand only temperatures up to 125 °C. A capillary stainless-steel probe tip could be mounted on the microphone head in order to increase the temperature range of the device up to 350°C (depending on the length). However, this implementation can limit the operating range of frequency due to the resonance of the system. It should be mentioned that for application of the probe microphone on the UniFi rig an additional cooling system is still needed as the target temperature for the rig is around 450 °C. Moreover, additional design steps shall be required to realize a support for the device.

3.12.2.4. Calibration test rig for acoustic sensor selection

Calibration tests in the acoustic laboratory at the University of Florence were carried out for comparing and investigating the three candidate sensors. A picture of the calibration test rig is shown in Figure 82. Basically, the rig is a waveguide with a square cross section whose dimensions are such

that only the plane wave can propagate up to 10 kHz. The rig is equipped with an anechoic termination at one end. An acoustic driver generates the test signal. A ¼" pressure field condenser microphone is installed flush at the duct wall in the middle of the duct which is used as the Reference Microphone (RM). The device under test (DUT) is installed flush in front of the reference microphone (Figure 83). An appropriate mounting system was used for each sensor to ensure the flush installation on the duct wall and to install the DUT exactly in front of the reference microphone in a co-axial manner. So that, both the DUT and the RM are expected to read the same acoustic pressure, considering the plane wave excitation. Other microphones are foreseen in different axial positions for other purposes, such as measuring the reflection coefficient inside the duct. The air flow could be provided inside the duct through a plenum as shown on the right of Figure 82. The measurements are collected through a high-speed 16 Bit A/D converter which allows the synchronous acquisition of both the signals from DUT and from RM. A software is used to manage the data acquisition and the test signal. More details about the rig configuration are available in the references [60], [65].

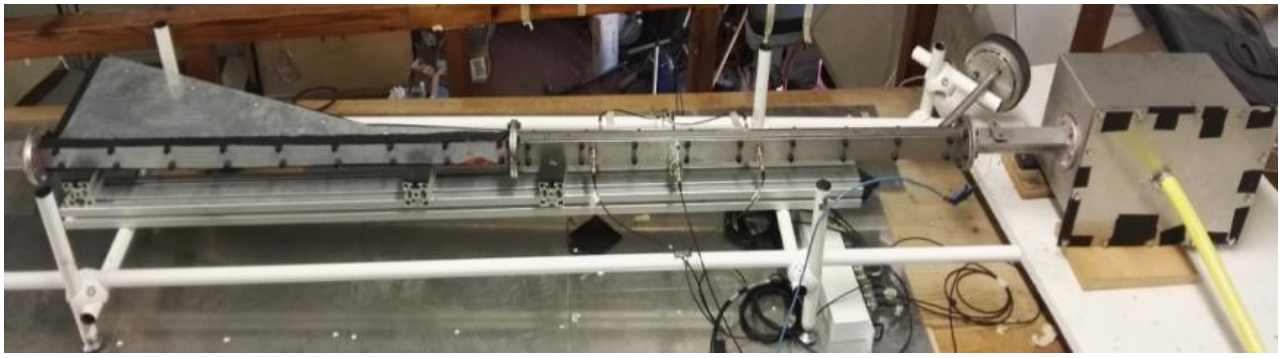

Figure 82, calibration test rig for acoustic measurements

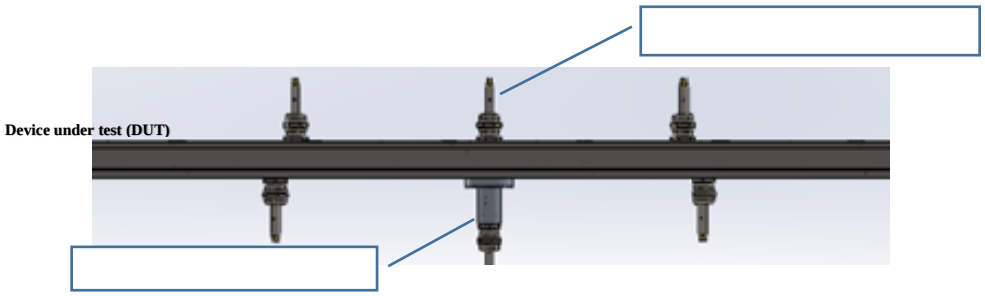

Figure 83, installation of reference microphone (RF) and device under test (DUT) on the calibration test rig

The objectives of the tests were mainly focused on:

1. Estimating the complex frequency response function (FRF) between RM and DUT
2. Estimating the floor noise of the DUT

3.12.2.5. Frequency response function with respect to the standard microphone

Each candidate sensor was installed on the calibration test rig to compare its acoustic behaviour with respect to the reference standard microphone. The FRF was the main objective of these tests. Figure 84 shows the comparison between the measured FRF for each sensor with respect to the standard microphone. According to the results, the piezo-resistive sensor has the best performance with respect to the piezo electric sensor and the 5 cm probe microphone. Apart from the small oscillations in FRF (within 0.5 dB at maximum) that could be due to the little misalignment in position between the piezo-resistive sensor and the RM and the small reflections from the anechoic termination, the piezo-resistive sensor has nearly the same behaviour of the standard microphone. The piezo-electric sensor has a very good performance as well, however it presents some pronounced fluctuations of FRF in the higher frequency range. For the probe microphone, the calibration curve is put to have a coherent comparison with the other sensors. This curve corresponds to a 5 cm probe microphone and the curve is provided by supplier. The performance of the probe microphone depends on the length of the probe which is mounted on the microphone tip.

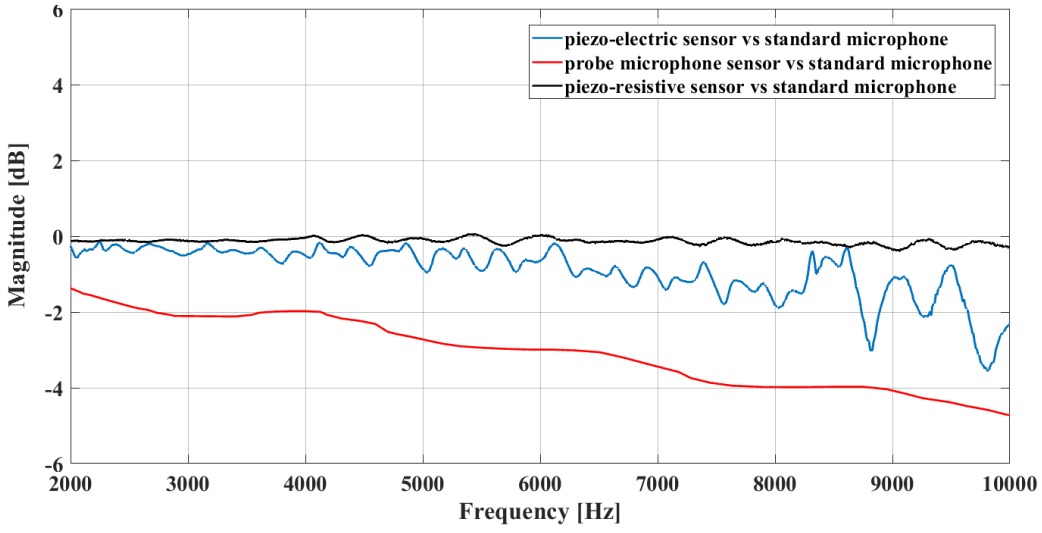

Figure 84, frequency response function comparison between three different sensors

3.12.2.6. Noise floor of the sensors

In Figure 85, the 1 Hz bandwidth spectra, estimated from the sensors output measured with no acoustic signal in the duct, are compared as equivalent SPL considering the static sensitivity. According to these results, both the piezo-resistive and piezo-electric sensors show a higher noise floor with respect to the standard microphone and the piezo-resistive sensor has higher noise floor than the piezo-electric one, however the overall noise floor level for all the candidate sensors meet the specifications given at the paragraph 3.12.2, i.e. a high enough SNR is ensured by all the tested sensors. Some peaks (usually at x50 Hz frequencies) are present in the curves could be due to electric disturbances in the laboratory and measurement chain and are not related to the sensor itself. The noise floor in general depends on the test ambient and the acquisition system as well. Provisions could be made in order to improve such result, e.g. by using higher quality signal conditioning device or a dedicated low noise amplifier.

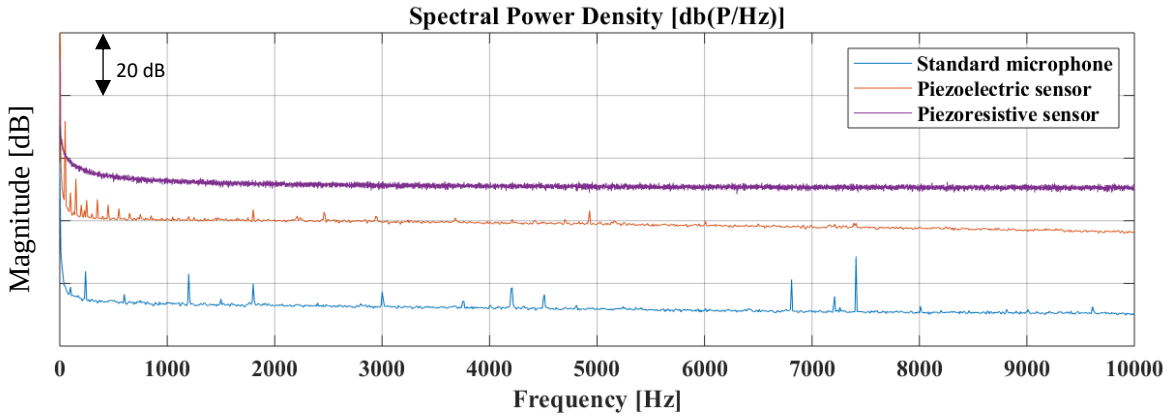

Figure 85, measured floor noise for different sensors

3.12.2.7. Overall Comparison and sensor selection

To down-select the best measurement device for acoustic testing in a grazing flow rig with hot flow, a dedicated study was carried out considering 3 possible solutions. To conclude, the piezo-electric sensor could be discarded mainly because of the higher sensor size and the operating temperature range, which is lower than required. Concerning the FRF for the piezoelectric sensor, it showed some non-linearities at the frequencies above 6 kHz. The probe microphone, although it has a very low floor noise, is discarded as well since it does not meet the required temperature requirements and implies the development of a cooling system. Furthermore, the flow effects in front of the probe tip could represent a concern and would require additional investigations. According to the results, piezo-resistive sensor demonstrates a good FRF within a high frequency range that is the most significant

parameter to be addressed. The operating temperature of the piezo-resistive sensor is sufficiently high and it does not require any auxiliary parts for cooling and thermal insulation. In addition, it has a small sensor dimension and it could be simply installed on the rig without special holders. Considering all the pros and cons among the suggested sensors, finally the piezo-resistive sensor is selected to be the acoustic measurement device for the UniFi test bench.

3.12.2.8. Auxiliary tests on Piezo-resistive sensor

Nominally, the selected sensor is suitable for hot measurement purposes however additional investigations are required for a deeper understanding of the temperature effects which are expected for piezo-resistive sensors. There are different sources of error that rise up at hot condition. Thermal sensitivity shift and Johnson noise could be the main aspects to be considered [66].

For the hot tests, the probe microphone was used as the reference microphone instead of the standard microphone alone since the standard microphone cannot be used at high temperatures. The objectives of the tests at hot conditions are listed below:

1. Estimating the complex frequency response function (FRF) of the piezo-resistive sensor with respect to the reference microphone (probe microphone in this case) at high temperature
2. Estimating the floor noise of the piezo-resistive sensor at high temperature
3. Checking the repeatability of the tests to find out if the high temperature alters the sensor behaviour in a permanent or reversible way

The sensor was heated up to 250 °C and then it was cooled down to ambient conditions. It was observed that rising the temperature does not change the floor noise level and, in addition, the test was completely repeatable because the behaviour at room temperature was recovered.

For what concerns FRF, 3 different temperatures were tested on the sensor. Figure 86 shows the measured FRF for the tested piezo-resistive sensor relative to the probe microphone at different temperatures.

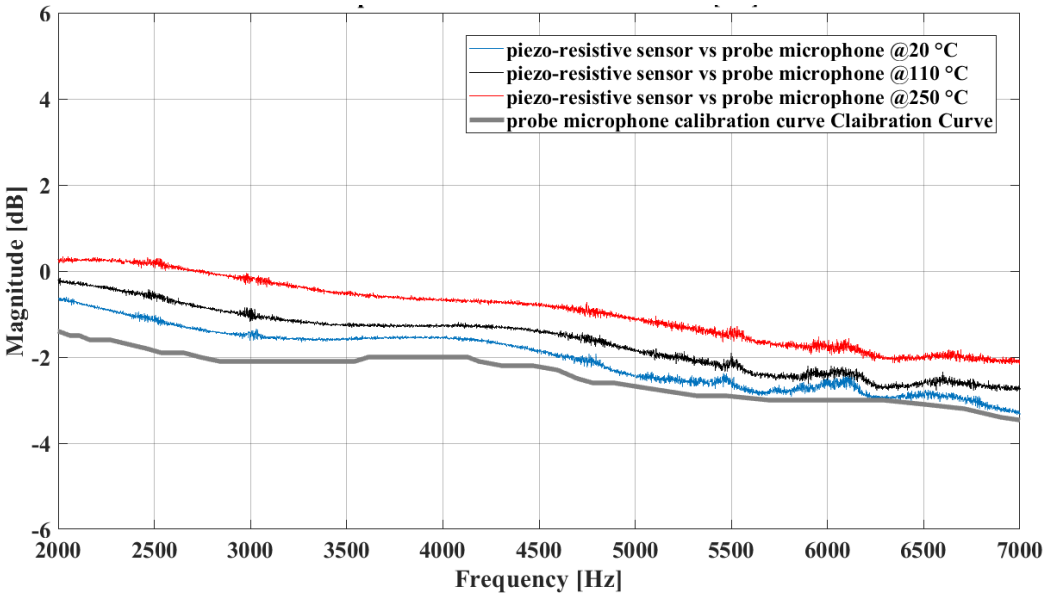

Figure 86, temperature effects on the frequency response function

As expected, there is a shift in the sensor sensitivity that causes some changes (less than 1 dB) in the FRF magnitude and it is within the specification for thermal sensitivity shift and thermal zero shift given by the manufacturer. This shift is very limited and, if needed, each sensor could be calibrated up to its maximum working temperature for better accuracy. There are no big changes in the curve shapes, implying that the sensor behaviour is predictable. FRF curve for cold condition before heating is completely reproducible after heating and cooling down, therefore the sensor gives same results over the time and there is no residual or side-effects due to the heating.

Chapter 4

Preliminary Rig Commissioning

Once the design and assembly of the rig is finished, a preliminary run was carried out to verify the rig testing capabilities. Through a set of aerodynamic measurements, the flow uniformity in the liner section was verified. From an acoustic point of view, basically two aspects have been checked: the achievable SNR (>10 dB is the requirement) and the acoustic performance of the anechoic terminations (R< 0.2 is the target).

Preliminary Aerodynamic results

A 2D map of the flow Mach number was produced by a set of measurement points at the liner section. Figure 87 shows the first results from the rig commissioning at average Mach 0.3. The main goal of the first test was to prove that at the test section the flow quality is good, with a fully developed and uniform profile. It can be seen that the relative deviations with respect to the higher measured Mach number were below 5% outside the boundary layer, so it can be concluded that an acceptable degree of flow uniformity is ensured at the test section.

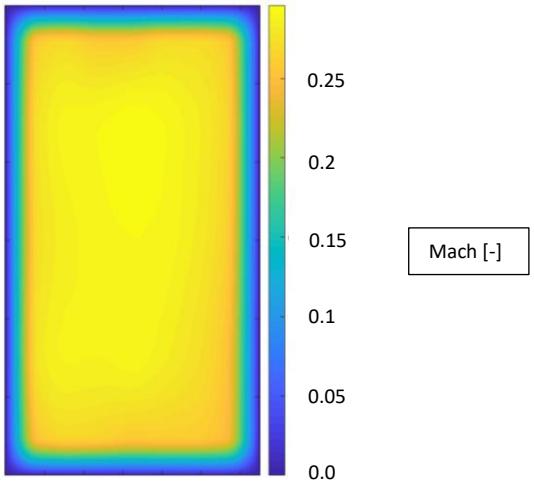

Figure 87, contour plot for the flow Mach number in the liner section

The flow yaw angle that determines the velocity direction with respect to the horizontal longitude axis is measured at the liner section. The measurement was carried out by traversing the probe at all

the five rows (top, mid top, mid span, mid bottom and bottom) of measurement sections and according to the results presented in Figure 88, there is no considerable flow rotation in front of the liner.

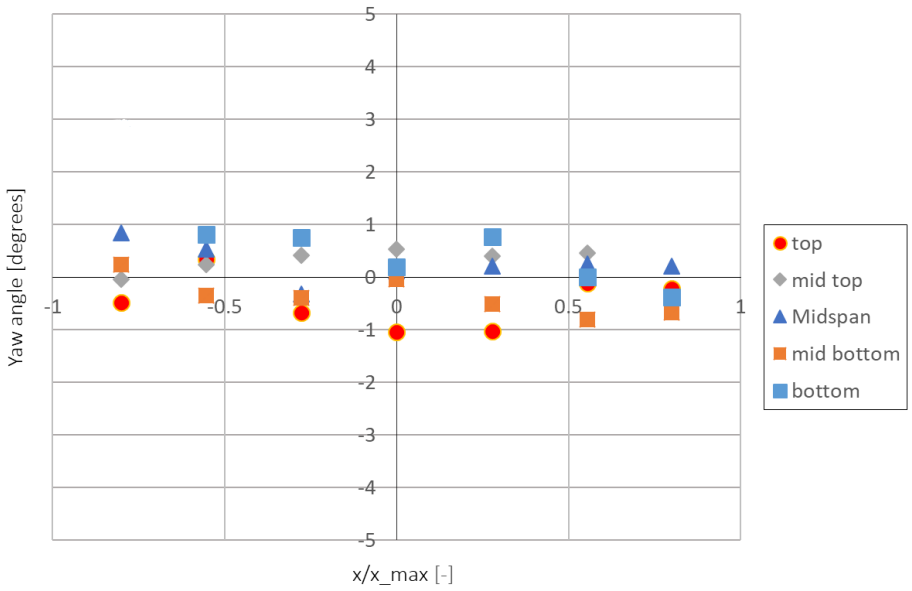

Figure 88, Flow yaw angle in the liner section Mach no. 0.3 at 5 different measurement rows in the liner section

The absolute static pressure values collected from the static taps in the test section are shown in Figure 89. The results, scaled with the atmospheric pressure, show that the pressure decrease linearly along the test section, as expected. The two groups of four measurement points at the leftmost and rightmost side of the graph are those which correspond, respectively, to the sections upstream and downstream of the liner. The point in the middle is the one measured at the liner section.

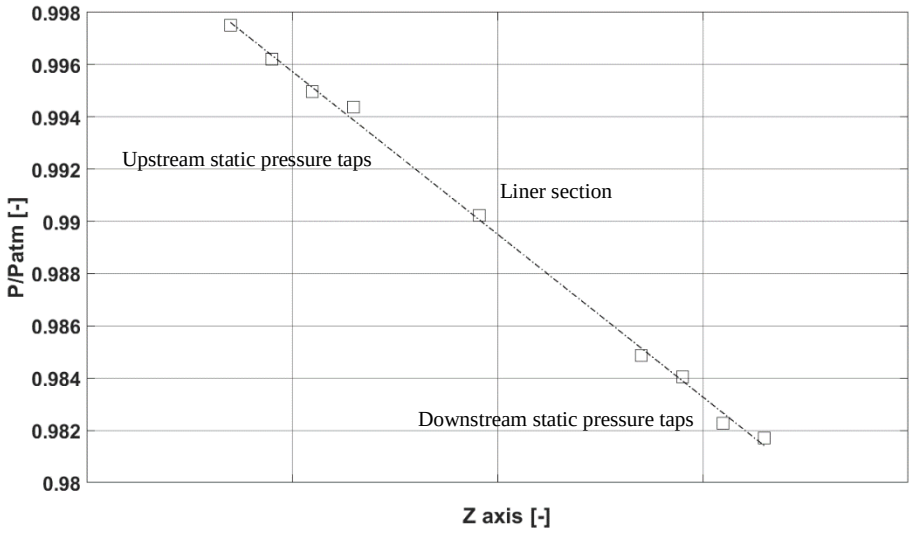

Figure 89, measured pressure losses along the duct

Preliminary Acoustic results

The preliminary rig commissioning was carried out at cold condition and a first set of acoustic data was obtained. The acoustic excitation is generated by the loudspeakers that are amplified to reach the desired sound pressure level. Standard capacitive microphones were used for this preliminary verification. A limited number of microphones was placed before and after the liner section in an axial array that provides the possibility of carrying out the two-microphone method for calculating the reflection coefficient and measure the SPL at both sides of the liner.

4.2.1. Flow noise and signal to noise ratio

The Signal to Noise Ratio (SNR) is defined as the ratio of the signal power to the background noise power and it must be sufficiently high to recognize and distinguish the desired signal from the background noise. Background noise could have two main sources: one is the fan noise and the other one is the pressure fluctuations due to the turbulence inside the flow. The flow noise can be considerable at high Mach numbers therefore the tests were performed for different flow speeds to ensure the quality of the SNR all over the rig envelope. Figure 90 shows the power spectral density of the flow noise at two different fan regimes (Mach1 and 3 × Mach1). According to the results in Figure 90, it is observed that rising the flow speed increases the flow noise. Therefore, a sufficiently high SNR (SNR>10 dB) must be guaranteed also for the tests at higher Mach numbers. Tonal excitations with high SPL could be employed to overcome the background noise. It is also observed that the measured background noise is mainly broadband as the fan does not produce any significant

tonal peak. The fan emissions are mostly observed at the lower frequencies, however the very low frequencies are not of interest for the rig mission. In case of need, an additional silencer could be installed before the inlet plenum to further reduce the fan noise. Moreover, there is the possibility of filtering out the flow noise from the excited source at the post processing stage through filtering methods based on coherence analysis. It is worth noting that, when the liner is installed attention must be paid to the SNR after the liner section: Here the SNR can be low because of the absorption caused by the liner itself and signal processing techniques to improve the SNR could be needed.

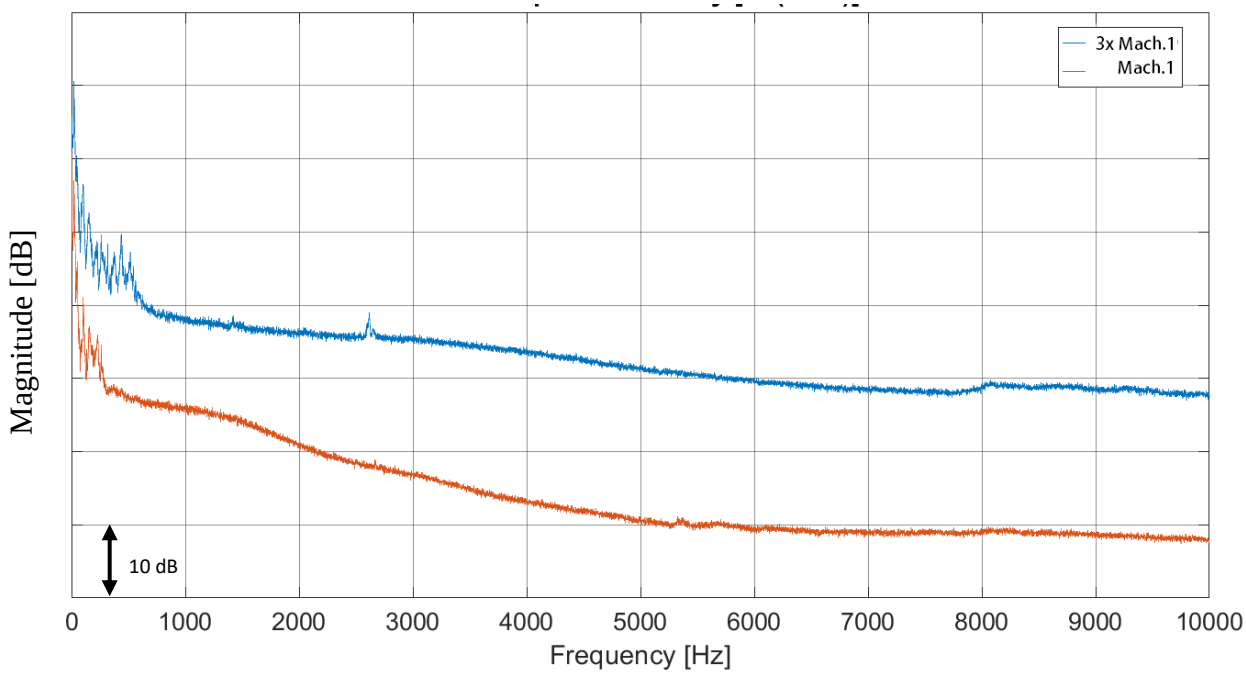

Figure 90, Measured flow noise (no signal excitation) at two different Mach numbers

4.2.2. Anechoic termination performance

Another important objective of the preliminary commissioning was to evaluate the effectiveness of the anechoic terminations. For this purpose, upstream speakers were used as the signal generator. They were set to work in phase and also the frequency was limited to the lower band to guarantee the plane wave regime. The two microphones closest to the anechoic termination (microphones at ring 5 and ring 4 downstream liner section, Figure 76) were used to calculate the reflection coefficient for the AT. The results are compared with the FEM model. Figure 91 shows the reflection coefficient at no flow condition and it is observed that it is less than 0.2 in the whole frequency band of the interest and also it is observed a qualitative agreement between numerical and experimental results. There are some mismatches between the FEM model and the experimental data that occur at certain frequencies

and they could be due to the differences between the actual construction of the AT which are not considered in the nominal FEM model.

The experimental results show also an excellent performance of the ATs at higher frequencies, as expected. It is worth mentioning that the FEM model is limited to lower frequencies to reduce the computation costs.

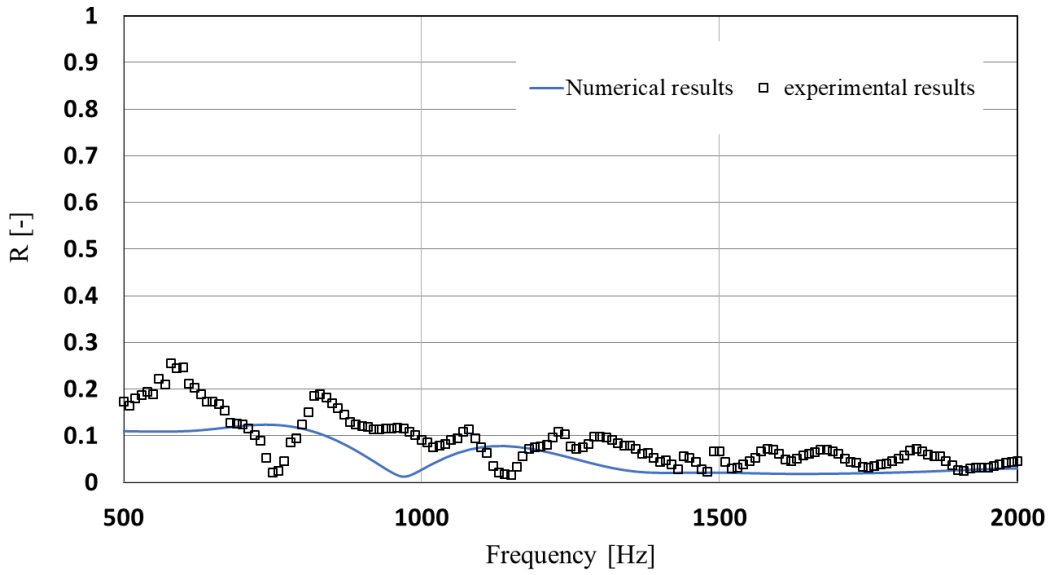

Figure 91, reflection coefficient with no flow: comparison between numerical prediction and the experimental measures

The reflection coefficient was evaluated also for the condition with flow and the results show no considerable effects on the acoustic performance (Figure 92). Two microphones at the downstream liner section were used for the measurement of the reflection coefficient under a broadband signal excitation. Different speeds were checked and according to the results presented in the Figure 92 in all the cases *R* is still below 0.2.

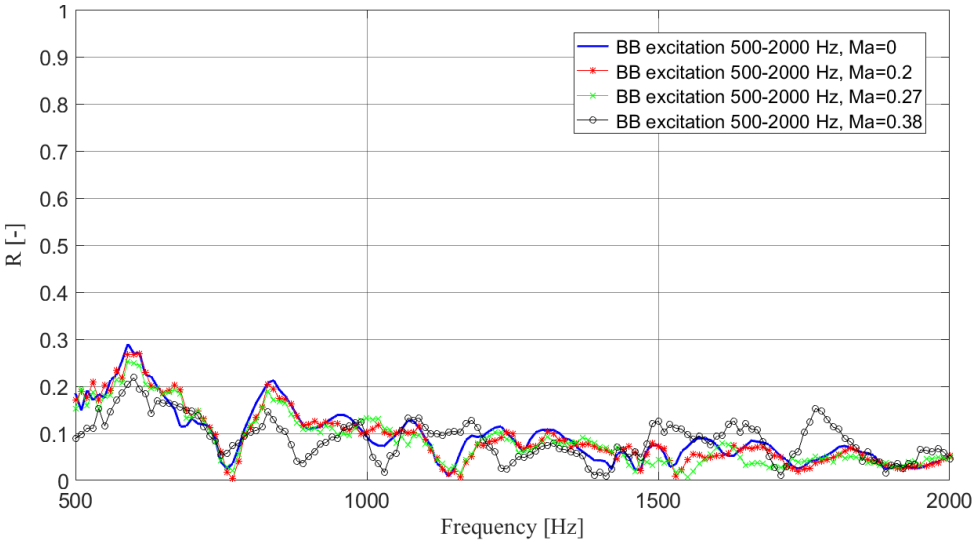

Figure 92, measured reflection coefficient at different flow speeds

4.2.3. Liner test, transmission loss measurement

In order to verify the suitability of the test rig at performing acoustic measurements for the characterization of the liners, a sample was installed on the rig and the measurements were acquired to get the transmission loss. The tested liner was a Single Degree of Freedom (SDOF) liner and was tested at cold condition because the temperature resistant sensors were not available yet.

The test was carried out at no flow and at two different flow Mach numbers. A series of tones was generated within the frequency band up to 2500 Hz, with a step of 250 Hz. Upstream speakers were used a tonal signal was considered. The transmission loss was obtained as it is described in the section (2.4) by means of 3 microphones: 2 microphones were installed upstream the liner (at rings 4 and 5) and a third microphone at the section downstream of the liner (ring 5, Figure 76).

Figure 93 depicts the results in terms of TL at 3 different flow conditions. The TL maximum takes place at the resonance frequency of the test article. The results show that the flow rises the maximum value of the transmission loss while its effect is quite negligible at lower frequencies. It is also observed that for increasing flow speed there is a shift in the frequency at which the maximum TL occurs. The results were compared also with the numerical outcomes that were provided by a partner within the ENOVAL European project. The comparison demonstrates a good agreement between the numerical and the experimental data.

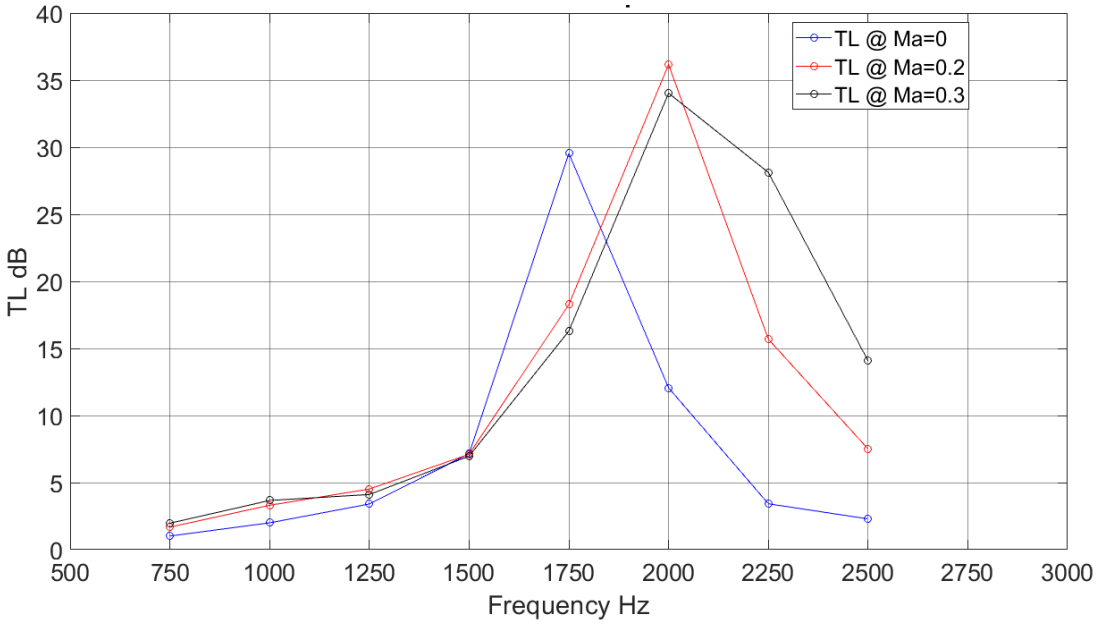

Figure 93, measured transmission loss due to a SDOF liner at different cold flow conditions

When the liner is installed, SNR could be critical at the liner downstream because of the action of the liner on the generated signal. For this purpose, the SNR was measured during the tests on the liner. In the picture below, the narrow band spectrum measured after the liner with a flow Mach number 0.3 is reported. The considered tonal signal was at 2 kHz, close to the maximum absorption of the investigated treatment. Figure 94 shows the measured signal and it can be seen that the signal amplitude is more than 15 dB above the flow noise which guarantees a good SNR.

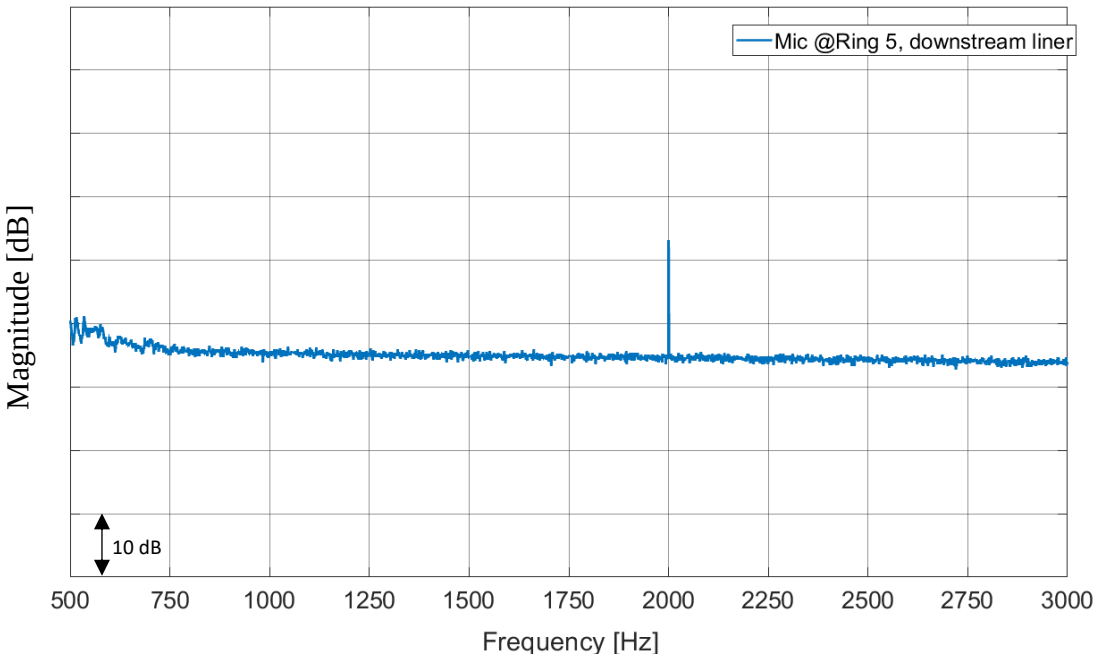

Figure 94, measured power spectral density of the signal downstream the liner, Ma=0.3

Conclusion and future works

Within the framework of technological research addressed to the reduction of noise emissions from modern aircraft engines, the use of acoustic liners has grown its importance in the recent years. Within this scenario, a dedicated test rig was designed and manufactured in the Department of Industrial Engineering at the University of Florence (Italy) with the aim of testing acoustic liners under hot and high-speed flow conditions, representative of the aeroengine exhaust. The apparatus is basically a waveguide where a controlled noise field is produced in the presence of a grazing flow. The final objective is to evaluate the liner impedance. The design of all the components were addressed carefully for working under high temperature (up to 450 °C) and the high flow speeds (up to Mach no. 0.5).

The rig was designed starting from scratch considering aerodynamical, mechanical, thermal and acoustical constraints.

A rectangular cross section has been selected to ease the installation of the liner and instrumentations. An optimized aspect ratio for the cross section has been estimated to ensure well separated cut-on frequencies for higher order acoustic modes as well as to reduce pressure losses in the test section.

The most important components, e.g. the plenum and the anechoic terminations were designed by means of finite element simulations using coupled analyses where thermal and mechanical effects were kept into account at the same time. The results showed satisfactory safety margins at all operating conditions.

FEA was used for the acoustic design of the anechoic terminations. A double slope shape was selected, and the results demonstrated low reflection coefficient within all the frequency band of interest.

After the design process was completed, the rig components have been realized and assembled together and the rig is operational.

From the point of view of acoustic measurements in hot flows, an experimental test campaign was performed to select a suitable dynamic sensor ensuring as much constant as possible frequency response function, together with low floor noise and resistance to high temperature. The results motivated the selection of a piezo-resistive sensor which met the requirements with a FRF deviation less than 0.5 dB within the band 2-7 kHz and acceptable noise floor. The thermal effects on FRF were

assessed experimentally: results showed a reversible effect on FRF which could be calibrated in a reproducible way.

A preliminary commissioning has been performed in order to have a first verification of the rig capabilities.

A first aerodynamic characterization has been performed and the Mach number distribution has been measured through a 3-holes probe at the inlet of the test-section. The results showed good uniformity of the flow field within the test section. The deviations from the expected profile were below 5% outside the boundary layer and the flow angle was below 1° at all the measurement positions. Such results demonstrate the effectiveness of the plenum and the nozzle at removing potential upstream flow distortions.

The acoustic performance of the anechoic terminations has been assessed through reflection coefficient measurement via 2 microphones method. A reflection coefficient below 0.2 has been verified within all the frequency band of interest which will ensure negligible impact of back-reflections at rig ends.

The rig background noise has been assessed at different flow regimes. The spectra revealed that the fan noise is limited to the very low frequency band and the absence of any fan-related tones within the measurement band. The turbulence-generated noise growth at increasing flow speed has been measured by flush mounted microphones: this determined the need of using tonal noise excitation in order to ensure a SNR higher than 10dB within all the frequency bands. This aspect is more of concern at the measurement section downstream of the liner where the amplitude of the excitation signal is reduced by the action of the liner itself. A preliminary test on a sample liner revealed that a SNR higher than 10dB is achievable even with a grazing flow condition.

Finally, a first test on a SDOF liner sample was performed and the transmission loss has been measured at ambient temperature (because the temperature resistant sensors were not available yet) in order to verify the rig functionality. The tests were performed at increasing flow speed and the outcomes revealed TL curves with the expected frequency shift due to the flow effect.

Future work

The rig is operating, and it will be used for testing liners under flow conditions representative of aero engine exhaust.

A comprehensive aerodynamic campaign is scheduled in order to assess accurately, by means of a high-resolution measurement grid, the mean flow field and the boundary layer profile at different

flow speeds within the test section. The results will be used to feed the impedance eduction algorithm in order to estimate the liner impedance.

Once the aero mapping will be completed, an acoustic experimental campaign will be performed to assess impedance of different liner samples.

References

[1] "https://commons.wikimedia.org/w/index.php?curid=4008470." [Online]. Available: https://commons.wikimedia.org/w/index.php?curid=4008470.

[2] "https://commons.wikimedia.org/w/index.php?curid=4005530." [Online]. Available: https://commons.wikimedia.org/w/index.php?curid=4005530.

[3] E. Piot, J.-P. Brazier, F. Simon, V. Fascio, C. Peyret, and J. Ingenito, "Design, manufacturing and demonstration of acoustic liners for air conditioning systems," 2016.

[4] M. Jones, M. Tracy, W. Watson, and T. Parrott, "Effects of Liner Geometry on Acoustic Impedance," 2012.

[5] M. Dannemann *et al.*, "Experimental Study of Advanced Helmholtz Resonator Liners with Increased Acoustic Performance by Utilising Material Damping Effects," *Appl. Sci.*, 2018.

[6] H. Matsuhisa, B. Ren, and S. Sato, "Semiactive control of duct noise by a volume-variable resonator," *JSME Int. Journal, Ser. 3 Vib. Control Eng. Eng. Ind.*, vol. 35, no. 2, pp. 223–228, 1992.

[7] J. M. De Bedout, M. A. Franchek, R. J. Bernhard, and L. Mongeau, "Adaptive-passive noise control with self-tuning Helmholtz resonators," *J. Sound Vib.*, vol. 202, no. 1, pp. 109–123, Apr. 1997.

[8] P. S. Liu, G. F. Chen, P. S. Liu, and G. F. Chen, "Characterization Methods: Physical Properties," *Porous Mater.*, pp. 493–532, 2014.

[9] *ISO 10534-1 Acoustics - Determination of Sound Absorption Coefficient and Impedance in Impedance Tubes - Part 1: Method Using Standing Wave Ratio*. 1996.

[10] A. Schoffman, *ISO 10534-2: 1998, Accoustics Determination of Sound Absorption Coefficient and Impedance Tubes Part 2 : Transfer Function Method*. Oxford University Press, 2007.

[11] R. Lanoye, G. Vermeir, W. Lauriks, R. Kruse, and V. Mellert, "Measuring the free field acoustic impedance and absorption coefficient of sound absorbing materials with a combined particle velocity-pressure sensor," *J. Acoust. Soc. Am.*, vol. 119, no. 5, pp. 2826–2831, May 2006.

[12] H. Lester and T. Parrot, "Application of a finite element method for computing grazing incidence wave structure in an impedance tube - Comparison with experiment<149>for duct

liner aeroacoustic design," 1979.

[13] M. Jones, W. Watson, M. Tracy, and T. Parrott, "Comparison of two acoustic waveguide methods for determining liner impedance," in *7th AIAA/CEAS Aeroacoustics Conference and Exhibit*, 2001.

[14] M. Jones, W. Watson, T. Parrott, and C. Smith, "Design and Evaluation of Modifications to the NASA Langley Flow Impedance Tube," in *10th AIAA/CEAS Aeroacoustics Conference*, 2004.

[15] W. R. Watson and M. G. Jones, "Impedance Eduction in Ducts with Higher-Order Modes and Flow."

[16] M. C. Brown, M. G. Jones, and W. R. Watson, "Uncertainty Analysis of the Grazing Flow Impedance Tube," Associate Fellow AIAA.

[17] C. H. Gerhold, R. H. Cabell, and M. C. Brown, "Development of an Experimental Rig for Investigation of Higher Order Modes in Ducts."

[18] C. H. Gerhold, M. C. Brown, M. G. Jones, and B. M. Howerton, "Report on Recent Upgrades to the Curved Duct Test Rig at NASA Langley Research Center."

[19] C. H. Gerhold, M. C. Brown, W. R. Watson, and M. G. Jones, "Investigation of Liner Characteristics in the NASA Langley Curved Duct Test Rig."

[20] S. Busse *et al.*, "Impedance Deduction Based on Insertion Loss Measurements of Liners under Grazing Flow Conditions," in *14th AIAA/CEAS Aeroacoustics Conference (29th AIAA Aeroacoustics Conference)*, 2008.

[21] S. Busse-Gerstengarbe, F. Bake, L. Enghardt, and M. G. Jones, "Comparative Study of Impedance Eduction Methods, Part 1: DLR Tests and Methodology," in *19th AIAA/CEAS Aeroacoustics Conference*, 2013.

[22] S. Busse-Gerstengarbe *et al.*, "Impedance eduction based on microphone measurements of liners under grazing flow conditions," in *AIAA Journal*, 2012, vol. 50, no. 4, pp. 867–879.

[23] E. R. Rademaker, S. T. Idzenga, H. N. Huisman, R. J. Nijboer, and S. L. Sarin, "A new facility for hot stream acoustic liner testing," 2003.

[24] E. R. Rademaker, H. M. M. van der Wal, and E. G. M. Geurts, "Hot-stream in-situ acoustic impedance measurements on various air-filled cavity and porous liners," 2009.

[25] K. Knobloch, C. Lahiri, L. Enghardt, F. Bake, and D. Peitsch, “Hot-acoustic-testrig (HAT) - A unique facility for thermoacoustic research,” in *Proceedings of the ASME Turbo Expo*, 2011, vol. 7, no. PARTS A, B, AND C, pp. 1023–1032.

[26] C. Lahiri, K. Knobloch, F. Bake, and L. Enghardt, “Acoustic Measurements of Perforated Liners in Hot and Pressurized Flow,” 2013.

[27] J. Primus, E. Piot, F. Simon, M. G. Jones, and W. Watson, “ONERA-NASA cooperative effort on liner impedance eduction,” in *19th AIAA/CEAS Aeroacoustics Conference*, 2013.

[28] E. Piot, J. P. Brazier, F. Simon, V. Fascio, C. Peyret, and J. Ingenitok, “Design, manufacturing and demonstration of acoustic liners for air conditioning systems,” in *22nd AIAA/CEAS Aeroacoustics Conference, 2016*, 2016.

[29] F. Mery, D. Sebbane, R. Roncen, E. Piot, and F. Simon, “Experimental impedance assessment of innovative liner under shear grazing flow,” 2019.

[30] J. Golliard, J.-C. Leroux, E. Portier, T. Humbert, and Y. Auregan, “MAINE Flow: Experimental facility for characterization of liners subjected to representative acoustical excitation and grazing flow,” 2019.

[31] S. V. Lympany, A. Z. Karon, M. L. Wadsworth, R. Funk, and K. K. Ahuja, “An experimental facility for measuring the acoustic reection and transmission of higher-order modes in heated flows, part 1: Design and methodology,” in *2018 AIAA/CEAS Aeroacoustics Conference*, 2018.

[32] S. V. Lympany and K. K. Ahuja, “An Experimental Facility for Measuring the Acoustic Reflection and Transmission of Higher-Order Modes in Heated Flows, Part 2: Experiments and Analysis,” in *2018 AIAA/CEAS Aeroacoustics Conference*, 2018.

[33] M. L. Munjal, *Acoustics of Ducts and Mufflers*. Wiley, 2014.

[34] D. C. Pridmore-Brown, “Sound propagation in a fluid flowing through an attenuating duct,” *J. Fluid Mech.*, vol. 4, no. 4, pp. 393–406, 1958.

[35] P. Mungur and G. M. L. Gladwell, “Acoustic wave propagation in a sheared fluid contained in a duct,” *J. Sound Vib.*, vol. 9, no. 1, pp. 28–48, 1969.

[36] U. Ingard, “Influence of Fluid Motion Past a Plane Boundary on Sound Reflection, Absorption, and Transmission,” *J. Acoust. Soc. Am.*, vol. 31, no. 7, pp. 1035–1036, Jul. 1959.

[37] M. K. Myers, “On the acoustic boundary condition in the presence of flow,” *Top. Catal.*, 1980.

[38] E. Brambley, “A Well-posed Modified Myers Boundary Condition,” in *16th AIAA/CEAS Aeroacoustics Conference*, 2010.

[39] E. J. Brambley, “Well-Posed Boundary Condition for Acoustic Liners in Straight Ducts with Flow,” *AIAA J.*, vol. 49, no. 6, 2011.

[40] S. W. Rienstra and M. Darau, “Reprint of: Mean flow boundary layer effects of hydrodynamic instability of impedance wall,” in *Procedia IUTAM*, 2010.

[41] M. G. Jones and T. L. Parrott, “Evaluation of a multi-point method for determining acoustic impedance,” *Mech. Syst. Signal Process.*, vol. 3, no. 1, pp. 15–35, 1989.

[42] U. Ingard, “On the Theory and Design of Acoustic Resonators,” *J. Acoust. Soc. Am.*, 2005.

[43] L. E. Kinsler, A. R. Frey, A. B. Coppens, and J. V. Sanders, “Fundamentals of acoustics. Third edition.,” 1982.

[44] C. Lahiri, “Acoustic Performance of Bias Flow Liners in Gas Turbine Combustors.”

[45] F. Fahy, *Foundations of Engineering Acoustics*. Elsevier Ltd, 2003.

[46] S. Rienstra, “Impedance Models in Time Domain, Including the Extended Helmholtz Resonator Model,” in *12th AIAA/CEAS Aeroacoustics Conference (27th AIAA Aeroacoustics Conference)*, 2006.

[47] A. F. Seybert and D. F. Ross, “Experimental determination of acoustic properties using a two-microphone random-excitation technique,” *J. Acoust. Soc. Am.*, vol. 61, no. 5, pp. 1362–1370, 1977.

[48] S.-H. Jang and J.-G. Ih, “On the multiple microphone method for measuring in-duct acoustic properties in the presence of mean flow,” *J. Acoust. Soc. Am.*, vol. 103, no. 3, pp. 1520–1526, 1998.

[49] M. Åbom and H. Bodén, “Error analysis of two-microphone measurements in ducts with flow,” *J. Acoust. Soc. Am.*, vol. 83, no. 6, pp. 2429–2438, 1988.

[50] J. S. Bendat and A. G. Piersol, *Random data : analysis and measurement procedures*. .

[51] W. R. Watson and M. G. Jones, “A Comparative Study of Four Impedance Eduction Methodologies Using Several Test Liners.”

[52] W. Watson and M. Jones, “Comparison of a Convected Helmholtz and Euler Model for Impedance Eduction in Flow,” in *12th AIAA/CEAS Aeroacoustics Conference (27th AIAA Aeroacoustics Conference)*, 2006.

[53] D. L. Armstrong, R. Beckemeyer, and R. F. Olsen, “Impedance measurements of acoustic duct liners with grazing flow,” *J. Acoust. Soc. Am.*, vol. 55, no. S1, pp. S59–S59, Apr. 1974.

[54] X. Jing, S. Peng, and X. Sun, “A straightforward method for wall impedance eduction in a flow duct,” *J. Acoust. Soc. Am.*, vol. 124, no. 1, pp. 227–234, Jul. 2008.

[55] X. Qiu, B. Xin, X. J.-J. of S. and Vibration, and undefined 2018, “Straightforward impedance eduction method for non-grazing incidence wave with multiple modes,” *Elsevier*.

[56] X. Jing, S. Peng, L. Wang, X. S.-J. of S. and Vibration, and undefined 2015, “Investigation of straightforward impedance eduction in the presence of shear flow,” *Elsevier*.

[57] U. Bolleter, R. Cohen, and J. Wang, “Design considerations for an in-duct soundpower measuring system,” *J. Sound Vib.*, vol. 28, no. 4, pp. 669–685, Jun. 1973.

[58] W. Neise and F. Arnold, “On sound power determination in flow ducts,” *J. Sound Vib.*, vol. 244, no. 3, pp. 481–503, Jul. 2001.

[59] *ISO 5136:2003, Acoustics-Determination of sound power radiated into a duct by fans and other air moving devices--In-duct method*. .

[60] F. Taddei, M. De Lucia, L. Bartolozzi, M. Salvestroni, and D. Torzo, “Setup of a test rig for the characterization of devices for acoustic measurements in hot flow,” in *23rd International Congress on Sound and Vibration*, 2016.

[61] D. A. Bies, “Acoustic Properties of Steel Wool,” *J. Acoust. Soc. Am.*, vol. 35, no. 4, pp. 495–499, 1963.

[62] *Gas Turbine Heat Recovery Steam Generators, ANSI/ASME PTC 4.4*. 1981.

[63] H.-W. Wang and J. Wei, “Blockage effect on the flow around a cylinder probe in calibration,” *J. Aerosp. Power*, vol. 7, 2007.

[64] U. Tapken and L. Enghardt, “Optimisation of Sensor Arrays for Radial Mode Analysis in Flow Ducts,” in *12th AIAA/CEAS Aeroacoustics Conference (27th AIAA Aeroacoustics Conference)*, 2006.

[65] F. Taddei *et al.*, “development of a measurement system for hot flow acoustic tests,” in

Proceedings of the 15th International Symposium on Unsteady Aerodynamics, Aeroacoustics & Aeroelasticity of Turbomachines, ISUAAAT15, 2018.

[66] R. Dieme, G. Bosman, T. Nishida, and M. Sheplak, "Sources of excess noise in silicon piezoresistive microphones," *J. Acoust. Soc. Am.*, vol. 119, no. 5, pp. 2710–2720, May 2006.